OPTICAL SPECTROSCOPY OF LUMINOUS INFRARED GALAXIES II. ANALYSIS OF THE NUCLEAR AND LONG-SLIT DATA

S. Veilleux[1],[2],[3], D.-C. Kim[1], D.B. Sanders[1],
J. M. Mazzarella[4], and B. T. Soifer[5]

Submitted to *The Astrophysical Journal*

Running Title: LUMINOUS INFRARED GALAXIES II.

[1] Institute for Astronomy, University of Hawaii, 2680 Woodlawn Drive, Honolulu, HI 96822

[2] Kitt Peak National Observatory, NOAO, P.O. Box 26732, Tucson, AZ 85726-6732.

[3] Hubble Fellow.

[4] Infrared Processing and Analysis Center, MS 100-22, California Institute of Technology, Jet Propulsion Laboratory, Pasadena, CA 91125

[5] Palomar Observatory, California Institute of Technology, 320-47, Pasadena, CA 91125.

ABSTRACT

A spectroscopic survey of a sample of 201 luminous IRAS galaxies (LIGs: $L_{ir} > 3 \times 10^{10} L_{\odot}$; HO = 75 km $s^{-1} Mpc^{-1}$) was carried out using the Palomar 5-meter amd University of Hawaii 2.2-m telescopes. Kim et al. (1 994, Paper 1) described the data-raking and data-reduction procedures and presented line and continuum measurements extracted from the nucleus of these objects. In this paper, the nuclear data are combined with circumnuclear measurements on 23 of these galaxies to investigate the properties of the line-emitting gas and underlying stellar population in and out of the nucleus. Great care was taken in classifying the nuclear spectra of these galaxies as "HII region-like" or "AGN-like" using a large number of line-ratio diagnostics correct cc] for the underlying stellar absorption features. This correction is an important source of errors in previous studies. The clnissioll-line spectra of many AGN were found to be of relatively low ionization level and were therefore classified as LINER. We confirm that both the fraction of LIGs with AGN spectra and the fraction of Seyferts among the AGN increase with infrared luminosity, both reaching a value of 54% at higher luminosity. The fraction of LINERs, on the other hand, is relatively constant at $\sim 25\%$. The source of the ionization of the emission-line gas often is a function of the distance from the nucleus. Based on the emission-line ratios and the strengths of the stellar absorption features, circumnuclear starburst activity is a common feature of LIGs, regardless of their nuclear spectral types. The emission-line, absorption-line, and continuum properties of the LINERs suggest that most of the LINER emission in these infrared-selectcd galaxies is produced through shock ionization]] rather than photoionization by a genuine active nucleus.

The nuclear region of Seyfert LIGs is found to be slightly less reddened than that of the LINERs and H II galaxies. The dust distribution generally is concentrated towards the nucleus, in agreement with the often peaky distribution of the molecular gas observed in these galaxies. Inverted dust profiles in which the nucleus appears less dusty than the circumnuclear region are observed in only five LIGs, four of which hare AGN emission-line characteristics. A possible explanation for these results is that galaxies with Seyfert emission lines are at a more advanced stage of dust destruction/expulsion than H II LIGs. Complex optical depth effects may also explain these results without invoking a smaller amount of dust in the nucleus. The slightly stronger Hβ and Mg Ib absorption features found in the nuclei of AGN (especially among the LINERs) may also indicate that these objects are at a more advanced stage of stellar evolution than H 11 LIGs. Further support "for this scenario comes from the fact that AGNs are found more frequently in advanced mergers than H 11 galaxies. However, this last result may be a luminosity effect rather than an effect related to the dominant nuclear source of ionization.

The [O III] profiles of both Seyfert anti LINER LIGs were found to be broader

on average than those of H II objects. Nearly *20%* of the LIGs in our sample have line widths larger than 600 km s-"[1]. We find that most of the galaxies in which we could determine the radial variations of the [0 III] line widths present broader profiles in the circumnuclear region than at the nucleus. When combined with published data on a few other ">vcll-studied LIGs, these results suggest that large-scale nuclear winds are common in these objects and are an efficient way of getting rid of the obscuring material in the nuclear region. The spatially extended LINER emission observed in many of these objects is probably due to shock ionization resulting from the interaction of the wind-accelerated gas with the ambient material of the host galaxy.

Subject headings : galaxies: nuclei - galaxies: stellar content - galaxies: Seyfert - infrared: sources

1. INTRODUCTION

Prior to the launch of the Infrared Astronomical Satellite (IRAS), relatively few galaxies were known to be extremely luminous at infrared wavelengths, $\lambda \gtrsim 10 \mu m$. Among them were the optically selected Seyfert 1 galaxies Mrk 231 and I Zw 1 (Rieke & Low 1972), and some optically identified merger galaxies like NGC 3690/IC 694 (Gherz, Sramek, & Weedman 1983). Since then, however, the IRAS survey has revealed that an important fraction of extragalactic objects emit the bulk of their radiation at far-infrared wavelengths (Houck et al. 1984; Soifer et al. 1984). In fact, above $\log(L/L_\odot) \approx 11.5$, this class of galaxies becomes the dominant extragalactic population in the local universe, exceeding even the space densities of optically selected quasars at comparable bolometric luminosity (Soifer et al. 1989; Sanders et al. 1991). Combined with the well-known relationship between galaxy interaction and high infrared luminosity (e.g., Lawrence et al. 1989; Leech et al. 1991), this discovery suggests that luminous infrared galaxies (LIGs) may provide important clues to the process of galaxy formation and the origin of nuclear activity in galaxies.

Perhaps the most important question regarding LIGs is the nature of their energy source. The debate often centers on what powers the most luminous infrared galaxies ($L \gtrsim 10^{11} L_\odot$) since the far-infrared flux in most of the weaker sources probably comes from dust heated by the old stellar population or as a consequence of star formation (e. g., Allen et al. 1985; Elston, Cornell, & Lebofsky 1985; Lawrence et al. 1986; Leech et al. 1988; Thronson et al. 1 990). Scenarios involving intense star formation (Norman & Scoville 1988; Rieke 1988; Condon et al. 1991; Radford et al. 1991), dust-enshrouded active galactic nuclei (AGN; Rieke & Low 1972; Norris et al. 1985; DePoy, Becklin, & Wynn-Williams 1986; Becklin 1986; Sanders et al. 1988a), and galaxy-galaxy collisions (Harwitt et al. 1987) have been suggested to explain the large luminosity of the brighter sources. There are several examples of known nuclear starbursts surrounding an active nucleus (e.g. Mrk 231 - Boksenberg et al. 1977; NGC 7469 -- Cutri et al. 1984), and given that all luminous infrared galaxies appear to be rich in star-forming molecular gas (Sanders, Scoville, & Soifer 1991), the main issue should be to determine which process is the *dominant* source of luminosity in LIGs.

Optical studies generally address this question by attempting to determine the main source of ionization of the line-emitting gas in LIGs and the role of galaxy interaction in triggering the large infrared luminosities of these objects (cf. review of Heckman 1991). The distinction between the source of the infrared radiation in these galaxies and the source-of ionization of their line-emitting gas is important to emphasize here as the former is believed to be deeply embedded in the core of these objects and is therefore invisible at optical wavelengths [and possibly optically thick at wavelengths up to 25 μm (Condon et al. 1991)]. Optical studies infer the nature of the energy source by assuming that the physical characteristics of the circumnuclear gas and underlying stellar population are good probes of the central energy source. This is also the approach that we will

follow in the present study. The weaknesses of this assumption will be reviewed in the discussion of our results,.

A major limitation of previous optical studies of LIGs has been the small size of their samples or the limited number of line and continuum diagnostics used in their analysis. In an attempt to remedy this situation wc have carried out a spectroscopic survey of a large sample of lRAS galaxies. Long-slit Palomar 5-meter spectra covering at least 3750 - 8000 Å (sometimes up to $\sim 1\ \mu m$) at a resolution of 8--10 Å and MKO 2.2m spectra Covering 5850 – 8870 Å were obtained of 201 IRAS galaxies, including 115 objects from the IRAS Combined Bright Galaxy Surveys (CBGS) (Soifer et al. 1989: Sanders et al. 1994a,b - hereafter refered to the CBGSs objects, scc Paper I) and 86 objects from the IRAS Warm Galaxy Surveys (WGS) selected on the basis of their "warm" infrared (60 tnn/100~m~) colors (hearafter refered to as the WGSS objects, see Paper I). A constant linear aperture of 2 kpc was used to extract the nuclear spectra from these data and therefore minimize aperture-rclatccl effects. An atlas of the nuclear spectra x-as presented in Kim ct al. (1994; hereafter Paper 1) along with tabulations of some of the results derived from these nuclear data. The present paper reports the results of our analysis of these nuclear data (§2) and also provides new information about the spatial variations of the various spectral parameters in" twenty-thr-ec objects of the sample (§3). In §4, we discuss the implications of this analysis, addressing the nature of the energy sources in luminous infrared galaxies and describing possible scenarios to explain the data. Finally, the main conclusions arc summarized in §5.

2. Results from the Nuclear Data

2.1. *Dust*

We start this section with a cautionary note. Far-infrared and radio surveys have shown the existence of large quantities of dust and molecular gas in LIGs, generally concentrated into compact regions of diameter less than 1 kpc (e.g., Scoville et al. 1986. 1989. 199]; Solomon et al. 1990; Radford ct al. 1991). As described in detail in Paper I. the "nuclear" data of our survey were derived using a fixed extraction window of 2 kpc. The size of this window implies that these data probably cover regions spanning a large range in optical depths. The extinction measurements derived from the nuclear dat a will therefore be lower limits to the true extinction as the observed line and continuum emission will come predominantly from regions of smaller optical depths (cf. discussion of I.etch et al. 1989).

The primary dust indicator used in the. present investigation is the emission-line Balmer decrement *corrected for the underlying stellar absorption features. The* observed intensity ratios of the two strongest Balmer lines, Hα and Hβ, were compared to the calculated values. Invariably, they were found to be steeper than the calculated values, with the difference being attributed to interstellar extinction. Stellar absorption features

underlying the emission lines of Hα and Hβ were taken into account in the measurement procedure (cf. Paper I, §4.2). No attempt was made to include the lower Balmer lines in the analysis because of their intrinsic weakness and because they are more strongly affect ed by the underlying stellar absorption lines. The Whitford reddening cur ve as parameterized by Miller & Mathews (1972) was used. All of the galaxies in our sample were classified as H II, LINER, or Seyfert 2 galaxies based on their emission-line spectrum. The method used for the classification will be discussed in detail in the nest section. Wc adopted an intrinsic Hα/Hβ ratio of 2.85 for H 11 galaxies (case B Balmer recombination decrement for $T = 10^4$ K and $N_e = 10^4$ cnl^{-}3, and 3.10 for AGN (Ferland & Netzer 1983; Péquignot 1984; Binette, Dopita, & Tuohy 1985; Gaskell & Ferland 1984).

The amounts of reddening derived from this method are listed as color excesses, E(B- V), in column (3) of Table 1. Note that these numbers include extinction due to the Galaxy. The distributions of E(B- V) for galaxies in the CBGSs and WGSs are shown in Figure 1. The median E(B–V) for objects in the CBGSs and WGSs are 1.1.3 and 0.91, respectively. A Kolmogorov-Smirnov (K-S) test shows that the probability that these two data sets are drawn from the same distribution is 0.01.

The amount of reddening found in LIGs can be compared with typical values measured in active galaxies. Dahari & De Robertis (1988) found median E(B–V) values of 0.37, 0.56 and 0.69 for Seyfert 1, Seyfert 2, and starburst galaxies, respectively. Similarly, typical reddening in nuclear H 11 regions is E(B- V) = 0.52 and even smaller in disk H II regions: E(B–V) = 0.36 (Kennicutt, Keel, & Blaha 1989). All of these values arc considerably smaller than the color cxccssc measured in LIGs and confirm the importance of dust in the infrared-selected objects. Figure 2 presents the distribution of E(B-V) for the various types of galaxies in the sample (cf. $2.2 for more detail). There may be a tendency for the optical spectra of Seyfert-2 LIGs [E(B- V) = 0.72] to be less reddened than H II LIGs [E(B–V) = 0.99], which may themselves be less reddened than the LINERs [E(B–V) = 1.14]. K-S tests indicate that the probability that the color excesses of Seyfert 2 galaxies and LINERs arc drawn from the sarnc distribution is only 0.009. It is 0.09 when the color excesses of Seyfert 2 galaxies arc compared with those of H II galaxies, and 0.1 when wc compare the color excesses of the LINERs and H I I objects.

No significant correlation was found between E(B- V) and the infrared luminosity for any class of objects. Mirabel & Sanders (1988) derived the H I column densities in the nuclei of 18. LIGs by measuring the strength of the H I 21 cm line seen in absorption against the nuclear radio source. The clnission-line Balmer decrement in twelve of these galaxies was measured in the present study: we find a tendency for the objects with large N(II 1) to have large cmissic~x~-line decrements.

Figure 3 shows that, contrary to elliptical galaxies, the Na ID and Mg Ib equivalent widths are not correlated. This result strongly suggests that most of the Na ID

absorption feature in LIGs is of interstellar origin, in contrast to the Mg Ib feature. The correlation between the reddening and the strength of the Na ID feature (Fig. 4) confirms the interstellar origin of the Na ID feature. Qualitatively similar results were found in the smaller sample of Armus, Heckman, & Miley (1989, hereafter .4 HM89). Figures 4 indicates, however, that the correlation between E(B-V) and EW(Na ID) is considerably weaker among the LINERs and Seyfert-2 objects than among the H II galaxies (the probability, P[null], that this correlation is fortuitous is 5 x 10^-10, 0.0002. and 0.01 for the H 11 galaxies, Seyfert galaxies, and J, INERs, respectively). A similar effect is observed when EW(Na ID) is replaced by the color of the continuum determined by the ratio of the continuum levels at 6563 Å and 4861 Å (C6563/C4861, Fig. 5): we obtain P[null] = 2 x 10^{-15}, 0.0003, and 0.8 for the H II galaxies, LINERs, and Seyfert 2 galaxies, respectively. This suggests that the scatter in the continuum colors of AGN is predominantly intrinsic, while in H 11 galaxies a large fraction of the scatter is due to variations in the amount of reddening from one object to the other. Indeed, if the continuum colors are assumed to be reddened by the same amount as the emission-line gas. we find that the distribution of the *de*reddened continuum colors in H 11 galaxies and in LINERs is 30 - .50 % narrower than before reddening corrections while the scatter in the continuum colors of Seyfert galaxies basically remains the same (cf §2.8).

2.2. Spectral Classification

Nearly all of the galaxies in our sample present a spectrum with emission lines. The characteristics of these lines are important indicators of the conditions of the thermal gas in these objects. The emission lines can be used to determine the density structure of the gas, its temperature, kinematics, and source of ionization. All of these properties will be discussed in the present and next three sections. Here, the issue of the main source of ionization of the line-emitting gas in LIGs is addressed using diagnostic line ratios.

The broad spectral coverage of our data allowed us to use many of the diagnostic tools known to be efficient at differentiating between the various ionization mechanisms. All of the line ratios used by Baldwin, Phillips, & Terlevich (1981, hereafter BPT) and Veilleux & Osterbrock (1987, V087) were included in our analysis. These are [O III] λ5007/Hβ, [O II] λ3727/[O III] λ5007, [N 11] λ6583/Hα, [S 11] $\lambda\lambda$6716,6731/Hα, and [O I] λ6300/Hα. *Note that the line ratios involving a Balmer line use the* intensity *corrected for the underlying stellar absorption* (cf. Paper 1). Heckman (1980, H80) *defined* the class of LINERs ("low-ionization nuclear emission-line regions") as having [O II] λ3727/[O III] λ5007 $>$ 1 and [O I] λ6300/[O III] λ5007 $\geq$ 1/3. This last line ratio was therefore also included in our analysis. More recently, the use of line ratios involving emission lines at longer wavelengths has been explored and found to help in determining the dominant ionization process in optically selected emission-line galaxies (Diaz, Pagel, & Terlevich 1985a,b; Morris & Ward 1988; Kirhakos & Phillips 1989; Osterbrock, Shaw,

& Veilleux 1990; Osterbrock, Tran, & Veilleux 1992 [hereafter OTV]). When possible, the values of [O II] $\lambda\lambda$7320,7330/Hα and [S III] $\lambda\lambda$9069,9531/Hα were thus measured and compared with the diagrams in OTV. All of the line ratios used in the present analysis have been corrected for reddening using the values of E(B–V) determined from the Hα/Hβ ratio and the Whitford reddening curve as parameterized by Miller & Matthews (1972: cf. previous section).

The results of our analysis are summarized in Tables 1 and 2. Figures 6 and 7 show the locations of the LIGs *without obvious companions in* the various diagnostic diagrams. Our discussion of the objects with double nuclei is postponed until §2.10, where the role of galaxy interaction in LIGs is assessed. All of the measurements in these tables and figures represent the *nuclear* values obtained by extracting the flux from the central 2 kpc. To avoid aperture-related effects, the more distant LIGs ($cz > 20000$ km s^{-1}; extraction window of 4 kpc) were not plotted in these diagrams. The spatial variations of the properties of the line-emitting gas in LIGs will be discussed in §3. Table 1 lists the various lines ratios used in the classification scheme of H80, BPT, and VO87. The uncertainty in these data is typically 10% and 25% for the entries with a colon (:). Columns 11, 12, and 13 list each of the spectral types determined from the location of the data points in the diagrams of [O III] λ5007/Hβ versus [N II] λ6583/Hα, [S II] $\lambda\lambda$6716,6731/Hα, and [O I] λ6300/Hα, respectively. We used the boundaries of VO87 to classify each object as H II galaxies or AGN. These boundaries were determined from an optically-selected sample of galaxies and based on the published results of photoionization models. A distinction was made among AGN between the objects of high ([O III] λ5007/H$\beta \geq 3$) and low ([O III] λ5007/H$\beta \leq 3$) excitation. The first group simply represents the "classic" Seyfert 2 galaxies while galaxies in the second group were called LINERs although a few of them do not satisfy the original LINER criteria of H80. We adopted this definition of LINERs because measurements of [O II] λ3727 were often not available. Finally, column 14 of Table 1 gives the adopted spectral type based on the previous four columns. A colon (:) next to the adopted spectral type indicates that the classification is ambiguous in the sense that the line ratios in these objects do not correspond to the same spectral type in all three diagrams of VO87. While differentiating between H II galaxies and AGN, more weight was given to the diagram of [O III] λ5007/Hβ versus [O I] λ6300/Hα than the other two diagrams of VO87 because the separation between the two classes of objects is more distinct in the diagram involving the [O I] line (cf. VO87). Table 2 lists the 11 objects for which [O II] λ7325 or [S III] $\lambda\lambda$9069, 9531 could be measured. Columns 8, 9, and 10 give the spectral types of each object based on their positions in the diagrams of OTV. Note that the classification based on these redder lines is more uncertain than the spectral types determined in Table 1 because it is based on fewer objects (cf. OTV). Nevertheless, we find that these two methods of classification give consistent results (column 11).

A summary of the results from the spectral classification is given in Table 3 and

in graphical form in Figure 8. The classification scheme was found to be relatively unambiguous: more than 90% of the galaxies in the sample have line ratios corresponding to the same spectral type in all three diagrams of VO87. Out of the 201 LIGs in the sample. 32 of them clearly are systems made up of two distinct nuclei. For these systems. we adopted in Table 3 the more Seyfert-like spectral type of the two nuclei: galaxy pairs with spectral types H 11- LINER, H II - Seyfert 2, H II - Seyfert 1, LINER - Seyfert 2, LINER - Seyfert 1, and Seyfert 1- Seyfert 2 were classified as LINER. Seyfert 2. Seyfert 1, Seyfert 2, Seyfert 1, and Seyfert 1, respectively. These interacting systems arc more common below $\log(L_{ir}/L_{\odot}) = 12$ (\$2. 10). Consequently, this classification method of the double-nucleus systems is conservative in the sense that it overestimates the fraction of AGN among tile lower luminosity objects and thus cannot explain the trends with infrared luminosity discussed below.

We found that 53% of the objects in the sample (106 galaxies) have spect ra characteristic of photoionization by hot stars (H 11 galaxies). AGN emission lines were observed in 76 nuclei (38% of the total sample) including 4 Seyfert 1 galaxies (2%. Mrk 231, IR0759+65, IR1334+24, and NGC 7469), 24 Seyfert 2 galaxies (12%), and 48 LINERs (24%). Finally, the spectral types of 19 galaxies could not be determined due to a lack of diagnostic emission lines.

Table 3 also shows the dependence of the LIG population on the infrared luminosity. *Perhaps the single most important result listed in Table 3 and shown in Figure* 8 is *the clear tendency for the more luminous objects to have A GN line ratios and for these objects to be more Seyfert-like.* In fact, three of the four Seyfert 1 galaxies in our sample have $\log(L_{ir}/L_{\odot}) > 12$. This trend was first observed in the relatively small sample of Sanders et al. (1988a). All of the objects in their sample were re-analysed using our more accurate treatment of the underlying Balmer absorption lines (cf. Paper I). Our measured [0 III] $\lambda 5007/H\beta$ ratios were found to be consistently smaller than the published values of Sanders et al. (1988). The difference is entirely attributable to underestimates of the equivalent widths of the Balmer absorption lines by Sanders et al. Indeed, errors in the estimates of the equivalent widths of the Balmer absorption lines have a larger effects at $H\beta$ than at $H\alpha$ because the Balmer decrement is steeper in emission than in absorption. Underestimates of the equivalent width of the Balmer absorption lines therefore produce a nearly vertical shift of the data points towards high [0 III]/$H\beta$ in all three diagrams of VO87. *We* believe *that the inaccurate treatment of the underlying stellar continuum in most of the earlier spectroscopic studies of LIGs has resulted in significant uncertainties in the vertical positions of the data points in the diagnostic diagrams.* Fortunately, such shifts do not generally affect the spectral classification of the objects as the boundary between H II galaxies and narrow-line AGN is nearly vertical. However, it does change the proportion of Seyfert 2s to LINERs among AGN. We find that the fraction of AGN in our sample which are genuine Seyfert galaxies is only about 54% even when $\log(L_{ir}) > 12$. These results arc consistent with the study of Allen et al.

(1991). but seem to disagree with the results of Leech et al. (1989) who found no dependence on infrared luminosity in their more distant sample. The origin of this apparent. discrepancy will be addressed in §3.2 where the spatial variations of the line ratios are discussed.

Finally, Table 3 shows that I, INERs contribute 20-- 25% of the LIG population. regardless of the infrared luminosity. The ionization process in LINERs has been the subject of considerable debate in the past decade (cf. Filippenko 1989 for a review). Our discussion of the processes relevant to the LINER LIGs is postponed until §4.1.1. once all of the quantities derived from the line and continuum emission of these objects have been presented.

.4 quick inspection of Figure 6 indicates that the upper-left region of these diagrams is devoid of any data points, reflecting the fact that essential all of the objects classified as H 11 galaxies have relatively low ionization level ([0 III]λ5007/Hβ < 3). This is to be contrasted with Figures 1 --3 of V087 where this region of the diagrams is populated with extranuclear H 11 regions and the low-luminosity H II galaxies from the sample of French (1980). Photoionization by hot (T_* 240000 K) stars with high ionization parameter and/or located in an oxygen-depleted environment [(0/H) = 0.1-0.75 $(O/H)_\odot$] can account for the high ionization level of these objects (Evans & Dopita 1985; McCall, Rybski, & Shields 1985; French 1980). This general lack of high-ionization H II galaxies among LIGs was also found in the samples of Leech et al. (1989), AHM89, Allen et al. (1991), and Ashby et al. (1992). Allen et al. have argued that the dozen of objects populating the high-[O III]/Hβ and 1ow-[N II]/Hα region of their diagram represent galaxies with a very recent burst of star formation ("extreme starburst galaxies" or ESB). These objects have emission-line and continumm properties which arc very similar to the galaxies studied by French (1980). No object in our sample is located in the ESB region defined by Allen et al. or have detectable WR features (e. g., combinations of He 11 λ4686, He I λ5876, C III λ5696, N IV λ5737, N 111 $\lambda\lambda$4634, 4640, and 4642).

2.3. Luminosities and Equivalent Widths of Hα

The values of the Hα luminosities of our sample of galaxies are listed in Table 4. These luminosities were derived from the nuclear spectra (cf. Paper I). Only data taken under photometric conditions were included in the final analysis. No correction was applied for Galactic and intrinsic dust. Figures 9 and 10 show the distributions of *observed* $L_{H\alpha}$ and EW(Hα) as a function of spectral types. LINER LIGs appear to be deficient in Hα emission relative to both Seyfert LIGs and H 11 LIGs: the median of the Hα luminosities (equivalent widths) for Seyfert LIGs, LINER LIGs and H II LIGs are 7.S x 10^{41} erg s-" · (63 Å), 3.5 x 10^{41} erg s^{-1} (29 Å), and 9.5 x 10^{41} crg S-l (55 l), respectively. The slight luminosity deficit in LINERs may be partially attributed to the larger amount of reddening found in these galaxies ($2.1). However, this scenario dots not explain the large differences in the equivalent widths unless one assumes that the

stellar continuum in LINERs is less reddened than the line emission. (This possibility could perhaps explain the fact that only a weak correlation was found in §2.1 between the continuum colors of LINER LIGs and E(B- V) determined from their emission-line Balmer decrement.)

The Hα luminosities of the H II LIGs of our sample are considerably larger than those found by Kennicutt, Keel, & Blaha (1989) in their sample of nuclear H II regions and bright disk H 11 regions ($L_{H\alpha} \simeq 3 \times 10^{39}$ erg s^{-1} for the objects with $\log[NII]/H\alpha \leq -0.15$), and they are somewhat brighter than the starburst galaxies of Balzano (1983; $L_{H\alpha} \simeq 5 \times 10^{40}$ erg s^{-1}). Reddening corrections would only amplify this discrepancy. On the other hand, the infrared-selected Seyfert 2 galaxies have observed Hα luminosities which are comparable to those of optically selected Seyfert 2 galaxies ($L_{H\alpha} \simeq 1 \times 10^{42}$ erg s^{-1} for an average color excess of 0.54; Dahari & De Robertis 19ss).

A strong (P[null] = 10–9) correlation between reddening-corrected Hα luminosities and infrared luminosities is observed among the H 11 LIGs but is much weaker in AGN LIGs (P[null] ≃ 0.01; Fig. 11). The H II LIGs in our sample have $L_{ir}/L_{H\alpha} \simeq 300 \cdot 3000$, significantly larger than the ratios typically observed in the disks of bright spiral galaxies (Persson & Helou 1987). A similar result was found by Leech et al. (1989). This 'deficit" of Hα emission may be due to an underestimate of the dust extinction or to fundamental differences in the production mechanisms of the Hα and infrared emission in these two types of objects. Leech et al. pointed out that slit losses may account for the large ratios in the nearby objects. We also observe in our sample of objects a weak tendency for $L_{ir}/L_{H\alpha}$ to increase with infrared luminosity.

As found by AHM89, the median log EW(Hα) of our H 11 LIGs (∼ 1.7) is closer to the values of the nuclear H II regions (∼ 1.5; Kennicutt, Keel, & Blaha 1989) than the values of disk H 11 regions (∼ 2.7; Kennicutt, Keel, & Blaha 1989). This low value of EW(Hα) in the H II galaxies of our sample can be explained if the time since the burst of star formation in these objects is of order ∼ 107 yr (using Fig. 1 of DeGioia-Eastwood 19S5 and the continuum colors of Jacoby, Hunter, & Christian 1980) or if an underlying old preexisting population is also contributing to the continuum light. This question will be addressed in more detail in §2.7 and $2.8 where the absorption features and the color of the continuum in these objects are discussed.

2.4. Densities

An estimate of the density of the line-emitting gas in luminous infrared galaxies may be derived from reddening-corrected line ratios. The density-sensitive lines [O II] λλ3726, 3729 could not be resolved in these galaxies because of their large intrinsic velocity widths and the 8 – 10 Å spectral resolution of the observations. The density was instead derived using the [S 11] λ6731/λ6716 line ratio and the five-level-atom calcula-

tions of De Robertis, Dufour, & Hunt (1987). Columns (9) and (10) of Table 1 list the values of this ratio and their corresponding densities for all of the galaxies in the sample. The flux of the individual [S II] lines was determined by fitting simultaneously two Gaussian profiles to the blend (cf. Paper I). Figure 12 shows the distribution of the density values for all of the LIGs of our sample as a function of their spectral type. The mean, median, and standard deviation around the mean of the density in the CBGSs LIGs arc 320, 250, and 260 cm^{-3}, respectively. The average density in Seyfert 2 galaxies (430 cm^{-3}) is somewhat larger than in H II galaxies (280 cm-3), while LINERs have intermediate values (350 cm--3). The average [S II] density in the AGN LIGs is considerably smaller than the average [S II] density found by Koski (1 978) in his sample of 30 Seyfert 2 and narrow-line radio galaxies ($n_e \simeq 2000$ cm^{-3}) but is comparable to the value found by Keel (1983) in his sample of LINERs ($n_e \simeq 450$ cm^{-3}). It is important to point out that the low ionization potential and critical density of these two [S II] lines (cf Osterbrock 1989) implies that the densities derived from this line ratio arc typical of regions of low ionization ancl density. In Seyfert galaxies and LINERs, densities derived from lines of higher ionization potential and critical density are often larger than the [S 11] density duc to stratification effects (e.g., De Robertis & Osterbrock 1986 and references therein). A possible explanation to the apparent difference between the [S 11] densities of AGN LIGs and optically selected AGN is that the extinction due to dust is more important in LIGs than in optically -selected AGN, preventing us to probe the inner, denser [S 11] line-emitting zone in the LIGs. A discussion of the density variations as a function of distance from the nucleus is postponed until §3.3.

2.5. Electron Temperatures

The electron temperature is a good discriminant to determine the source of ionization of the line-emitting gas. The two optical line ratios most often used in temperature measurements involve [O 111] $\lambda\lambda$4363, 5007 and [N II] $\lambda\lambda$5755, 6583. Unfortunately, this last line ratio could not be used in our analysis because of the extreme faintness of [N 11] λ5755 in all of the objects in the sample. Similarly, [0 III] λ4363 is generally quite faint and is blended with Hγ and complex absorption features. Overall. the [0 111] λ5007/λ4363 temperature could bc determined (estimated) in three (eight) H II galaxies. eight (ten) Seyfert '2 galaxies, but, unfortunately, in none of the LINERs. Table 5 lists the values of this ratio along with the electron temperatures derived using the five-level-at.om calculations of De Robertis, Dufour, & Hunt (1987) and densities of 10^3 cm^{-3} and 10^6 cm^{-3}. Typical [0 III] temperatures predicted from low-density models for photoionization by hot stars, an active nucleus, and collisional ionization by shocks arc *4000-14000* K, *9000-18000 K,* and *25000-30000* K, respectively. (McCall, Rybski, & Shields 1985; Ferland & Netzer 1983; Binette, Dopita, & Tuohy 1985). The temperatures listed in Table 5 arc all consistent with photoionization either by stars (for the LIGs classified as H II galaxies) or by an active nucleus (for the Seyfert 2 LIGs).

2.6. Line Widths

The rather low spectral resolution of our data prevents us from carrying out a detailed analysis of the emission-line profiles. Results from high-resolution studies of emission-line galaxies have shown that the effects of finite instrumental resolution on the measured line widths and line asymmetries can be quite dramatic (e.g., Whittle 1985a; Veilleux 1991 b). Discrepancies between measurements derived from low and high resolution data come from the uncertainties associated with using the quadrature method to correct the observed widths for the finite instrument resolution. This method assumes that the intrinsic and instrument profiles are Gaussian and gives corrected widths that are systematically too high for profiles which are more pesky than Gaussians (e.g., the emission-line profiles in AGN; Whittle 1985a; Veilleux 1991 b). For this reason. line asymmetries will not be considered in the present discussion and the conclusions derived from our analysis of the line widths will be treated with caution.

The [0 III] λ5007 line was selected for line width measurements because it is strong in most LIGs and free of any nearby emission lines or absorption features (in contrast to Hα). A large spread in line widths was found in the objects of the sample. As shown in Figure 13, there is a tendency for objects with large line widths to be luminous in the infrared domain. Figure 14 shows that the median line width of AGN LIGs is larger than the median line width of H 11 LIGs (320 km s^{-1} versus 250 km S–l), but with considerable overlap in the various line width distributions. A K-S test on the line widths of AGN and H 11 galaxies shows that the probability that these two data sets are drawn from the same distribution is 0.09 (it is 0.07 when only the LINERs are compared with the H 11 galaxies). A similar result was found in the smaller sample of AHM89. Line widths larger than 600 km s^{-1} are observed in nearly 20% of the objects in our sample. These objects deserve more attention and should be observed at higher spectral resolution. These objects will be discussed in considerable detail in §3.5 and 54.2?.

Comparisons with the [0 111] line widths of other emission-line galaxies taken from the recent literature (Whittle 1992a,b; Veilleux 1991a) indicate that the line widths of AGN LIGs are comparable to those of optically -selected AGN. H II LIGs have line profile: with widths similar to those of the starburst galaxies of Balzano (1983) and Feldman et al. (1982) but larger than those of H II galaxies (i.e. late-type galaxies with act ive star-forming regions; e.g., Gallagher & Hunter 1983; French 1980).

2.7. Stellar Absorption Features

A large number of stellar absorption features arc present in the spectra of our objects. Among the strongests of thcm arc the Balmer lines, Mg Ib $\lambda\lambda$5176, 5200 -! MgH. Na ID λ5892, Ca II H+K (only visible in the galaxies with higher redshift). the G band due to CN and CH near 4250 Å, TiO bands at 6180, 7100, and 7700 Å, and the Ca II triplet at $\lambda\lambda$8498, 8542, 8662 Å (observed in our few long-wavelength spec-

tra). The Na ID feature was found in §2.1 to be mostly of interstellar origin; it will not be discussed any further in the present section, All of the other lines can be used to derive the properties of the dominant underlying stellar population in these objects. The equivalent widths of Hβ and Mg Ib of the objects in our sample were listed in Table 3 of Paper I (cf. \$3.2 of that paper for a description of the technique used to measure these features and estimate the uncertainties in these measurements). No attempts were made to measure the strength of Ca II H+K and the G band because they were often blended with Hϵ and [Ne 111] λ3967 and with [S II] λ4069, 4076, Hδ, Hγ, and (O 111] λ4363. respectively.

Balmer absorption in the spectra of LIGs is the signature of an intermediate-age (10^8 - 10^9 yr) population of stars. The average Hβ equivalent widths of LIGs (1.85 Å. including all of the objects without apparent Hβ in absorption) was found to be similar to the values observed in non-active spiral galaxies (- 1.44 Å; Keel 1983). The data show a slight tendency for the ultraluminous infrared galaxies [log $(L_{ir}/L_{\odot})>12$] to have weaker Hβ absorption feature than the other LIGs. However, this result is based on only twenty-one objects so it is uncertain. LIGs with LINER spectra appear to have stronger Hβ features on average than H II and Seyfert 2 LIGs: the medians of EW($H\beta_{abs}$) for H II galaxies, Seyfert 2 galaxies, and LINERs are 1.25, 1.63, and 2.30 Å, respectively. K-S tests show, however, that these differences are marginal. A qualitatively similar difference is seen among optically-selected LINERs and Seyfert 2 galaxies (e.g., Filippenko & Sargent 1986).

The strength of Mg Ib is a good indicator of the presence of an old ($\gtrsim 10^9$ yr) stellar population (Bica, Alloin, & Schmidt 1990; and references therein). The median equivalent width of detected Mg Ib ~5176 features in our sample of galaxies is $\sim$ 1.3 Å, with the AGN (especially the LINER LIGs) having a stronger Mg Ib feature than the H II objects ($\sim$ 1.5 Å versus $\sim$ 1.1 Å, Fig. 15; cf. also AHM89). K-S tests indicate that the probability that the EW(Mg Ib) of LINERs and H II galaxies are drawn from the same distribution is only 0.003. It is 0.7 and 0.4 when the values of the Seyfert LIGs are compared with those of H 11 galaxies and LINERs, respectively. This result may imply that the stellar population in H II LIGs is younger than in the LINER nuclei. Note, however, that all of these equivalent widths are considerably smaller than the equivalent widths observed in non-active spiral galaxies (EW[Mg Ib] = 3.5- 6.0 Å; Keel 1983a; Stauffer 1982; Heckman, Balick, & Crane 1980; AHM89). Dilution of the old-star continuum by a power-law continuum produced by an AGN or the featureless continuum of hot. young stars could explain this result. In the case of a young starburst ($\sim 10^7$ yr), the small EW(Mg Ib) can also be produced by red supergiants in the starburst itself without the need for an old preexisting stellar population (cf. Bica et al. 1990).

The equivalent width of the Ca II absorption triplet at $\lambda\lambda$8498, 8542, 8662 Å was also measured when possible. This feature is the strongest feature in the deep-red spectrum of late-type stars and normal galaxies. Of the fourteen objects with spectral

coverage extending up to these wavelengths, the equivalent widths of both Ca II λ8542 and λ8662 could only be measured reliably in three objects. In the other objects. one of these lines was either not strong enough to be measured or the observed central wavelength of the apparent λ8542 feature was shifted by more than 20 Å to the blue and therefore corresponded instead to Fe I A8515. These three galaxies arc 1215-s06 (, H 11). 1344+14 (H II), and 1344+11 (Seyfert 2/H II). The EW(Ca 118542, 8662) of these objects were found to be 6.44, 6.15, and 4.37 Å, respectively. These values arc comparable to the results of Terlevich, Diaz, & Terlevich (1990) who obtained Ca II equivalent widths corrected for broadening of $\sim$ 7 Å in normal *and* Seyfert galaxies. The broadening correction of Terlevich et al. is always less than 1 Å and can therefore be neglected for our purposes. This result is quite remarkable considering the fact that EW(Mg Ib) for these three objects is 0.99, 0.61, and 0.97 Å, respectively, i.e. considerably smaller than the values typically found in normal spiral galaxies. The equivalent widths of Mg Ib in these three objects is clearly too small relative to the equivalent widths of the Ca 11 triplet to be explained by dilution effects caused by the presence of any reasonable featureless continuum of the form produced by active nuclei (e.g., $F_\nu \sim \nu^{-1.5}$) or hot stars (e.g., Bica, Alloin, & Schmidt 1990). Terlevich et al. (1990) found a similar result in their sample of optically selected objects. They explained their results by invoking the presence of a cluster of relatively young ($\sim$ 107 yr) red supergiants which dominates the deep-red continuum light of these objects and produce large EW(Ca 11) but small EW(Mg Ib). A similar effect can be taking place in at least the two H II galaxies 1215+06 and 1344+14.

Ca 11 triplet data on a larger number of LIGs will be needed before drawing any statistically significant conclusions about the presence of a large population of red supergiants in LIGs. Our analysis of the spatial variations of these stellar features will provide further constraints on the stellar population of these objects (cf. §3.6).

2.9. *Continuum Colors*

In §2.1, wc noted that the observed continuum colors, C6563/C4861, corl-elate with the reddening determined from the emission-line Balmer decrement (Fig. 5). Although this result dots not strictly imply that the line-emitting gas and stellar continuum are reddened by exactly the same amount, wc will use the amount of dust derived from the emission-line spectrum to deredden the continuum colors of our objects. An histogram showing the dereddened continuum colors as a function of spectral types is presented in Figure 16. *There are no significant continuum color differences between H II LIGs and A GN LIGs* OT *between LINER LIGs and infraTed-selected Seyfert 2s (all classes have* $[C6563/C4861]_0 \approx 0.4$). Assuming that most of the optical continuum is produced by the underlying stellar population and using the continuum colors of the stellar cluster models of Jacoby, Hunter, & Christian (1980), wc find that most of the objects in our sample have colors characteristic of a stellar population less than 10^9 yr old

([C6563/C l]$_0 \lesssim 0.54$). AHM89 arrived at a similar results from their smaller sample.

Leech et al. (1989) found that luminous galaxies generally have cent inuum colors (uncorrected for extinction) which are bluer than objects of lower infrared luminosity. They observed a similar effect when considering the equivalent width of the Ho emission line instead of the infrared luminosity. These correlations cannot be directly verified in our sample because the flux level at 3800 Å used in their analysis was not measured in the present study. However, there is a weak tendency for [C6563/C4861]$_0$ among the CBGSs objects to decrease with increasing infrared luminosity (P[null] = 0.01. Fig. 17b). This effect is not present when the *observed* continuum colors are considered (P[null] = 0.57). Objects in our sample with large Hα equivalent widths also have small C6563/C4861 (but not [C6563/C4861]$_0$; Fig. 18).

Contrary to what is observed in normal galaxies (e.g., Heckman, Balick, & Crane 1980), no correlation was found between the reddening-corrected continuum colors of LIGs and their Mg Ib equivalent widths (Fig. 19). This result remains the same when H 11 LIGs or AGN LIGs arc considered independently. This lack of correlation can be understood if a star-burst or an AGN is affecting (C6563/C4861)$_0$ and/or EW(Mg Ib). The unusually small Mg Ib equivalent widths in LIGs (cf. §2.7) is consistent with this idea. In the case of H II galaxies, the starburst contribution can be estimated using the models of Bica, Alloin, & Schmidt (1990). The median values of (C6563/C4861)$_0$ and EW(Mg Ib) measured for this class of objects are 0.39 and 1.11 Å, respectively. The combination of such small Mg Ib equivalent width and blue continuum matches their model in which the burst-to-galaxy mass ratio is $\sim$ 10% and the burst age is less than $\sim 10^7$ yr. .4s discussed in §2.7 and in Bica et al. (1990), such young starburst reproduces the weak Mg Ib feature and the continuum colors without the need for an underlying old preexisting population.

2.9. *Radio Fluxes*

A strong correlation is known to exist between radio continuum fluxes and mid-to-far infrared fluxes in the nuclei and disks of normal late-type galaxies as well as in the nuclei of starburst galaxies (e. g., van der Kruit 1973; Helou, Soifer, & Rowan-Robinson 1 985; Condon & Broderick 1986; Condon & Broderick 1988; Wunderlich, Klein, & Wielebinski 19S7; Condon, Anderson, & Helou 1991). The existence of this correlation suggests that the radio and infrared continua have a common origin in these objects. The infrared emission is probably produced by warm dust heated by ultraviolet radiation from massive .($M \gtrsim 8\ M_\odot$) stars. The radio emission, on the other-hand, is primarily non-thermal, synchrotrons radiation associated with supernova explosions (and their remnants) from the same population of massive stars, plus a smaller contribution of thermal emission from the H 11 regions produced by these stars (Condon & Yin 1990). Thronson et al. (1990) and Condon, Anderson, & Helou (1991) suggested that lower-mass stars may also contribute to the heating of the dust in these objects (the '-infrared

cirrus-' component).

The radio-infrared correlation is found to be considerably weaker in optically selected Seyfert galaxies than in starburst galaxies (Condon et al. 1982; Condon & Broderick 1988). Quantitatively, if q is defined as the logarithmic FIR-radio flux-density ratio (cf. Condon et al. 1991), we have <q> = 2.34 for star-burst galaxies with very little scatter around the mean while radio-selected active galaxies have q < 2, suggesting an additional source of radio emission in these objects. The values of q for the objects in our sample were calculated using the IRAS fluxes and the 1.49 Ghz fluxes of Condon et al. (1990, 1991). The results of this analysis arc presented in Figure 20. Alt bough the scatter is considerable, Seyfert 2 galaxies have somewhat smaller values of q than H II galaxies and LINERs (2.17 versus 2.37 and 2.42, respectively). However, only four Seyfert 2 galaxies have q < 2: NGC 1068, NGC 1143/44, NGC 5256 NE, and NGC 7674. Con don et al. (1991) found a tendency in their sample for the scatter in q to increase with infrared luminosities. A similar result is found, in our slightly larger sample. Condon et al. attributed this result to large free-free optical depths in the more compact, generally more luminous galaxies. Correction for this effect decreases the scatter in q considerably (cf. Fig. 5 of Condon et al. 1991) and suggests that the infrared and radio emission originating on the subarcsecond scale in most of these LIGs (except perhaps for some of the Seyfert 2 galaxies) is produced by starbursts. However, as Lonsdale, Smith. & Lonsdale (1993) recently discovered, this result does not exclude the possibility of milliarcsecond-scale AGN cores with log $T_b \gtrsim 5$ in many (and perhaps *all*) of these objects, contributing only a small ($\sim$12%) fraction of the total radio power. The implication of this important result will be discussed in §4.1.2.

In Figure 21a, we have plotted the ratio of 20-cm continuum fluxes to Hα line fluxes for most of the objects in our sample. The value expected for free-free emission at ν = 1.49 Ghz from a 10000 K extinction-free gas is 1.0 x 10^{-12} erg cm^{-2} s^{-1} mJy^{-1} (Kaufman et al. 1987). Figure 21b shows this same ratio after correcting the Hα fluxes for extinction using the values of E(B-V) determined from the emission-line Balmer decrements. Although this ratio is considerably smaller than the uncorrected ratio. we find that r_c is still two orders of magnitude larger than the expected thermal value. with the I. INTERs showing the larger excesses (H 11: 54, S: 66, and L: 151). The large values of r_c arc probably due to a combination of two effects: (1) most likely, the reddening determined from optical emission lines are underestimates of the actual amount of dust. and (2) non-thermal radio processes associated with supernova explosions and their remnants. shock ionization, or directly related to the AGN are present in the cores of these objects. One or both of these effects is affecting LINERs more than the other LIGs. The -'"- nature of LINER LIGs will be discussed in more detail in §4.

2.10. Morphological Properties and Presence of Companions

Galaxy interactions are well known to play an important role in luminous in-

frared galaxies (Lonsdale, Persson, & Matthews 1984; Cutri & MacAlary 1985: Sanders et al. 1987; Vader & Simon 1987; Telesco, Wolstencroft, & Done 1988; Hutchings & Neff 19SS: Jones & Stein 1989; Lawrence et al. 1989; Leech et al. 1989, 1991; AHM90: Melnick & Mirabel 1990; Rowan-Robinson 1991). In order to address the issue of galactic interaction in our sample, We used the definition of Tinney et al. (1990) for the interact ion class (IA C): IAC= 1, isolated objects with no extended tails and no companion within three optical diameters; IAC=2, galaxies with an asymmetric or distorted appearance, but no evidence of a close-by companion; IAC=3, galaxies with an ongoing inter-action as judged from the presence of two overlapping or nearby galaxies: IAC=4, advanced merger systems as indicated by the presence of tidal tails or shells around a single stellar system. The interaction classes of 92 objects belonging to the CBGSs were extracted from the tabulations of Sanders et al. (1991) and Tinney et al. (1990). The interaction classes of 9 objects from the WGSS were also included in the analysis. Our group is presently involved in a multiwavelength imaging study aimed at determining more accurately the stage of interaction of many of these objects.

As in previous studies, wc find a strong correlation between infrared luminosity and interaction class among the objects of the CBGSs. The mean IAC of the objects in the $\log(L_{ir}/L_{\odot})$ bins 10- 11, 11- 12, and above 12 are 2.53, 2.90, and 3.62, respectively. A w-taker but significant correlation is also observed between spectral types and interaction class in the sense that AGN and especially Seyfert 2 galaxies arc more advanced merger systems than H II objects (IAC = 3.17, 2.91, and 2.78 for Seyfert 2s, LINERs, and H 11 galaxies, respectively). This result was expected since the proportions of AGN and Seyfert 2 galaxies increase with infrared luminosity (§2.2). The larger strength of the IAC -- L_{ir} correlation suggests that the infrared luminosity rather than the spectral type is the driving parameter in these correlations (cf. §4 .3).

Wc also searched for any variations in the [0 III] λ5007 line widths as a function of the stage of interaction. No significant trend was observed. A similar result was found by Leech et al. (1989) using the Hα and [N II] line widths of the H 11 galaxies of their sample. Finally, we calculated the average equivalent width of the Hα emission line as a function of the interacting class IAC (Fig. 22). Differences were observed between the various classes: 42 Å, 81 Å, and 67 Å for galaxies with IAC = 2, 3, and 4, respectively (only two objects belong to IAC = 1). The differences between IAC = 2 and IAC = 3 are fairly significant (P[null K-S] = 0.09) but the others are not (P[null K-S] = 0.6 · 0.7). These numbers can be compared with the results of Keel ct al. (1985) who found that the median nuclear Hα equivalent width of *single* galaxies is roughly 8 Å, while for interacting galaxies it is approximately 25 Å. lhe strongly interacting (IAC = 3 and 4) . L] Gs of our sample do indeed show stronger Hα emission than the isolated objects of Keel et al. (1985). Both Keel et al. and Kennicutt et al. (1987) noticed that the average EW(Hα) decreases with projected separation of the pairs. It may therefore be surprising to find that merged systems (IAC=4) generally have smaller EW(Hα) than

systems with double nuclei (IA C=3). However, it is important to note that equivalent widths of a number of the objects with IAC=4 may be affected by the presence of an active nucleus. Moreover, systems in this interaction class are sometimes difficult to differentiate from objects in the lower interaction classes and so errors in the classification are likely. In contrast, Leech et al. (1989) did *not* see *a* difference between the equivalent widths of interacting and non-interacting LIGs but this apparent discrepancy may be attributed to the lack of strongly interacting objects in their sample relative to the sample of Keel et al. (1985) and Kennicutt et al. (1987).

Systems with double nuclei (IAC = 3) were investigated further in an attempt to quantify the effects of galaxy interactions in these objects. Figure 23 shows the line ratios of 17 CBGSs and 6 WGSS systems with double nuclei. Each physical pair is indicated by two data points joined by a line. Filled symbols are ultraluminous infrared galaxies [$\log(L_{ir}/L_{\odot})>12$], squares with an "X" in the middle are objects with $10 < \log(L_{ir}/L_{\odot}) < 11$, and open squares are systems with $\log(L_{ir}/L_{\odot}) <11$. First, we find that many of the double nuclei have ambiguous spectral types in the sense that the line ratios in these objects do not correspond to the same spectral type in all three diagrams of VOS7. This result suggests that a mixture of ionization processes (e.g., photoionization by hot stars and shock ionization, or photoionization by hot stars and an active nucleus) are taking place in the cores of these objects. Another important result is the presence of a Seyfert 2 galaxy (NGC 5256 NE) and a number of LINERs among this sample. This result shows that, at least in a few cases, the formation of active nuclei *precedes* the final merger phase of the *present* galactic interaction.

2. 11. Infrared Spectral Properties

The infrared spectral properties of the various classes of LIGs were investigated. We used the definitions of Dahari & De Robertis (1988) for the IRAS color indices [$\alpha_1 = -\log(S_{60}/S_{25})/\log(60/25), \alpha_2 = -\log(S_{100}/S_{60})/\log(100/60)$] and for the "infrared color excess)' [$IRCE = ((\alpha_1 + 2,48)^2 + (\alpha_2 + 1.94)2)0"0$]. The infrared color excess is a measure of the deviation from colors of nonactive spiral galaxies ($\alpha_1 = -1.48$ and $\alpha_2 = -1.94$: Sekiguchi 1987). The "spectral curvature" as defined by Condon et al. (1991; $C60 = \alpha_1 - \alpha_2$) was also used in the analysis.

The objects in our sample which belong to the CBGSs were found to have average $\alpha_1, \alpha_2, IRCE$, and $C60$ of –2.44, –0.77, 1.27, and 1.66, respectively. Differences in the selection criteria of the objects in the warm sample resulted in significantly different average infrared properties: $\alpha_1 = -1.74$, $\alpha_2 = -1.01$, $IRCE$ = 1.30, and $C60 = 1.22$. A tendency for the infrared colors of Seyfert galaxies to be warmer than those of H 11 galaxies is well known to exist in both optically and infrared selected objects (e.g., Miley et al. 1984; Miley, Neugebauer, & Soifer 1985; Osterbrock & De Robertis 1985; de Grijp, Miley, & Lub 1987; Dahari & De Robertis 1988). These differences were also observed in our sample: $\alpha_1, \alpha_2, IRCE$, and C60 = -1.72, -0.59, 1.67, and 1.07 for the

Seyfert 2 LIGs while they are -2.10, -0.95, 1.20, and 1.49 for H II LIGs. Interestingly, objects with LINER properties generally have infrared properties which are more similar to those of H II galaxies than those of Seyfert LIGs: α_1, α_2, $IRCE$, and $C60$ = -2.-4S. -0.81.1.28, and 1.62, respectively.

Soifer & Neugebauer (1991) found that the mean infrared colors of IRAS galaxies vary systematically with infrared luminosity in the sense that S_{60}/S_{100} increases and S_{12}/S_{25} decreases with increasing infrared luminosity (see also Soifer et al. 1987: Allen et al. 1991). Our combined (CBGSs + WGSs) sample does *not* show any systematic trend in the average value of α_2 with infrared luminosity but this is due to the presence of the WGSS objects. Indeed, α_2 and $IRCE$ (but not $C60$) are, observed to increase with infrared luminosity when only the objects in the CBGSs are considered (P[null] = 5×10^{-7} and 2×10^{-6}, respectively). Excluding all of the AGN from the CBGSs does not significantly affect the strength of these correlations. None of these correlations are observed in the WGSS . There is no tendency for α_1 of the CBGSs objects to vary with infrared luminosity.

Correlations between the redshift and α_2 and $IRCE$ are also present in our CBGSs sample. Considering only the H II galaxies in the CBGSs does not affect the strength of these correlations. Once again, none of these correlations are observed in the WGSS , and the values of α_1 among the CBGSs or WGSS objects do not correlate with redshift. A similar correlation between α_2 and redshift was found in the sample of Allen et al. (1991). The existence in our flux-limited CBGSs sample of a correlation between infrared luminosity and redshift (cf Paper I, §2.1) makes it difficult to determine whether the infrared luminosity or the redshift is driving the correlations involving the infrared properties.

As discussed by Allen et al., the α_2 – redshift correlation can be understood if dust has been gradually cooling down due to ageing of the stars in the starbursts. However, they rejected that possibility based on the fact that their "extreme starbursts" (which they interpret as the youngest starburst galaxies in their sample; §2.2) did not have hotter dust than the other starbursts of their sample. Another explanation for these correlations is based on the results discussed in $2.10, namely that the more luminous objects generally arc at a more advanced stage of galactic interaction. As the interaction proceeds, intense star formation is taking place, the kinetic energy of the galactic collision is converted into shocks, and an active nucleus may b, forming in the merger system. All of these processes result in an increase of the infrared luminosity ant] the dust temperature, (Sanders .1992). The relative importance of these processes in the final energy budget will be discussed in 54.1.2. The presence of these correlations among H IILIGs suggest however that the formation of an active nucleus cannot be 'the sole driver of these correlation. In this galactic interaction scenario, the important parameter in these correlations is the infrared luminosity and the α_2-redshift correlation is simply a consequence of the L_{ir} -- z correlation of our flux-limited sample.

In contrast to Mazzarella & Bothun (19S9) and Mouri & Taniguchi (1992]. we do not find any strong correlation between the infrared colors (dust temperatures) and the intensity ratios [O 1] λ6300/Hα and [0 111] λ5007/Hβ in our infrared-selected sample of H II galaxies (Figs. 24 and 25). However, we confirm th, correlations between infrared colors and Hα equivalent widths observed by Mozzarella, Bothun, & Boroson (1991, in a sample of optically-selected star-burst galaxies. Optical and infrared-selected H II galaxies with large Hα equivalent widths tend to have low F[12]/F[25] and high F[60]/F[100] (P[null] = 0.006 and 10-6, respectively; Fig. 26). This result suggests that the most active star-forming regions produce far-infrared emission with the warmest. dust temperatures (Mozzarella et al. 1'391). Perhaps surprisingly, similar (but weaker) correlations are observed among the infrared-selected Seyfert 2 galaxies (P[null]= 0.0S and' 0.0007. respectively).

Figure 27 shows the well-known correlations between the optical-to-infrared luminosity ratio and the infrared luminosity (P[null] = 10^{-n^8}, 0.03, and 0.06 for the H II galaxies, LINERs and Seyfert) or the IRAS flux ratio F[60]/F[1 00) (only present among the H II galaxies; P[null]= 0.003, 0.3, and 0.7 for the H II galaxies, LINERs. and Seyferts). In this figure, the optical continuum luminosity, 1,(4861), is defined as P(4861) x 4861 where P(4861) is the monochromatic power of the continuum at 4861 Å. No reddening correction was applied to the continuum luminosity. This correlation has been interpreted in the past as an indication that high global dust temperature is associated with large infrared dust emission or small optical continuum extinction. The tendency for the color excess of H II galaxies (P[null] = 10^{-n^3}) and, to a lesser extent, LINER LIGs (P[null]= 0.06) to decrease with log 1,(4861)/L_{ir} is consistent with this hypothesis (Fig. 27). The first two correlations essentially vanish when the continuum luminosities are corrected for dust extinction using the emission-line Balmer decrements (Fig. 28). The existence of a strong *positive* correlation between E(B-V) and $L(4861)_0/L_{ir}$ (P[null] = 10^{-17} when considering all the objects) suggests that the reddening correction derived from the emission lines may overestimate the actual extinction of the optical continuum.

Finally, we find that there is a weak tendency for α_2 and $IRCE$ to be larger in objects with bluer intrinsic continuum colors, $(C6563/C4861)_0$ (P[null] = 0.08 and 0.09. respectively). This result may be due to the fact that the more luminous infrared galaxies have somewhat bluer dereddened continuum colors (cf. §2.8).

3. *Spatial Information*

Recent studies of optically-selected active galaxies have shown that the circumnuclear gas surrounding the cores of these objects can be an excellent probe of the active nuclei on much smaller scale (cf. review Wilson 1991). By analogy, it is natural to expect that the extended line emission in LIGs will reveal something about the energy source lurking in these objects. In §2, we focussed on the properties of the nuclear gas (R <2 kpc); we will now discuss the behavior of many of these properties as a function

of the distance from the nucleus. A total of twenty-three objects from our sample could be used for this exercise. The names of these galaxies are listed in Table 6 along with their redshifts, infrared luminosities, and spectral types. One can see from this table that the condition for extended emission introduces a bias in this subsample, favoring nearby low-luminosity objects. Note that the data-taking procedure was not optimized to obtain spatial information on the objects of our sample but rather to obtain nuclear information of a maximum of objects: the slit was positioned along the line joining double nuclei rather than along the major axis of the individual galaxies. This fact explains the relatively small number of objects from which wc were able to extract spatial information.

3.1. Reddening

Figure 29 shows the radial variations of E(B-V) as determined from the emission-line Balmer decrement (cf. §2.1). For simplicity, we assumed that the intrinsic Balmer decrements outside of the nucleus is the same as in the nucleus (i.e. $[H\alpha/H\beta]_0$ = 2.85 in and out of the H II nuclei and 3.1 in and out of the AGN). This assumption does not affect our results. The numbers next to the profiles correspond "to the identification number in Table 6. Irrespective of their infrared luminosities, the amount of reddening in the objects of this subsample generally decreases outward from the nucleus. The extinction at R $\approx$ 5 kpc sometimes reaches values less than half the amount found in the nuclear region. This high degree of dust concentration is consistent with the compact distribution of molecular gas in many of these luminous infrared galaxies (Scoville et al. 1986, 1989, Solomon et al. 1990; Radford et al. 1991).

Interestingly, inverted reddening profiles in which the color excess in the center of the galaxy is less than outside of the nucleus occur among four AGN (tile Seyfert 2 galaxy IR 2211-11 and the LINERs IR 1525+36, IR 2055-42, and IC 5135) but in only one H II galaxy (IR 1541+32). A possible explanation for these inverted profiles is that the dust in the center has been partially expelled or destroyed by the AGN. These observations are also consistent with the evolutionary scenario in which H II objects evolve into AGN after shredding most of their nuclear dust (e.g., Sanders et al. 1988a). 130th of these hypotheses predict that the nuclear dust content should be lower in Seyfert galaxies than in H 11 galaxies, a result found in §2.1. Note, however, that complex optical depth effects may produce inverted dust profiles without invoking a smaller amount of dust in the nuclei of these objects (Leech et al. 1989; Keel 1992). We will return to this discussion in §4.2 and §4.3.

3.2. *Spectral Classification*

The variations of the line ratios as a function of aperture sizes are shown in Figures 30 - 32. Some of the objects in this subsample have line ratios which change sig-

nificantly with the size of the aperture. The most noteworthy examples are ZW453.062, NGC 5953, and NGC 7679. The line ratios of NGC 5953 and ZW453.062 are AGN-like in the nucleus but are H II region-like in the circumnuclear gas. The line ratios of NGC 7679 behave in a similar fashion with the exception of the [S II]/Hα ratio which remains H 11 region-like in and out of the nucleus. The general tendency of the nuclear AGN-like line ratios to become H II region-like when a larger aperture is used can be understood if there is a circumnuclear starburst which dilutes the AGN emission from the nucleus of these objects. A starburst surrounding a nuclear AGN line-emitt.ing region is already known to exist in other LIGs and in some optically selected AGN (e.g., Mrk 231 and NGC 7469; Sanders et al. 1988b, Wilson et al. 1991). Evidence for circumnuclear starbursts in many of these objects also comes from the strength of the absorption features outside of the nuclei (§3.6). The presence of these circumnuclear starbursts may explain the smaller fraction of AGN LIGs found in fainter IRAS surveys (Lawrence et al. 1989; Leech et al. 1989; Rowan-Robinson 1991). In these studies, the ultraluminous infrared galaxies are typically three times more distant than objects from the CBGSs, so the aperture includes more of the circumnuclear (H II region-like) emission than in the more nearby objects. This result emphasizes the fact that a constant linear-size aperture is crucial when classifying the nuclear spectra of LIGs using emission-line ratio diagnostics.

On the other hand, the line ratios in the nuclei of 2055-42 and, to a lesser extent. 1s29-34, MCG-0304014, and Mrk 331 are H II region-like but become I. IINER-like at larger distances from the nucleus. A similar effect was observed by AHM89 and Heckman, Armus, & Miley (1990; HAM90) in M82. They explained this type of ionization structure in the context of a supernovae-driven wind model in which the circumnuclear gas collisionally ionized by strong shocks caused by the interaction of the outflowing nuclear gas with the ambient material. This scenario could also explain the ionization gradient in 2055-42, 1829-34, MCG-0304014, and Mrk 331.

3.3. *Densities*

The density profiles were measured in seven objects of our sample using the [S 11 λ6731/λ6716 ratio. The results are presented in Figure 33. Measurements near the low-density limit ($n_e \simeq 150$ cm^{-3}) should be treated with caution. Complex density variations are observed in all of these objects. However, there is a weak trend for lower densities to be found at larger distances from the nucleus. One notable exception to this rule is MCG-0304014 in which the density is near the low-density limit at the nucleus but reaches 1400 cm^{-3} at R $\simeq$ 3.1 kpc. The radial density *profiles* of AGN were not found to be different from those measured in H II objects apart from a generally higher normalization factor (see §2.4). Unfortunately, the density profiles could not be determined for any of the ultraluminous infrared galaxies of our sample, so no statement can be made about the reported variations in the density profiles of LIGs as a function

of infrared luminosity (HAM90).

3..4. *Temperatures*

Due to the faintness of (O 111] λ4363 in nearly all the objects of our sample, a study of the temperature gradients could be carried out for only two galaxies: the Seyfert 2 galaxy NGC 7679 and the H II/LINER galaxy IR2222-08. Their temperature profiles are presented in Figure 34 in the cases where $n_e = 10^3$ and 10^6 cm^3. First. note that the temperatures measured in the H 11/LINER object are considerably higher than in the Seyfert 2 galaxy, suggesting that shock ionization may be important in IR2222-08. The clear tendency in this object to find larger temperatures at larger distances from the nucleus ($T_e \approx 35000$ K at R = 12 kpc) also suggests that shock ionization gradually becomes important in the outer parts of the line-emitting region. The density profile of this object could not be measured from our data so the possibility that the variations of [0 111] λ4363/λ5007 may be clue to density variations cannot be formerly excluded but appears unlikely considering the amplitude and monotonic nature of the [O III] ratio variations. Shock ionization may be responsible for the LINER emission in and out of the nucleus of this object. A similar though less significant positive temperature gradient is observed in NGC 7679. In this galaxy, higher temperatures in the outskirts of this galaxy may be due to hardening of the AGN ionizing field, density variations, shock ionization, metallicity gradients, or a combination of these processes.

The spatial variations of the [0 III] λ4363 line were measured in only a handful of other LIGs (HAM90). New data with signal-to-noise ratio higher than in the present data and taken at a number of position angles are needed to determine if positive temperature gradients are a common feature of these objects.

3..5. *L ine Widths*

The rather poor spectral resolution of our data ($\sim 8 - 10$ Å) prevents us from studying any line profile parameters other than the line width. The spatial variations of the line widths of both [O 111] λ5007 and Hα were examined. In spite of the larger strength of Hα, blends of this line with [N II] $\lambda\lambda$6548, 6583 ancl stellar Hα make the width of Hα more uncertain than that of [O III]. The results of these measurements arc presented in Figures 35 and 36. We note a general tendency for the [O III] line widths to reach a maximum *outside* of the nucleus. This effect is somewhat weaker when the more uncertain Hα line widths are examined. The only objects which have smaller *[0* III] . . widths outside of their nucleus are the Seyfert 2 galaxy NGC 7674 and the LINER NGC 5953/Arp 91. We cannot completely rule out the possibility that this effect is due in part to numerical broadening associated with Poissonian noise (noisier signals tent] to pull in more of the emission in the wings away from the peak and so broaden the fitted line profile), Observations at higher signal-to-noise ratios and spectral resolution arc

needed to confirm these results.

Nevertheless, the highly non-Gaussian profiles found at intermediate radii in about 4 of these 12 galaxies suggest that the larger line widths observed outside of the nucleus are produced by organized, large-scale bulk motion rather than by chaotic. turbulent motion. We speculate that the broad profiles outside of the nucleus are produced by (unresolved) line splitting where two or more elnission-line components having different velocities are present. Such Extra-nuclear line splitting is a relatively common feature in the handful of LIGs for which high-resolution kinematic data exist in the literature (e.g.. Ulrich 1978; Axon & Taylor 1978; Bland & Tully 1988; HAM90; Filippenko & Sargent 1992; Veilleux et al. 1994 and references therein). With the exception of the remarkable object NG C 3079, the velocity separations in all of these objects were observed to be less than ~ 400 km s^{-1}. Line splitting of this amplitude would be difficult to detect at the resolution of our data. The broad non-Gaussian profiles outside the nucleus of these objects arc therefore interpreted as being the kinematic signature of large-scale bipolar outflows from the nucleus. Data of higher spectral resolution are needed to confirm the presence of line splitting in the circumnuclear nebulae of our sample of LIGs.

3.6. *Stellar Absorption Features*

The Mg Ib equivalent widths measured in LIGs were found in §2.7 to be considerably smaller than the equivalent widths observed in non-active spiral galaxies. Dilution of the old-star continuum by a featureless continuum produced by an AGN or by hot, young stars can explain this result. If this hypothesis is valid, the study of radial variations of the strength of this feature with distance from the nucleus may help determine the size of the continuum source and therefore distinguish between point-like AGN and extended starbursts (the compact star-bursts suggested by Condon et al. [1991] to exist in many ultraluminous infrared galaxies cannot be differentiated from AGN using this method alone).

All of the radial EW(Mg I) profiles that could be derived from our data are presented in Figure 37. Note, first of all, that essentially all of the nuclear *and* circumnuclear Mg Ib equivalent widths of our subsample of LIGs are considerably lower than the values measured in the nuclei of normal, field spiral galaxies (~ 4 Å; Heckman, Balick, & Crane 1980; Stauffer 1982). This result suggests that the source of dilution of the old stellar continuum is extended and, consequently, that circumnuclear starbursts are important contributors to the optical continuum in most of.the objects in our subsample. Another explanation is that we are seeing the red supergiant phase of. spatially extended, young starbursts (age $\approx 10^7$ yr). In this scenario, there is no need for an underlying old stellar population because the weak Mg Ib absorption feature is entirely produced by the red supergiants (Bica, Alloin, & Schmidt 1990). In both cases, the continuum is expected to be flat or even rising to the blue (Bica et al. 1990). The issue of radial varia-

tions of the continuum colors will be discussed in §3.7. Metallicity gradients in the host galaxy may be another source of variations in EW(Mg Ib) (Edmunds 1989; Diaz 1989; Thomsen & Baum 1987).

The radial EW(Mg Ib) profiles of Figure 37 do not show any trend with infrared luminosity or nuclear spectral types. Indeed, the equivalent widths of Mg Ib in many of the AGN (including nearly all Seyfert 2 galaxies) either *decrease* with radius or do not show any significant radial dependence. A similar result is found for the H II objects. Once again, this strongly points to the presence of starburst activity in the circumnuclear region of LIGs, regardless of their nuclear spectral types. The strength of the Mg Ib feature alone thus cannot be used to determine the size and nature of the *nuclear* source of energy in these objects.

Of the three objects for which we have reliable *nuclear* Ca II triplet $\lambda\lambda$8542, 8662 equivalent widths (1215+06 [H II], 1344+14 [H II], and 1344+11 [S2/H 11], cf. §2.7), long-slit data could be extracted for only the last one. EW(Ca 11) in 1344+11 was found to be 5.49, 4.99, 4.35, and 8.84 Å at a distance from the nucleus of 0.0- 0.5 kpc, 0.5- 1.0 kpc, 1.0 -2.0 kpc, and 2.0 -4.0 kpc, respectively. For comparison, EW(Mg Ib) varies from 1.26 Å in the nucleus down to 0.81 Å at a distance of 2- 4 kpc. Dilution effects by an active nucleus cannot explain these results. However, we cannot exclude the possibility that some of the *line emission* in this object is produced by an AGN.

The radial behavior of the Hβ equivalent widths is shown in Figure 38. Complex, non-monotonic variations are observed in many objects of our sample. However, essentially all LIGs with Seyfert spectral characteristics (unfortunately, we have no data on 1344+11) present Hβ equivalent widths which are smaller in the nucleus than in the circumnuclear region. *This is the strongest evidence from absorption line data that a featureless AGN continuum may be contributing to the optical continuum in the nuclei of Seyfert LIGs.* The fact that the LINER LIGs in our sample do not show this behavior suggests that AGN continuum emission is not a major contributor to the optical continuum of these objects. This last statement is based on a few objects so it is uncertain.

3.7. *Continuum Colors*

The continuum color, C6563/C4861, was measured as a function of distance from the nucleus for all twenty-three objects in the subsample. With the notable exceptions of the Seyfert 2 galaxies U08696, NGC 7674, and ZW475.056 (and, to a lesser extent, IR1530+30) and the H II object IR1829-34, the continuum colors of the objects in our sample are redder in the nucleus than in the outskirts of the host galaxy (Fig. 39), with a tendency for the color gradients to be steeper in the redder nuclei. The continuum colors are all too red to be produced by an *unreddened* stellar population less than 109 year old. Undoubtedly, dust is affecting the continuum colors of the nuclear region and, to a lesser degree, the circumnuclear stellar populations. The radial gradient of the

dust Distribution is producing differential reddening which is dominating the continuum color profiles. In Seyfert galaxies, the nuclear continuum is anomalously blue with respect to its surroundings, perhaps because it is strongly affected by the hard, power-law continuum produced by the AGN.

In Figure 40, the continuum colors were corrected for reddening effects using the measured Hα/Hβ emission-line ratios. The vertical dashed lines in this figure represent the colors of star clusters of various ages (from Jacoby, Hunter, & Christian 1984). First of all, note that some of the data points in Figure 40 are *bluer* than the colors of the ZAMS. In the cases of the Seyfert 2 galaxies NGC 34 and NGC 7679 (and perhaps also the LINER NGC 1204), the extreme nuclear colors are probably due to dilution effects of the stellar continuum by the blue, AGN continuum. However, it is interesting to note that the radial behavior of the dereddened continuum colors is not particularly sensitive to infrared luminosity or spectral types of the objects. The continuum colors in the nuclear region of most galaxies are bluer than in the outskirts. These results support the presence of an AGN and/or a starburst in the nuclei of these objects. On the other hand, the sometimes extreme *negative* color gradient observed in NGC 660 minor (L), IC 5135 (H II), MCG-0304014 (H II), IR1541+28 (S2) and NGC 7591 (L) maybe caused by the presence of a young *circumnuclear* starburst region. The negative EW(Mg Ib) gradient found in these five galaxies (cf. §3.6) is also consistent with this hypothesis.

4. DISCUSSION

4.1. *Energy Sources*

First, an important distinction should be made between the source of energy responsible for ionizing the line-emitting gas in LIGs (thereafter called the source of ionization) and the source of energy powering the quasar-like bolometric luminosities and violent outflows observed in some of these objects (cf. §3.5 and §4.2). In §2.3, we found that $L_{H\alpha}$(nucleus) $\simeq$ 0.001--0.0001 L_{ir} in most of the objects in our sample. The imaging study of AHM90 found that $L_{H\alpha+[NII]}$(nucleus) $\gtrsim$ 0.1 $L_{H\alpha+[NII]}$(total) so $L_{H\alpha}$(total) $\approx 10^{-2} - 10^{-3} L_{ir}$. Furthermore, since both shock ionization or photoionization models predict that the total emission-line luminosity is about 30 times the Hα luminosity (e.g., Dinette, Dopita, & Tuohy 1985; Ferland & Netzer 1983) and the total bolometric luminosity of LIGs is typically less than twice their infrared luminosity (e.g., Rice et al. 1988; Soifer et al. 1987) we have that L_{neb}(total) $\simeq$ 0.1-0.01 L_{bol}. Although correction for reddening effects makes the value of this ratio rather uncertain, the fraction of the total energy produced by LIGs which is used in ionizing the line-emitting gas observed at optical wavelengths is therefore likely to be small ($\lesssim$ 10%: cf. also AHM90). In the present section, we will first address the issue of the nature of the ionization source in LIGs and then attempt to provide further constraints on the more

d:..cult question of the origin of the large bolometric luminosity in these objects.

4.1.1 *Source of Ionization*

We found in §2.2 that both the fraction of LIGs with AGN (Seyfert and LINER) spectra and the fraction of Seyfert galaxies among the AGN increase with infrared luminosity. In contrast, the proportion of LINERs was found to be 20 – 25% regardless of the infrared luminosity. There is very little question that the main source of ionization in LIGs with H II region-like spectra is photoionization by hot O – B stars. The debate centers on the ionization process in AGN and more particularly in the galaxies with LINER spectra. .4 considerable amount of work over the last ten years has been devoted to this issue (see Heckman 1987 and Filippenko 1989 for reviews). .41 most certainly *optically-selected* LINERs constitute a heterogeneous class made of objects (1) photoionized by a weak AGN continuum (Ferland & Netzer 1983; Filippenko & Halpern 1984; Pequignot 1984; Stasinska 1984; Binette 1985; Filippenko 1985; VO87; Ho, Filippenko, & Sargent 1993), (2) shock ionized by the interaction of outflowing gas with the ambient medium of the host galaxy or resulting from galaxy collisions (Koski & Osterbrock 1976; Fosbury et al. 1978; H80; HAM90; Harwit et al. 1987), (3) photoionized by a population of hot, high metallicity stars lying perhaps in a dense environment (Terlevich & Melnick 1985; Terlevich 1992; Filippenko & Terlevich 1992; Shields 1992). (4) associated with cooling accretion flows (Mathews & Bregman 1978; Kent & Sargent 1979; Heckman 1981; Cowie et al. 1983; Hu, Cowie, & Wang 1985; Phillips et al. 1986; Fabian et al. 1986) or ionized by a combination of some of these processes.

In the infrared-selected objects of our sample, emission from cooling flows can be discarded rather con: ently based on the fact that galaxies associated with cooling flows are generally asso:.ted with dominant early-type galaxies in X-ray clusters rather than the late-type, morphologically disturbed host galaxies of LIGs (§2. 10). The results presented in §2 and §3 can be combined with those of previous studies to address the importance of each of the other processes in AGN LIGs. It is important at this stage to emphasize once again that the LINER definition used in the present study does not exactly correspond to the original definition of H80 (§2.2). In the cases where [0 II] λ3727 could be measured reliably, a few LINER LIGs were found not to be "genuine.. LINERs. These fcw objects may well be photoionized by normal hot stars. Filippenko & Terlevich (1992) pointed out that LINERs with [0 1] $\lambda 6300/H\alpha \lesssim 1/6$ may also be produced through photoionization by hot (T 245000 K) main-sequence O stars. However, this mechanism leaves the spectrum of most of the LINER LIGs -in our sample unexplained. Photoionization by hot stars in a density-stratified environment with solar abundances modified by normal grain depletion was suggested by Shields (1992) to explain LINERs with larger [0 I]. This process may be responsible for the line emission of some well-organized, optically-selected LINERs but the application of these models to LINER LIGs, highly irregular and dusty systems, may not be realistic. Note, how-

ever, that the larger nuclear [S II] densities found in LINER LIGs compared with [hose of H II objects are consistent with this picture. In any case, the high densities required to produce LINER emission by O-star photoionization arc unlikely to be present over extended areas *outside* of the galactic nucleus of our objects and, consequently, this process cannot explain the extended, circumnuclear LINER emission observed in some of our objeers.

The importance of photoionization by a cluster of unusually hot stars ("Warmers": Phases 2 and 3 in the scenario of Terlevich 1992) in the AGN LIGs is difficult to assess as there is relatively little information available at the present time which can discriminate between this ionization process and photoionization by a genuine active nucleus (as in the case of their optically-selected counterparts). The presence of a blue continuum in the "nuclear regions of many of the Seyfert 2 LIGs of our sample (cf. §3.6 and §3.7) can be explained in both the Warmer and AGN scenarios. As discussed in §2.7 and §3.6, the sample of LIGs for which we have reliable measurements of a large number of absorption lines spanning a broad wavelength range (including the important Ca II triplet feature) is too small in the present study for any statistical analysis. Measurements of this kind are needed to determine the importance of dilution effects by a featureless AGN continuum in these objects and to find out whether the presence of red supergiant stars is affecting the strengths of any of these features. Observations outside the optical window and into the infrared domain may provide the best tests. Detection of well-collimated radio jets in some LIGs [e.g., the LINER LIG NGC 3079 (Irwin & Seaquist 1988)] are difficult to reconcile with the Warmer scenario. Spectroscopy at ultraviolet wavelengths may help uncover the presence of strong stellar winds from massive stars (Maeder 1990). A search for hard X-rays in LIGs would also be very valuable in that context as a detection of radiation above ~ 100 keV from these objects would seriously undermine the possibility of Warmers producing the bulk of the ionization.

The nebulae of most LIGs are entities which are morphologically irregular as a result of galactic encounters and/or the interaction of nuclear outflowing gas with the circumnuclear region (cf §2.6, 2.10, 3.5 and references therein). LINER emission associated with shock ionization is a natural consequence of such violent processes. In this scenario, the kinetic energy involved in the large relative gas motion is efficiently thermalized via shocks, producing very hot ($T \approx 10^6 - 10^7$ K) gas at the interface of the interaction. LINER emission is produced in the $10^4 - 10^5$ K post-shock gas or in gas photoionized by dilute bremmstrahlung radiation emitted by the hot-gas phase. In either case, the LINER emission is expected to be produced from a region which is spatially extended. This is particularly true in the case of shock ionization caused by galaxy encounters where the region of interface is expected to be many kpc in extent. Spatially extended LINER emission was indeed observed in many of the nearby LIGs of our sample (§3.2) and in the sample of HAM90. Moreover, LINER emission was found to be particularly frequent in advanced mergers (IAC = 3 and 4; cf. 52,10) and in objects with

broad emission-line profiles (§2.6). The high values of r(20 cm/Hα) in LINER LIGs (cf. §2.9) may be explained in the context of shock ionization through an abundant production of relativistic electrons.

Additional support for a shock ionization origin to some of the AGN emission comes from the null or positive radial gradient of the [O III] λ5007/Hβ ratio in some of these objects (cf. §3.2). This ratio is known to be highly dependent on the ionization parameter (U = density of ionizing photon/electron density $\propto n^{-1} R^{-2}$; e.g., Ferland & Netzer 1983). The null or positive [O III]/Hβ radial gradients are therefore inconsistent with the idea that the circumnuclear gas is being photoionized by a nuclear source of hard photons (be it an AGN or Warmers) unless the circumnuclear density profile follows $n(r) \propto r^n$ with $n \gtrsim 2$. Such steep density profiles are not observed in LIGs (cf. §3.3 and HAM90). Most likely, photoionization and shock ionization are both taking place in many of these objects. Energy arguments also support this scenario: the Hα luminosity expected from shock ionization is $\sim 2.4 \times 10^{26} n_0 A V_s^3$ erg S–l, where n_0 is the density of the ambient gas (in cm^{-3}), A is the shock surface (in pc^2), and V_s is the shock velocity (in km s^{-1}) (Binette, Dopita, & Tuohy 1985). This value is smaller than the reddening-corrected Hα luminosities of most of the objects in our sample even if we use conservatively high values for the parameters (e.g., $n_0 = 100$ cm^{-3}, $A = 10^6$ pc^2, and $V_s = 300$ km s^{-1}). Moreover, shock models predict strong correlations between line widths and [O I]/Hα, [S II]/Hα, or [N II]/Hα, but Figure 41 shows that a large scatter exists in these relations for our sample of objects.

Finally, it is important to emphasize that the Seyfert-like emission is considerably more difficult to produce from shock ionization than LINER emission. Indeed, a very restrictive range of shock conditions are needed to produce the high-excitation spectrum of Seyfert galaxies (e. g., Binette, Dopita, & Tuohy 1985; Pequignot 1985; Innes 1992). Shock ionization is thus unlikely to be the dominant ionization process in Seyfert 1,1 Gs. The values of the electron temperature determined in the ten Seyfert 2 LIGs of our sample in which [O III] λ4363 was detected are indeed consistent with photoionization by a hard continuum of a 10^3-106 cm^{-3} medium (§2.5 and 3.4).

4.1.2 Source of the Luminosity

There is a general consensus that much of the infrared luminosity of LIGs is thermal radiation from "heated dust grains. The dilemma consists in finding the *dominant* heat source of these grains. The radiation field from a dust-enshrouded AGN (e.g., Becklin & Wynn-Williams 19.87; Sanders et al.. 1988a; Lonsdale, Smith, & Lonsdale 1993). extended or compact nuclear starbursts (e.g., Rieke et al. 1985; Condon et al. 1991). or the old underlying stellar population (Thronson et al. 1990) have all been suggested to be the main heating process in LIGs. The possibility of producing the large infrared luminosity by tapping into the kinetic energy involved in violent galaxy collisions was also explored by Harwit et al. (1987). From a theoretical point of view. all of

these models are rather successful at explaining objects with $\log(L_{ir}/L_{\odot}) \lesssim 12$. The real test however is to explain the ultraluminous galaxies. At these high luminosities. the scenario involving radiation from an old stellar population starts to break down (Thronson et al. 1990), while the scenario of Harwit et al. (1987) requires the galaxy collisions to be nearly face-on. The lack of correlation between the total kinetic energy in the interacting system and the infrared luminosity per unit Hz mass is also inconsistent with this last scenario (Sanders, Scoville, & Soifer 1991; cf. Condon et al. 1991 for another argument against the galaxy-collision model). We will therefore focus our attention on the starburst and AGN scenarios, but keeping in mind that the other two scenarios may be important for lower luminosity objects.

Observationally, the difficulty in evaluating the importance of starbursts relative to AGN lies in the fact that the source of energy of LIGs is embedded in a very dense nuclear concentration of molecular gas which is essentially impenetrable at all wavelengths except perhaps in the hard X-rays or at radio wavelengths (Condon et al. 1991). For this reason, optical studies which attempt to determine the central energy source of LIGs heavily relies on the assumption that the physical characteristics of the circumnuclear gas and stellar population reflect the dominant processes taking place in the very core of LIGs. This assumption about the line-emitting gas in turn implies that the nuclear source, as seen from the circumnuclear region, is not completely covered by molecular clouds, so that some of the radiation emitted in the center leaks out to distances of order ~ 1 kpc.

Until recently, this assumption was supported by radio observations. Norris et al. (1988, 1990) found for instance that the detection of compact ($R \lesssim 200$ pc), high-brightness temperature ($T_b \gtrsim 10^5$ K) radio cores generally attributed to the presence of a genuine AGN were far more common among LIGs optically classified as AGX than among the others. In contrast, the deeper survey of Lonsdale et al. (1993) recently found no correlation in their sample of LIGs between the detection of compact. radio cores and their optical classification (this conclusion remains qualitatively the same when using the improved classification of the present paper although differences in the spectral types are rather frequent). However, one comes to a slightly different conclusion when all of the LINER LIGs are excluded from their sample. Indeed, we find that Seyfert LIGs have a slightly higher probability of radio-core detection than H II objects. This result reinforces the idea discussed in §4.1.1 that the dominant source of ionization in many LINER LIGs is *not* photoionization by a genuine AGN and therefore that many of these objects should not be included in the AGN class. The higher dust content of LINERs relative to that of H II LIGs (§2.1 and §2.9) is also inconsistent with the hypothesis that the LINER emission is produced by an AGN which is less obscured than in H II objects (Lonsdale et al. 1993). In any case, one should be cautious when drawing any conclusions concerning the dominant energy source of LIGs based on radio data since the energy at these wavelengths actually represents less than $\sim 10^{-4}$ of the total

bolometric luminosity of these galaxies. Moreover, the luminosity of the compact cores detected by Lonsdale et al. are only $\sim$ 10% of the total *radio* luminosity. Consequently, the AGN detected at radio wavelengths may not contribute significantly to **the** large infrared luminosity of these objects. Knowledge of the distribution of the radio emission on the pc–kpc scales and its relationship with the powerful infrared emission will be needed before one can assess accurately the relative importance of compact-core radio emission in the total energy budget of LIGs.

The importance of starbursts in LIGs can be estimated by comparing the prediction of the starburst model with some of the results from our sample. We choose this method of reasoning rather than comparing our results with the predictions of the AGN model because we feel that the relationship between the various energy regimes of star formation (optical, infrared, and radio) is better understood than in AGN. In Figure 28. we plotted the ratio of the continuum luminosity at λ = 4861 Å corrected for reddening. $L(4861)_0$, to the infrared luminosity of the objects in our sample. Using these numbers, we find that the average values of log $L(4861)_0/L_{ir}$ for H II galaxies, LINERs, and Seyfert galaxies are all about the same (- 0.74, –0.82, and –0.70, respectively) but that the scatter among Seyfert LIGs is nearly twice as large as among the other two classes of objects. These results suggest that the source of continuum in some of these Seyfert galaxies is different from H II and LINER LIGs, and that many LINER LIGs may be more directly related to the H II objects than to the Seyfert galaxies (cf. §4.1.1 and above). For a more direct comparison with published starburst models, we need to transform the infrared luminosities of our objects into bolometric luminosities. The results of Rice et al. (1988), Soifer et al. (1987), and Sanders (1991) show that $L_{ir}/L_{bol} \gtrsim 0.5$ rind therefore the continuum luminosity, L(4861), is $\sim$ 5% of the bolometric luminosity. This ratio can be compared with the theoretical predictions of Wyse (1985) in the case of a young (10^6--107 yr) starbursting stellar population taking into account the appropriate bolometric corrections (e.g., Bruzual 1981): $L(4861)/L_{bol} \approx$ 10-- 20%. Therefore, we find that up to 5070 of the bolometric luminosity of the LIGs in our sample could be powered by the starburst if all of the optical continuum is indeed produced by young stars. Underestimates in the reddening corrections of the optical continuum would increase this value (see note at the end of ~2.11, however). On the other hand, part of the optical continuum may be produced by an old stellar population or, in some Seyfert LIGs, a power-law AGN continuum, thus decreasing the percentage of the bolometric luminosity produced by the starburst.

In the "pure" starburst model, the infrared and Hα luminosities are measures of the total and" ionizing luminosity produced by the stars, respectively. These two quantities can therefore be used to determine the star formation rates in galaxies. Using the derivations of Gallagher, Hunter, & Tutukov (1984) and Hunter et al. (1986), we have

$$SFR(IR) = 26\ \beta^{-1} L_{ir,11}\ M_\odot\ yr^{-1} \quad (1)$$

$$SFR(H\alpha) = 2700\ \eta^{-1} L_{H\alpha,11} \quad M_\odot\ yr^{-1} \tag{2}$$

where the infrared and Hα luminosities arc in units of $10^{11} L_\odot$, β is the fraction of the bolometric luminosity radiated by stars and η is the fraction of ionizing photons that produce observable Hα emission (see also Kennicutt 1983). Equations (1) and (2) assume that the star formation rate is constant over the lifetime of stars with $M \geq 10\ M_\odot$ and that the initial mass function (IMF) extends up to $\sim 100\ M_\odot$ with slope $\gamma = 2.35$ (Salpeter 1955). Further assuming that $\beta \approx \eta \approx 1$ in LIGs, we get SFR(Hα)/SFR(IR) $\sim 10^3\ L_{H\alpha}/L_{ir}$. In §2.3, we found that $L_{H\alpha}$ of H 11 LIGs correlate very well with L_{ir} with most of these objects having $L_{ir}/L_{H\alpha} = 300 - 3000$. In these galaxies, we thus have SFR(IR) ≃ SFR(Hα) ≃ 1-500 $M_\odot yr^{-1}$, where the first equality takes into account the large uncertainties in the Hα luminosities related to reddening corrections. Another potential source of scatter in the Ha-to-infrared luminosity ratio in these objects is variations in the form of the IMF (more specifically the IMF slope γ and the upper and lower mass limits; Condon & Yin 1990). In contrast, the correlation between Hα and infrared luminosities is much weaker (if at all present) among AGN LIGs, and especially Seyfert galaxies. The presence of an additional, non-stellar source of energy in some of the Seyfert LIGs is probably changing the value of this ratio from the nominal value for star formation.

Another constraint on the star formation rate in these galaxies can be derived from the radio data. If we assume that most of the radiation from LIGs is due to a nuclear starburst, the radio luminosities of our objects can be used to estimate the Type II supernova rate using the prescription of Condon & Yin (1990):

$$SNR = 7.7 \times 10^{-24} (\nu/1\ Ghz)^{0.8} L_{NT}\ yr^{-1} \tag{3}$$

where L_{NT} is the non-thermal component of the radio luminosity. Note that this supernova rate takes into account the production of relativistic electrons after the adiabatic (Sedov) phase of supernova remnants and that it depends very little on the upper mass limit of the IMF (in contrast to the star formation rates derived from Hα luminosities [eqn. 2]). Condon & Yin argue that the ratio of non-thermal to thermal radio flux is approximately the same for most spiral galaxies:

$$L_{NT}/L_T \sim 10\ (\nu/1\ GHz)^{-0.7}. \tag{4}$$

Assuming that this ratio also applies to LIGs, we can use the radio fluxes tabulated by Condon et al. (1990, 1991; $\nu = 1.49$ GHz) for the objects in our sample to find SNR ≃ 0.005 -1.0 yr^{-1}. This value of the supernova rate is related to the star formation rate through the form of the IMF. For instance, Elson, Fall, & Freeman (1989) estimated that a star-formation rate of 10 $M_\odot yr^{-1}$ would produce one supernova every 15 yr (using a Salpeter IMF with an upper mass cutoff of 100 MO). The star formation rate predicted from the supernova rate calculated above is therefore of the same order of magnitude as the values derived from the infrared and Hα luminosities.

It is important to point out the implications of the star formation rates derived from the radio, infrared, and Hα luminosities. Results from Sanders, Scoville, & Soifer (1991) show that the infrared luminosity to H_2 mass ratio increases with the infrared luminosity with the approximate form

$$L_{\rm ir}/M(H_2) \approx 10\ L_{\rm ir,11}\ \ {\rm L}_\odot\ {\rm M}_\odot^{-1}. \qquad (5)$$

The star formation rate derived above will therefore transform the entire inter-stellar medium into massive stars in about 4 x $10^8 {\rm L}_{\rm ir,11}^{-1}$ yr, neglecting the mass loss of these stars back into the interstellar medium and assuming no low-mass stars are formed. In this picture, the ultraluminous phase of these galaxies would therefore be only 10 million years or so. This timescale is considerably shorter than the lifetime estimated by Carico et al. (1990) from the rate of detection of double nuclei in these systems. Furthermore, the Hα luminosities observed in our sample (10^{40} - 10^{44} erg s^{-1}) would correspond to a total mass in OB stars of $\sim 10^2$ -- $10^{10} {\rm M}_\odot$ in the nuclear region alone. Including the stars with lower masses would increase these numbers by factors of 3 – 10. These masses should be detectable in studies of the nuclear velocity field of these objects. The time scales for gas depletion and the required masses in OB stars become less extreme if we only apply the starburst model to H II LIGs.

4.2. *Evidence for Outflows in Luminous Infrared Galaxies*

HAM90 have argued that many of the fourteen LIGs in their sample show evidence for violent outflows. They compared multiwavelength data on their objects with the predictions of a number of analytical and numerical models published in the literature (e.g., Castor, McCray, & Weaver 1975; Weaver et al. 1977; Chevalier & Clegg 1985: Tomisaka & Ikeuchi 1988; Mac Low & McCray 1988; Mac Low, McCray, & Norman 1989; Norman & Ikeuchi 1989) to argue that the gas motion in these objects is regulated by the interaction of supernovae-driven winds with the ambient material of the host galaxy.

In spite of the large uncertainties affecting the line width measurements from our data (cf. §2.6), there is strong evidence that violent outflow is also present in at least some of the objects in our sample. Nearly 20% of the LIGs in our sample have nuclear [O III] λ5007 line widths larger than 600 km S–l. The majority of the objects presenting such broad profiles have an AGN emission-line spectrum. Unfortunately, a quantitative comparison between the width of the observed -profiles and the line widths expected from gas motion in the gravitational field of the host galaxy is very difficult because we know so very little about the mass distribution of LIGs. Consequently, powerful tools like the Faber-Jackson and Tully-Fisher relations cannot be used to determine rigorously the importance of gravity relative to non-gravitational forces as in the case of optically-selected active galaxies (Whittle 1989a,b; Veilleux 1991a,b; Whittle 1992a, b).

Line widths can be produced by two gravitational effects: smearing of the rotation curve across the nuclear aperture or broadening effects related to the nuclear stellar velocity dispersion. In the first case, line widths larger than 600 km s^{-1} would require extremely steep velocity gradients in the nuclear region of LIGs which are not observed in normal spiral galaxies (Rubin et al. 1985; however, see Bland-Hawthorn, Wilson, & Tully 1991). In the second case, massive host galaxies with $M_B(\mathrm{bulge}) \lesssim -22$ are needed (although this value of M_B is somewhat dependent on the exact structure of the gravitational potential: Kormendy & Illingworth 1982; Kormendy 1982b; Dressier & Sandage 1983; Kormendy & Illingworth 1983). We also consider this possibility unlikely based on the late-type morphologic and the fairly modest total B magnitudes of these galaxies (e. g., Soifer et al. 1987). Line broadening due to galactic interaction also appears doubtful since no correlation between line widths and the phase of interaction was found in our sample (§2.10).

Other, perhaps more convincing evidence for non-gravitational motion in the LIGs of our sample comes from our long-slit data. In §3.5, we found that 10 of the *12* galaxies in which we could determine the radial variations of the [0 III] λ5007 line widths present broader profiles in the circumnuclear region than in the nucleus. These results suggest that some of the line-emitting gas in these galaxies is being accelerated outward. Large uncertainties in the line profiles and lack of complete two-dimensional spatial coverage prevent us from determining the exact geometry of this outflow. The detection of emission-line substructures (density enhancements) in the circumnuclear region of some of these objects suggests that most of the line emission may be produced by the '-walls" of spatially-resolved hollow structures (cf. also HAM90; Veilleux et al. 1994). Jet-induced line splitting cannot be formally excluded (e.g., Axon et al. 1989) although poorly collimated outflows arc more likely. In any case, the outflowing component is likely to interact with the ambient material of the host galaxy or with the slow-moving gas of a previous outflow event; extended LINER emission might result from this interaction (§4.1.1). The positive temperature gradient found in the two galaxies with [0 111] λ4363 strong enough to be measured outside of the nucleus also supports the possibility that shock ionization is important outside of the nucleus of some of these objects (cf. §3.4). Finally, the presence of inverted dust profiles in a few of these objects (§3.1) is also consistent with the possibility that the dust in the nuclear region of these objects has been ejected in a violent outflow event along with the gas component. Note. however, that the smaller nuclear reddening can also be explained by dust *destruction* in the nucleus or by complex optical depth effects (Leech et al. 1989; Keel 1992).

The widths of the nuclear and circumnuclear [0 III] line profiles were not found to correlate strongly with the infrared luminosity of the galaxy (§2.6 and 3.5). This result is somewhat surprising since the infrared luminosity of LIGs is a substantial fraction of their total bolometric luminosity and therefore it should be a good measure of the energy powering the outflow. A number of parameters other than the energy injection

rate are determining the outflow velocity, however. In the case of a wind-blown bubble expanding into an infinite homogeneous medium (Weaver et al. 1977). the velocity of the bubble (v in km s^{-1}) is related to the (kinetic) energy injection rate (dE/dt in erg s^{-1}) as well as the radius of the bubble (R in kpc) and the density of the medium (n_0 in c $^{-3}$ according to

$$V^3 = 3 \times 10^{-36} (dE/dt) R^{-2} n_0^{-1}. \quad (6)$$

Consequently, the lack of correlation between line widths and infrared luminosity may reflect variations in the properties of the ambient medium of the galaxies, the size (age) of the expanding bubbles, or the fraction of the bolometric luminosity which is used in powering the outflows. This last parameter probably depends on the nature of the energy source: AGN or starburst. In the case of the H II LIGs of our sample, we can use the supernova rate derived in §4.1.2 (SNR $\simeq$ 0.005 -- 1.0 yr^{-1}) and assume an energy output per supernova of $\sim 10^{51}$ erg to derive an energy injection rate of order $\sim 10^{41.2} - 10^{43.5}$ erg s^{-1} Assuming typical values for the radius of the expanding bubble of $\sim$ kpc and no $\simeq$ 10 cm^{-3}, we obtain bubble velocities $\sim 40 - 210$ km s^{-1}, which are of the same order as half the line widths observed in most of our objects. LIGs with broader emission-line profiles may require an additional source of energy such as an AGN (cf. the discussion of NGC 3079 by Veilleux et al. 1994). Note, however, that the previous calculations assume that the bubble has not "blown out" of the host galaxy. Therefore, according to Mac Low & McCray (1988) and Mac Low, McCray, & Norman (1 989), the following condition must be fulfilled:

$$D \simeq 3.0 \times 10^{-42} (dE/dt) H_{kpc}^{-2} P_7^{-3/2} n_0^{1/2} < 100, \quad (7)$$

where H_{kpc} is the scale height of the galaxy in kpc and P_7 is the ambient pressure, P/k, *in* units of 10^7 K cm^{-3}. U-sing conservative estimates ($H_{kpc} \sim 0.5$, $P_7 \sim 1 - 5$ from HAM90, and $n_0 \sim 10$), we find that this condition is satisfied when $dE/dt \lesssim 10^{43}$ erg s^{-1}, a value which probably only applies to the lower-luminosity objects in our sample. A more rigorous analysis of the ultraluminous infrared galaxies of our sample would thus require using wind flow models (e.g., Schiano 1985, 1986; Duric & Seaquist 1988; Smith 1993). We feel that the fragmentary kinematic data presented here do not warrant such an analysis.

4.3. Origin *and Evolution*

The results from the present study emphasize once again the importance of galactic interactions in LIGs (e.g., Lonsdale, Pesson, & Matthews 1984; Joseph & Wright 1985; Cutri & MacAlary 1985; Allen et al. 1985; Vader & Simon 1987; Sanders et al. 1988a; Telesco, Wolstencroft, & Done 1988; Hutchings & Neff 1988; Bushouse et al. 1988; Jones & Stein 1989; Leech et al. 1989; AHM90; Melnick & Mirabel 1990; Saunders et al. 1990; Rowan-Robinson 1991). Previous studies have also found that the nuclear

concentration of the molecular gas and the infrared luminosity per unit H_2 mass is larger for the more luminous objects and the more advanced merger systems (Telesco, Wolstencroft, & Done 1988; Bushouse et al. 1988; Young et al. 1986; Solomon & Sage 19SS; Tinney et al. 1991; Sanders, Scoville, & Soifer 1991; Scoville et al. 1991; Sanders 1992). N-body simulations show that such high nuclear concentration of molecular gas is a natural consequence of the merger of two late-type spiral galaxies (Negroponte & White 19s3: Noguchi 1988; Barnes & Hernquist 1991). Violent tidal forces resulting from the interaction triggers the" formation of a central bar which "funnels" the gas to the central kpc-scale region of the merger. However, such models have difficulties predicting the subsequent evolution of this gas concentration. Star formation (not included in the N-body simulations) is undoubtedly important in the central region of the merger. Such nuclear starbursts may disrupt the gas phase of the merger through deposition of a large amount of mechanical energy by supernovae and stellar winds. If, on the other hand, the gas concentration becomes sufficiently dense to be self-gravitating, fragmentation and instability can lead to further radial inflow (Toomre *1964;* Begelman, Blandford, & Rees 1984: Lin. Pringle, & Rees 1988; Norman & Scoville 1988; Shlosman, Frank, & Begelman 1989). In these circumstances, the physical conditions become favorable to the formation of a central massive black, hole (MBH) or to the fueling of a pre-existing black hole (Spitzer 1971; Saslaw 1973; Begelman & Rees 1978; Lightman & Shapiro 1978; Weedman 1983: Spitzer 1985, 1987; Quinlan & Shapiro 1989). An active nucleus results, further disrupting the surrounding gas through its intense radiation field, x-ray heated wind, and possible radio jets (Begelman, McKee, & Shields 1983; Begelman, Blandford. & Rees 1984).

The high frequency of AGN among advanced merger systems found in §2. 10 is indeed consistent with the formation of an active nucleus during the infrared luminous phase. On the other hand, the presence of AGN in loosely interacting systems (e. g., NG C 5256; §2.10) suggests that the formation of MBH may precede the *present* phase of merger formation in at least a few systems. However, this scenario does not exclude the possibility that the preexisting MBH was formed by a galaxy encounter at an earlier epoch. Tidal forces induced by the present galaxy interaction may be responsible for reacti~-sting these black holes before the final merger phase. Although considerable debate exists on the time scale for the formation of MBH from a nuclear starburst {e.g., Weedman 1983; Quinlan & Shapiro 1989; and references therein), this time scale may be sufficiently short to allow such a process to occur within the merging time (10^7 - 10^8 yr).

A few other results from the present study support an evolutionary sequence in which *some* of the H 11 LIGs may evolve into AGN/QSOs: (1) The amount of dust derived from the emission-line Balmer decrement is observed to be smaller in the nucleus of Seyfert LIGs than in H II objects. Four of the five objects in our sample which present a larger dust content outside of the nucleus than in the nucleus have AGX op-

tical spectra. Although the optical method used in the present study is likely to underestimate e the actual dust content of these galaxies (Leech et al. 1989; Keel 1992). this result is consistent with Seyfert LIGs being at a more advanced stage of dust destruction than H 11 galaxies. (2) Another indication that AGN LIGs may be at a more advanced stage of evolution than H II LIGs is the presence of stronger Mg Ib and $H\beta$ absorption features in the first class of objects. These features indicate that the optical continuum of AGN LIGs is produced in part by an old (10^8 – 10^9 yr) stellar population which is either not present in H II LIGs or is being swamped by a younger starburst. Note. however. that this effect is stronger among AGN LIGs with LINER characteristics. These objects were found to have a larger dust content that any other classes of LIGs. and may not be powered by a genuine AGN. The strength of the absorption features is a good indicator of the time interval since the last starburst but dots not necessarily reflect the stage of dust destruction in the nucleus.

5. SUMMARY

We have conducted a spectroscopic survey of a sample of 201 luminous IRAS galaxies (LIGs). The nuclear data, presented in Paper I, were combined with circumnuclear measurements on a subsample of 23 of these galaxies to investigate the properties of the line-emitting gas and underlying stellar population in and out of the nucleus. The main conclusions of this study can be summarized as follows:

1. It is important to use a large number of line-ratio diagnostics corrected for the underlying stellar absorption features to determine the dominant ionization process in these galaxies. The removal of these absorption features is a delicate process which has often been neglected in previous studies. We find from our analysis of the nuclear spectra that both the fraction of LIGs with AGN spectra and the fraction of Seyferts among the AGN increase with infrared luminosity, both reaching a value of 54% (Table 3). The fraction of LINERs, on the other hand, is relatively constant at ~ 25 %.

2. The origin of the line emission often is a function of the distance from the nucleus. Based on the emission-line ratios, the strengths of the stellar absorption features, and the dereddened continuum colors, circumnuclear starburst activity appears to be a common feature of LIGs, regardless of their nuclear spectral types.

3. The infrared, radio, and optical properties of LINER LIGs suggest that most of the LINER emission in these infrared-selected galaxies is produced through shock ionization rather than photoionization by a-genuine active nucleus. In contrast, the most likely ionization process in Seyfert LIGs appears to be photoionization by an AGN or Warmers. Observations at high energies ($E \gtrsim 100$ keV) will provide a good test to differentiate between these two possibilities.

4. The dust content of these galaxies was estimated using the emission-line Balmer decrement. The nuclear region of Seyfert LIGs is found to be slightly less reddened than that of LINERs and H II objects. The dust distribution generally is concentrated towards the nucleus, in agreement with the often pesky distribution of the molecular gas in these galaxies and their positive [S II] density gradients. Inverted dust profiles in which the nucleus appears less dusty than the circumnuclear region are observed in only five LIGs, four of which have AGN emission-line characteristics (1 Seyfert galaxy and 3 LINERs). A possible explanation for these results is that galaxies with Seyfert emission lines are at a more advanced stage of dust destruction/expulsion than H 11 LIGs. Complex optical depth effects may also explain these results without invoking a smaller amount of dust in the nucleus. Long-slit infrared spectroscopy and spectropolarimetry of these objects would be useful to evaluate the importance of these optical depth effects (e.g., Goldader et al. 1994; Hines 1991; Hines & Wills 1993).

5. The strengths of the nuclear $H\beta$ and Mg Ib absorption features indicate that the stellar population characterizing the nuclei of AGN (and especially the LINERs) is on average older than that of H 11 LIGs. This result is consistent with the evolutionary scenario in which some of the H II LIGs evolve into AGN LIGs.

6. We confirm the importance of galactic interaction in triggering the luminous infrared emission and perhaps also the nuclear activity in these galaxies: the ultraluminous objects and those with AGN spectra are found more frequently in advanced mergers. In at least one case (NGC 5256), however, Seyfert activity *precedes* the final merger phase of the interaction, implying perhaps that the massive black hole which is presumed to exist in this object was formed in a previous encounter and has been reactivated by the present interaction.

7. We measured the line widths of [0 III] λ5007 and $H\alpha$ to study the gas dynamics in these objects. The relatively low spectral resolution of our data prevented us from studying the other moments of the line profiles. The [O 111] profiles of both Seyfert and LINER LIGs are found to be somewhat broader on average than those of H II objects, a result also observed in optically-selected samples. Nearly 20% of the LIGs in our sample have line widths larger than 600 km s^{-1}. We find that most of the galaxies in which we can determine the radial variations of the [0 111] line widths present broader profiles in the circumnuclear region than at the nucleus. When combined with published data on a few other well-studied LIGs, these results suggest that large-scale nuclear winds are common in these objects and are an efficient way of getting rid of the obscuring material in the nuclear region. The spatially extended LINER emission observed in many of these objects is probably due to shock ionization resulting from the interaction of the wind-accelerated gas with the ambient material of the host

galaxy. Positive temperature gradients derived from the spatial variations of the [O III] $\lambda 5007/\lambda 4363$ ratio in two galaxies are consistent with this idea. The dynamical importance of non-gravitational motions in the cores of these galaxies is difficult to estimate without having complete two-dimensional coverage of these complex emission-line structures. Fabry-Perot spectroscopy has proven to be a very powerful tool in that respect thanks to its unique combination of high spectral resolution and complete spatial coverage (e.g., Veilleux et al. 1994). A few more of these objects are now being studied using this technique.

We are grateful for support of this research by NASA grant NAG5-1251 to the University of Hawaii (I). B. S., D. C. K.). S. V. gratefully acknowledge the financial support of NASA through grant number HF-1039.01-92A awarded by the Space Telescope Science Institute which is operated by the AURA, Inc. for NASA under contract No. NAS5-26555. B.T.S. is supported by grants from NASA and NSF. J.M.M. received support from the Jet Propulsion Laboratory, California Institute of Technology, under a cent ract with NASA. This research has made use of the NASA/IPAC Extragalactic Database (NED) which is operated by the Jet Propulsion Laboratory, California Institute of Technology, under contract with the National Aeronautics and Space Administration.

REFERENCES

Allen. D. A., Norris, R. P., Meadows, V. S., & Roche, P. F. 1991, MNRAS, 248, 528

Allen. D. A., Roche, P. F., & Norris, R. P. 1985, MNRAS, 213, 67p

Armus. L., Heckman, T. M., & Miley, G. K. 1989, ApJ, 347, 727

_____ 1990, ApJ, 364, 471

Ashby. M., Houck, J. R., & Hacking, P. B. 1992, AJ, *104, 980*

Axon. D. J., et al. *1989,* Nature, 341, 631

Baldwin, J. .4., Phillips, M. M., & Terlevich, R. 1981, PASP, 93, 5

Barnes, J. E., & Hernquist, L.. E. 1991, ApJL, 370, 65

Begelman, M." C., Blandford, R. D., & Rees, M. J. 1984, Rev. Mod. Phys., 56, 255

Begelman. M. C., McKee, C. F., & Shields, G. A. 1983, ApJ, 271, 70

Begelman, M. C., & Rees, M. J. 1978, MNRAS, 185, 847

Beichman, C. A., et al. 1986, ApJL, 308, 1

Bica, E., Alloin, D., & Schmidt, A. 1990, MNRAS, 242, 241

Binette. L., Dopita, M. A., & Tuohy, I. R. 1985, ApJ, 297, 476

Bland, J., & Tully, R. B. 1988, Nature, 334, 43

Bland-Hawthorn, J., Wilson, A. S., & R. B. Tully 1991, ApJL, 371, 19

Boksenberg, A., Carswell, R. F., Allen, D. A., Fosbury, R. A. E., Penston, M. V., & Sargent. W. L. W. 1977, MNRAS, 178, 451.

Bruzual, G. A. 1981, PhD Thesis, University of California, Berkeley

Bushouse. H. A., Lamb, S. A., & Werner, M. W. 1988, ApJ, 335, 74

Carico. D. P., et al. 1990, ApJL, 349, 39

Castor. R., McCray, R., & Weaver, R. 1975, ApJL, 200, 107

'Chevalier. R. A., & Clegg, A. W. 1985, Nat, 317, 44

Cid Fernandes, R., Dottori, H. A., Gruenwald, R. B., & Viegas, S. M. 1992, MNRAS. 255, 165

Condon, J. J., Anderson, M. L., & Helou, G. 1991, ApJ, 376, 95

Condon. J. J., & Broderick, J. J. 1988, AJ, 96, 30

Condon, J. J., Helou, G., Sanders, D. B., & Soifer, B. T. 1990, ApJS, 73, 359

Condon. J. J., Huang, Z.-P., Yin, Q.-F., & Thuan, T. X. 1991, ApJ, 378, 65

Condon, J. J., & Yin, Q. F. 1990, ApJ, 357, 97

Cutri, R. M., Rudy, R. J., Ricke, G. H., Tokunaga, .4. T., & Winner, S. P. 1984. ApJ. 245, 818.

Dahari, O., & De Robertis, M. M. 1988, ApJS, 67, 249

DeGioia-Eastwood, K. 1985, ApJ, 288, 175

de Grijp, M. H. K., Miley, G. K., & Lub, J. 1987, A & A Suppl., 70, 95

DePoy, D. L., Becklin, E. E., & Geballe, T. R. 1987, ApJL, 316, 63

De Robertis, M. M., Dufour, R. J., & Hunt, R. W. 1987, JRASC, 81 195.

De Robertis, M. M., & Osterbrock, D. E. 1986, ApJ, 301, 727

Diaz, A. I. 1989, in Evolutionary Phenomena in Galaxies, eds. J. E. Beckman and B. E. J. Pagel, (Cambridge: Cambridge University Press), p. 377

Diaz, A. I., Pagel, B. E. J., & Terlevich, E. 1985a, MNRAS, 214, 41p

Diaz, .4. 1., Pagel, B. E. J., & Wilson, I. R. G. 1985b, MNRAS, 212, 737

Dressler, .4., & Sandage, .4. 1983, ApJ, 265, 664

Duric, N. & Seaquist, E. R. 1988, ApJ, 326, 574

Edmunds, M. G. 1989, in Evolutionary Phenomena in Galaxies, eds. J. E. Beckman and B. E. J. Pagel, (Cambridge: Cambridge University Press), p. 356

Elson, R. .4. W., Fall, S. M., & Freeman, K. C. 1989, ApJ, 336, 734

Fabbiano, G., Heckman, T. M., & Keel, W. C. 1990, ApJ, 355, 442

Ferland, G. J., & Mushotzky, R. F. 1984, ApJ, 286, 42

Ferland, G. J., & Netzer, H 1983, ApJ, 264, 105

Filippenko, A. V. 1985, ApJ, 289, 475

_____ *1989,* in Active Galactic Nuclei, ed. D. E. Osterbrock and J. S. Miller, (Dordrecht: Kluwer), 495

_____ 1991, in Relationships between Active Galactic Nuclei and Starburst Galaxies, cd. A. V. Filippenko, (San Franscisco: Astronomical Society of the Pacific). 253

Filippenko, .4. V., & Halpern, J. P. 1984, ApJ, 285, 458

Filippenko, A. V., & Sargent, W. L. W. 1985, ApJS, 57, 503

_____. *1986,* in Structure and Evolution of Active Galaxies, eds G. Giuricin et al., (Dordrecht: Reidel), 21

_____ 1988, ApJ, 324, 134

.- —.—._-. 1992, AJ, 103, 28

Filippenko, .4. V., & Terlevich, R. 1992, ApJL, 397, 79

Ford. H. C., Dahari, O., Jacoby, G. H., Crane, P. C., & Ciardullo, R. 1986, ApJL. 311.7

French. H.B. 1980, ApJ, 240, 41

Gallagher, J. S., Hunter, D. A., & Tutokov, A. V. 19S4, ApJ, 2S4, 544

Gherz. R. D., Sramek, R. .4., & Weedman, D. W. 1983, ApJ, 267, 551.

Goldader, J. D., Joseph, R. D., Doyon, René, & Sanders, D. B. 1994, ApJ, submitted

Hacking. P., Condon, J. J., & Houck, J. R. 19S7, ApJL, 316, 15

Halpern, J. P., & Steiner, J. E. 1983, ApJL, 269, 37

Harwit. M. O., Houck, J. R., Soifer, B. T., & Palumbo, G. G. C. 1987, ApJ, 315, 28

Heckman. T. M. 1980, A&A, 87, 152

_____ 1987, in Observational Evidence of Activity in Galaxies, ed. Ye. Khachikian et al., (Dordrecht: Kluwer), 421

_____ 1991, in Massive Stars in Starbursts, eds. C. Leitherer, N. R. Walborn, T. M. Heckman, and C. .4. Norman, (Cambridge: Cambridge University Press), p. 289

Heckman, T. M., Armus, L., & Miley, G. K. 1987, AJ, 92, 276

_____ 1990, ApJS, 74, 833 (HAM90)

Heckman, T. M., Balick, B., & Crane, P. C. 19S0, A&A Suppl., 40, 295

Heiles C. 1990, ApJ, 354, 4S3

Hclou. G., Soifer, B. T., & Rowan-Robinson, M. 1985, ApJL, 298, 7

Hill, G. J. Heasley, J. H., Becklin, E. E., & Wynn-Williams, C. G. 19SS, AJ, 95, 1031

Hines. D. C. 1991, ApJL, 374, 9

Hines. D. C., & Wills, B. J. 1993, ApJ, 415, 82

Ho, L. C., Filippenko, .4. V., & Sargent, W. L. W. 1993, ApJ, 417, 63

Houck. J. R., et al. 1984, ApJL, 278, 63

Houck. J. R., et al. 1985, ApJL, 290, 5

Hunter. D. .4., et al. 1986, ApJ, 303, 171

Innes. D. E. 1992, A&A, 256, 660

Irwin, J. A., & Seaquist, E. R. 198S, ApJ, 335, 658

Jacoby. G. H., Hunter, D. A., & Christian, C. A. 1984, ApJS, 56, 256

Joseph. R. D., & Wright, G. S. 1985, MNRAS, 214, 87

Keel. W. C. 1983, ApJ, 269, 466

_____ 1992, in Massive Stars: Their Lives in the ISM, eds. J. P. Cassinelli and E. B. Churchwell, (San Francisco: Astronomical Society of the Pacific), 49S

Keel. W. C., Kennicutt, R. C. Jr., Hummel, E., van der Hulst, J. M. 1985, AJ. 90. 708

Kennicutt, R. C. 1983, ApJ, 272, 54

_____ 1984, ApJ, 277, 361

Kennicutt, R. C. Jr., Keel, W. C., & Blaha, C. A. 1989, AJ, 97, 1022

Kim. D.-C., Sanders, D. B., Veilleux, Sylvain, Mozzarella, J. M., & Soifer, B. T. 1994. ApJS, submitted (Paper I)

Koo, B.-C., & McKee, C. F. 1992a, ApJ, 388, 93

_____ 1992b, ApJ, 388, 103

Kormendy, J., & Illingworth, G. D. 1982, ApJ, 256, 460

_____ *1983,* ApJ, *265, 632*

Kormendy, J., & Sanders, D. B. 1992, ApJL, 390, 53

Koski. A. T. 1978, ApJ, 223, 56

Lawrence, A., et al. 1985, ApJ, 291, 117

Lawrence, A., et al. 1989, MNRAS, 240, 329

Leech. K. J., et al. 1989, MNRAS, 240, 349

Leech. K. J., Rowan-Robinson, M., Lawrence, A., & Hughes, J. D. 1991, in Dynamics of Galaxies and Their Molecular Cloud Distributions, ed. F. Combes and F. Casoli (Dordrecht: Kluwer), p. 432

Lightman, A. P., & Shapiro, S. L. 1978, Rev. Mod. Phys., 50, 437

Lin, D. N. C., Pringle, J. E., & Rees, M. J. 1988, ApJ, 328, 103

Lonsdale, C. J., Smith, H. E., & Lonsdale, C. J. 1993, ApJL, 405, 9

Mackenty, J. W., & Stockton, .4. 1984, ApJ, 283, 64

Mac Low, M.-M., & McCray, R. 1988, ApJ, 324, 776

Mac Low, M.-M., McCray, R., & Norman, M. I,. 1989, ApJ, 337, 141

Maeder, A. 1990, in Massive Stars and Starburst Galaxies, ed. C. Leitherer, N. R. Walborn, T. M. Heckman, & C. A. Nor-man (Cambridge: Cambridge University Press), 97

Mazzarella, J. M., & Bothun, G. D. 1989, in Active Galactic Nuclei, ed. D. E. Osterbrock and J. S. Miller (Dordrecht: Kluwer), 490

Mazzarella, J. M., Bothun, G. D., & Boroson, T. A. 1991, AJ, 101, 2034

McCall, M. L., Rybski, P. M., & Shields, G. A. 1985, ApJS, 57, 1

McCarthy, P. J., Heckman, T. M., & van Breugel, W. 1987, AJ, *92, 264*

Melnick, J., & Mirabel, I. F. 1990, A & A, 231, L19

Miley, G., et al. 1984, ApJL, 278, 79

Miley, G. K., Neugebauer, G., & Soifer, B. T. 1985, ApJL, 293, 11

Mirabel, I. F., & Sanders, D. B. 1988, ApJ, 335, 104

Morris, S. L., & Ward, M. J. 1988, MNRAS, 230, 639

Mouri, H., & Taniguchi, Y. 1992, ApJ, 386, 68

Negroponte, J., & White, S. D. M. 1983, MNRAS, 205, 1009

Neugebauer, G., Soifer, B. T., & Miley, G. K. 1985, ApJL, 295, 27

Noguchi, M. 1988, A&A, 203, 259

Nor-man, C. "A., Ikeuchi, S. 1989, ApJ, 345, 372

Norman, C. A., & Scoville, N. 1988, ApJ, 332, 124

Norris. R. P., et al. 1990, ApJ, 359, 291

Norris. R. P., Kesteven, M. J., Allen, D. A., & Troupe, E. 1988, MNRAS, 234, 51p

Osterbrock, D. E. 1989, Astrophysics of Gaseous Nebulae and Active Galactic Nuclei (Mill Valley: University Science Books)

Osterbrock, D. E., Shaw, R. A., & Veilleux, S. 1989, ApJ, 352, 561

Osterbrock, D. E., Tran, H. D., & Veilleux, S. *1992,* ApJ, 389, 196

Persson, C. J., & Helou, G. 1987, ApJ, 314, 513

Phillips, et al. 1986, AJ, 91, 1062

Quinlan, G. D. & Shapiro, S. L. 1989, ApJ, 343, 725

Radford, S. J. E., Solomon, P. M., & Dowries, D. 1991, ApJL, 368, 15

Rice, W. L., et al. 1988, ApJS, 68, 91

Rieke, G. H., et al. 1985, ApJ, 290, 116

Rieke, G. H. 1988, ApJ, 331, L5

Rieke, G. H., & Low, F. J. 1972, ApJL, 176, 95

Rowan-Robinson, M., et al. 1991, Nature, 351, 719

Rubin. V. C., et al. 1985., ApJ, 289, 81

Sandage, A., & Tammann, G. A. 1987, A Revised Shapley-Ames Catalog of Bright Galaxies, second edition (Carnegie Institution of Washington, Washington)

Sanders, D. B. 1991, in Dynamics of Galaxies and Their Molecular Cloud Distributions, ed. F. Combes and F. Casoli (Dordrecht: Kluwer), 417

Sanders. D. B. 1992, in Relationships between Active Galactic Nuclei and Starburst Galaxies, ed. A. V. Filippenko, (San Franscisco: Astronomical Society of the Pacific), 303

Sanders, D. B., Egami, E., Lipari, S., Mirabel, I. F., & Soifer, B. T. 1994a, ApJ, submitted.

Sanders, D. B., Scoville, N. Z., & Soifer, B. T. 1991, ApJ, 370, 158

Sanders, D. B., Soifer, B. T., Egami, E., Mirabel, I. F., & Lipari, S. 1994b, ApJ, submitted.

Sanders, D. B., Soifer, B. T., Elias, J. H., Madore, B. F., Matthews, K., Neugebauer, G., & Scoville, N. Z. 1988a, ApJ, 325, 74

Sanders, D. B., Soifer, B. T., Elias, J. H., Neugebauer, G., & Matthews, K. 1988b, ApJL, 328, 35

Saslaw. W. C. 1973, PASP, 85, 5

Saunders, W., et al. 1990, MNRAS, 242, 318

Schiano. A. V. R. 1985, ApJ, 299, 24

Scoville. N., & Norman, C. 1988, ApJ, 332, 163

Scoville. N. Z., Sargent, .4. I., Sanders, D. B., & Soifer, B. T. 1991, ApJL, 366, 5

Sekiguchi, K. *1987,* ApJ, 316, 145

Shields. J. C. 1992, ApJL, 399, 27

Shlosman, I., Frank, J., & Begelman, M. C. 1989, Nature, 338, 45

Shull, J. M., & McKee, C. F. 1979, ApJ, 227, 131

Smith. S. J. *1993,* ApJ, preprint

Soifer. B., Boehmer, L., Neugebauer, G., & Sanders, D. 1989, AJ, 98, 766

Soifer. B. T., & Neugebauer, G. 1991, AJ, 101, 354

Soifer. B. T., Sanders, D. B., Madore, B. F., Neugebauer, G., Danielson, G. E., Elias. J. H.. Lonsdale, C. J., & Rice, W. 1..1987. ApJ, 320, 238

Soifer. B. T., Sanders, D. B., Neugebauer, G., Danielson, G. E., Lonsdale. C. J.. Madore. B. F. & Persson, S. E. 1986, ApJL, 303, 41

Soifer. B. T., et al. 1984a, ApJL, 278, 71

Soifer. B. T., et al. 1984b, ApJL, 283, 1

Solomon. P., Radford, S., & Dowries, D. 1990, ApJL, 348, 53

Solomon. P. M., & Sage, L.. J. 1988, ApJ, 334, 613

Spitzer. L. 1971, in Nuclei of Galaxies, ed. D. O'Connell (Amsterdam: North-Holland), p. 443

_____ 1985, in IAU Symposium 113, Dynamics of Star Clusters, ed. J. Goodman and P. Hut (Dordrecht: Reidel), p. 109

_____ 1987, Dynamical Evolution of Globular Clusters (Princeton: Princeton University Press)

Stasinska. G. 1984a, A&.4 Suppl., 55, 15

Stasinska. G. 1984b, A&A, 135, 341

Stauffer, J. R. 1982, ApJS, 50, 517

Stockton. A. 1990, in Dynamics and Interactions of Galaxies, ed. R. Wielen (Berlin: Springer), 440

Telesco, C. M., Wolstencroft, R. D., & Done, C. 1988, ApJ, 329, 174

Tenorio-Tagle, G., & Bodenheimer, P. 1988, ARAA, 26, 145

Tenorio-Tagle, G., Bodenheimer, P., k Rózyczka 1987, A&A, 182, 120

Tenorio-Tagle, G., Terlevich, R., France, J., & Melnick, J. 1992, in Relationships between Active Galactic Nuclei and Starburst Galaxies, ed. .4. V. Filippenko, (San Franscisco: Astronomical Society of the Pacific), 147

Terlevich. R. 1992, in Relationships between Active Galactic Nuclei and Starburst Galaxies, ed. A. V. Filippenko, (San Franscisco: Astronomical Society of the Pacific), 133

Terlevich. E., Díaz, A. I., & Terlevich, R. 1990, MNRAS, 242, 271

Terlevich. R., & Melnick, J. 1985, MNRAS, 213, 831

Terlevich. R., Melnick, J., & Moles, M. 1987, in Observational Evidence of Activity in Galaxies, cd. E. Ye. Khachikian et al. (Dordrecht: Kluwer), 499

Terlevich. R., Tenorio-Tagle, G., France, J., & Melnick, J. 1992, MNRAS, 255, 713

Thomsen. B. & Baum, W. A. 1987, ApJ, 315, 460

Thronson. H. A., Majewski, S., Descartes, L., & Hereld, M. 1990, ApJ, 364, 456

Tinney, C. G., et al. 1990, ApJ, 362, 473

Tomisaka, K., & Ikeuchi, S. 1988, ApJ, 330, 695

Toomre, A. 1964, ApJ, 139, 1217

Vader, J. P., & Simon, M. 1987, Nature, 327, 304

van der Kruit, P. C. 1973, A&A, 29, 263

Veilleux, S. 1991a, ApJS, 75, 383

——— 1991b, ApJ, 369, 331

Veilleux, S., Cecil, G., Tully, R. B., Bland-Hawthorn, J., & Filippenko, A. V., & Sargent, W. L. W. 1994, ApJ, in press

Veilleux, S., & Osterbrock, D. E. 1987, ApJS, 63, 295

Weaver, R., et al. 1977, ApJ, 218, 377

Weedman, D. W. *1983,* ApJ, *243, 756*

Whittle, M. 1985a, MNRAS, 213, 1

——— 1985b, MNRAS, 213, 33

——— 1989a, in Highlights Astr., 8, 423

——— 1989b, in IAU Symposium 134, Active Galactic Nuclei, ed. D. E. Osterbrock & J. S. Miller (Mill Valley: Univ. Science Books), 349

——— 1992a, ApJ, 387, 109

——— 1992b, ApJ, 387, 121

Wills, B. J., et al. 1993, ApJ, 400, 96

Wilson, A. S., Helfer, T. T., Haniff, C. A., & Ward, M. J. 1991, ApJ, 381, 79

Wyse, R. F. G. 1985, ApJ, 299, 593

Wunderlich, E., Klein, U., & Wielebinski, R. 1987, A&AS, 69, 487

Wynn-Williams, C. G., & Becklin, E. E. 1993, ApJ, 412, 535

Young, J. S., Schloerb, F. P., Kenney, J. D., & Lord, S. D. 1986, ApJ, 304, 443

Young, J. S., Claussen, M. J., & Scoville, N. Z. 1987, ApJ, 324, 115

FIGURE CAPTIONS

Figure 1. Distribution of the color excesses for the CBGSs (solid line) and WGSs , short-dash line) galaxies of our sample. The CBGSs galaxies are slightly more reddened than the WGSS galaxies.

Figure 2. Distribution of the color excesses as a function of spectral types. The Seyfert 2 galaxies are slightly less reddened than the other galaxies.

Figure 3. Equivalent widths of Na ID as a function of the equivalent widths of Mg Ib. The stars are the H II galaxies, the open circles are the LINERs, and the filled circles are the Seyfert galaxies. There is no obvious correlation for any of the galaxies.

Figure **4.** Color excesses as a function of the equivalent widths of Na ID for each spectral type. The meaning of the symbols is the same as in Fig. 3. A correlation is observed.

Figure **5.** Color excesses as a function of the observed continuum colors for each spectral type. The continuum color is defined as the ratio of the continuum level near $H\alpha$ to the continuum level near $H\beta$. The meaning of the symbols are the same as in Fig. 3. A correlation is observed.

Figure 6. Dereddened *flux* ratios as a function of infrared luminosities for single nucleus systems in (a) the CBGSs sample and (b) the WGSS sample. The open squares represent galaxies with $\log(L_{ir}/L_{\odot}) < 11$, the squares with an "X" in the middle are galaxies with $11 \leq \log(L_{ir}/L_{\odot}) \leq 12$, and filled squares are galaxies with $\log(L_{ir}/L_{\odot}) > 12$. H II galaxies (H) are located to the left of the solid curve while AGN are located to the right of that curve. AGN were further classified as Seyferts or LINERs depending on whether or not [O III] $\lambda 5007/H\beta \geq 3$ (indicated by a solid horizontal segment). The filled square with an arrow pointing upward in the CBGSs sample is Arp 220.

Figure 7. Dereddened flux ratios involving [0 II] $\lambda 3727$/[O III] $\lambda 5007$. Meaning of the symbols are the same as in Fig. 6.

Figure **8.** Summary of the results of the spectral classification as a function of the infrared luminosity.

Figure 9. Distribution of the $H\alpha$ luminosities for each spectral type. The average $H\alpha$ luminosity of LINERs is somewhat smaller than that of H II galaxies.

Figure 10. Distribution of the Hα equivalent widths for each spectral type. The average Hα equivalent widths of LINERs is significantly smaller than that of H II galaxies.

Figure 11. Distribution of the ratios of the reddening-corrected Hα luminosities to the infrared luminosities for each spectral type. Note the larger scatter among Seyferts and (to a lesser extent) LINERs.

Figure 12. Distribution of the electron density for each spectral type.

Figure 13. [0 III] λ5007 line widths as a function of the infrared luminosities for each spectral type. The meaning of the symbols is the same as in Fig. 3. The objects with large [0 111] λ5007 line widths generally have high infrared luminosity.

Figure 14. Distribution of [O III] λ5007 line widths for each spectral type. "The average line of H II galaxies is somewhat smaller than that of the LINERs and (to a lesser extent) the Seyfert 2 galaxies.

Figure 15. Distribution of the equivalent widths of Mg Ib for each spectral type. LINERs have significantly larger Mg Ib equivalent widths than H 11 galaxies. Seyfert galaxies have intermediate values.

Figure 16. Distribution of dereddened continuum colors, $(C6563/C4861)_0$, for each spectral type. No significant difference is observed between these various distributions.

Figure 17. Continuum colors as a function of the infrared luminosities. (a) observed colors, (b) dereddened colors. There is a weak tendency for the dereddened colors to decrease with increasing infrared luminosity.

Figure 18. Continuum colors as a function of the Hα equivalent widths in emission. (a) observed colors, (b) dereddened colors. H 11 objects with large Hα equivalent widths present blue observed continuum colors.

Figure 19. Dereddened continuum colors as a function of the equivalent widths of Mg Ib for each spectral type. The meaning of the symbols is the same as in Fig. 3.

Figure 20. Logarithmic FIR-radio flux-density ratios as a function of the infrared luminosities for each spectral type. The meaning of the symbols is the same as in Fig. 3.

Figure 21. Logarithmic radio-Ha flux-density ratios as a function of the infrared luminosities for each spectral type: (a) using observed Hα fluxes, (b) using dereddened Hα fluxes. The value expected for free-free emission from a 10000 K extinction-free gas is 12.

Figure 22. Distribution of the Hα equivalent widths in emission as a function of the interaction class. Galaxies with an asymmetric or distorted appearance. but no evidence of a close-by companion have IAC = 2; galaxies with an ongoing interaction as judged from the presence of two overlapping or nearby galaxies have IAC = 3: and advanced merger systems as indicated by the presence of tidal tails or shells around a single stellar system correspond to IAC = 4.

Figure 23. Dereddened flux ratios for double nucleus systems. The meaning of the symbols and the solid lines is the same as in Fig. 6.

Figure 24. IRAS color-s as a function of [0 I] λ6300/Hα. The meaning of the symbols is the same as in Fig. 3. There is no strong correlation for any spectral type.

Figure 25. IRAS colors as a function of [0 III] λ5007/Hβ. The meaning of the symbols is the same as in Fig. 3. There is no strong correlation for any spectral type.

Figure **26.** IRAS colors as a function of the equivalent width of Hα in emission. The meaning of the symbols is the same as in Fig. 3. Correlations are observed among H II galaxies and possibly also among Seyfert 2 galaxies.

Figure 27. Infrared luminosity, IRAS 60-to-100 μm flux ratio and color excess as a function of the optical-to-infrared luminosity ratio. The meaning of the symbols is the same as in Fig. 3. A negative correlation is observed among the H II galaxies in all three panels.

Figure 28. Same as Fig. 26 except that the optical continuum luminosities have now been corrected for dust extinction using the emission-line Balmer decrements. The meaning of the symbols is the same as in Fig. 3. A strong positive correlation is observed in the lower panel.

Figure **29.** Radial profiles of the color excess. The asterisks are the nuclear values and the numbers correspond to the objects listed in Table 6.

Figure 30. [0 III] λ5007/Hβ versus [N II] λ6583/Hα as a function of the size of the extraction aperture (top panel), and the distance from the nucleus (lower panel). In

both panels, the asterisks mark the nuclear values and the numbers correspond to the objects listed in Table 6. In the top panel, the size of the extraction aperture doubles between each data point while, in the lower panel, it is the mid-dist ante of the extraction aperture from the nucleus which doubles.

Figure 31. [0 III] $\lambda 5007/\mathrm{H}\beta$ versus [S 11] $\lambda\lambda 6716, 6731/\mathrm{H}\alpha$ as a function of the size of the extraction aperture (top panel), and the distance from the nucleus (lower panel). In both panels, the asterisks mark the nuclear values and the numbers correspond to the objects listed in Table 6. In the top panel, the size of the extraction aperture doubles between each data point while, in the lower panel, it is the mid-distance of the extraction aperture from the nucleus which doubles.

Figure 32. [0 III] $\lambda 5007/\mathrm{H}\beta$ versus [0 1] $\lambda 6300/\mathrm{H}\alpha$ as a function of the size of the extraction aperture (top panel), and the distance from the nucleus (lower panel). In both panels, the asterisks mark the nuclear values and the numbers correspond to the objects listed in Table 6. In the top panel, the size of the extraction aperture doubles between each data point while, in the lower panel, it is the mid-distance of the extraction aperture from the nucleus which doubles.

Figure 33. Radial profiles of the electron density. The asterisks are the nuclear values and the numbers correspond to the objects listed in Table 6.

Figure 34. Radial profiles of the electron temperature derived from the [0 III] $\lambda 4363/\lambda 5007$ flux ratio. The temperatures are given for two electron densities (103 and 10^6 cm^{-3}) The asterisks are the nuclear values.

Figure 35. Radial profiles of the [0 111] $\lambda 5007$ line widths. The asterisks are the nuclear values and the numbers correspond to the order in Table 6. Note that, in many cases, the line widths reach a maximum *outside* of the nucleus.

Figure 36. Radial profiles of the $\mathrm{H}\alpha$ line widths. The asterisks are the nuclear values and the numbers correspond to the order in Table 6.

Figure 37. Radial profiles of the equivalent widths of Mg Ib. The asterisks are the nuclear values and the numbers correspond to the order in Table 6. The Mg Ib equivalent widths are lower at all radii than the value typically found in non-active spiral galaxies (~ 4 Å).

Figure 38. Radial profiles of $\mathrm{EW}(\mathrm{H}\beta_{\mathrm{abs}})$ in the galaxies of our sample. The asterisks are the nuclear values and the numbers correspond to the order in Table 6.

Figure 39. Radial profiles of the observed continuum colors. The asterisks are the nuclear values and the numbers correspond to the order in Table 6. Note the general tendency for the observed colors to be redder in the nuclei.

Figure 40. Radial profiles of the dereddened continuum colors. The asterisks are the nuclear values and the numbers correspond to the order in Table 6. The vertical dotted, short-dashed, and long-dashed lines represent the continuum colors of star clusters with ages O (ZAMS), 10^7, and 10^9 yr, respectively.""

Figure 41. [0 III] λ5007 line widths as a function of [N 11] λ6583/Hα, [S 11] $\lambda\lambda$6716, 6731/Hα, and [0 I] λ6300/Hα.

Table 1a. Observed and Dereddened Line Ratios, Densities, Spectral Classification - IRAS Bright Galaxies

Name	H_α / H_β	E(B-V)	[OIII] / H_β	[NII] / H_α	[s11] / H_α	[01] / [OIII]	[OII] / 6731	6731 / 6716	N_e	Spectral Types [NII]	[SII]	[OI]	Adopted
(1)	(2)	(3)	(4)	(5)	(6)	(7)	(8)	(9)	(10)	(11)	(12)	(13)	(14)
*NW 23	5.89	0.74	-0.38	-0.23	-0.49	-1.44	—	0.95	480	H	H	H	H
	2.85		-0.42	-0.23	-0.51	-1.41	---	0.95					
*NGC 34	24.55	2.08	0.60	0.11	-0.27	-1.03	—	0.55	a	S2	S2	S2	S2
	3.10		0.50	0.10	-0.33	-0.93	--	0.55					
● MCG-0JOI051S	6.92	0.90	-0.15	-0.35	-0.58	-1.54	---	0.91	390	}1	H	H	H
	2.85		-0.20	-0.36	-43.60	-1.50	--	0.91					
● N4CGW3105IN	4.27	0.40	-0.59:	-0.43	-0.71	-1.75	—	0.74:	80:	H	H	H	H
	2.85		-0.61:	-0.43	-0.72	-1.73	---	0.74:					
'NGC 232	10.47	1.31	0.24	-0.13	-0.67	-1.37		- ·	—	I.	H	H	H:
	2.85		0.18	-0.14	-0.71	-1.31	---	---					
* UGC 555	9.77	1.15	--0.14	-0.22	-0.28	-0.90	---	0.83	250	L	L	L	L
	3.10		-0.20	-0.23	-0.31	-0.84	--	0.83					
*IC 1625\	3.98	0.32	0.12	-0.56	-0.58	-1.45	—	0.28:	a	H	H	H	H
	2.85		0.10	-0.56	-0.59	-1.43	—	0.28:					
● IC 1623SE	3.47	0.20	0.37	-0.67	-0.62	-1.56	-1.30:	0.71	40	H	H	H	H
	2.85		0.36	-0.67	-0.63	-1.55	-1.21:	0.71					
*MCG-W4014	8.51	1.10	-0.37	-0.28	-0.63	-1.66	—	0.85	260	H	H	H	H
	2.85		-0.42	-0.29	-0.66	-1.61	—	0.83					
* MCG +0294025	8.71	1.12	-0.01	-0.40	-0.51	-1.41	0.25	0.79	160	H	H	H	H
	2.85		-0.06	-0.41	-0.54	-1.36	0.73	0.78					
*UGC 903	9.33	1.18	-0.07	-0.34	-0.42	-1.40:	--	0.83	230	H	L	H	H:
	2.85		-0.13	-0.35	-0.46	-1.34:		0.81					
*NGC 520	32.36	2.37	—	-0.15	-0.26	-1.27	---	0.76	110	—	---	---	—
	3.10			-0.16	-0.33	-1.15	—	0.74					
● IR 01364-1042	10.96:	1.27:	0.27:	-0.01:	-0.19:	-0.53:	---	0.68	a	L	L	L	L
	3.10		0.21:	-0.02:	-0.23:	-0.46:		0.68					
•NGC 660	16.60	1.69	0.42	0.01	-0.32	-1.21		0.91	410	L	L	L	L
	3.10		0.34	0.00	-0.37	-1.12	—	0.91					
*III Zw 35S	10.00;	1.18;	0.12;	0.02	-0.27	-0.74	—	1.00	590	L	L	L	L
	3.10		0.07;	0.01	-0.31	-0.68		1.00					
'III Zw 35N	3.89	0.31	0.29	-0.72	-0.51	-1.35		0.65	a	H	H	H	H
	2.85		0.28	-0.72	-0.52	-1.33		0.65					
* NGC 695	7.94	1.03	-0.50	-0.35	-0.77	-1.28	---	0.69	a	H	H	H	H
	2.85		-0.55	-0.35	-0.80	--1.23	--	0.68					
•NGC 873	8.71	1.13	-0.27	-0.33	-0.61	-1.75		0.71	30	H	H	H	H
	2.85		-0.33	-0.33	-0.64	-1.69	—	0.71					
NGC 1050	6.17	0.77	-0.48	-0.23	-0.60	-1.64		0.91	390	H	H	H	H
	2.85		-0.51	-0.24	-0.62	-1.60		0.91					
NGC 1056	6.61	0.85	-0.10	-0.41	-0.43	-1.38	—	0.76	110	H	H	H	H
	2.85		-0.14	-0.42	-0.46	-1.34		0.76					
•NGC 1068	6.17:	0.68:	1.19	0.11:	-0.47:	-0.92:		- - -		S2	S2	S2	S2
	3.10		1.16	0.10:	-0.49:	-0.89:	--	-					
*NGC 1083	5.50	0.65	-0.26	-0.40	-0.42	-1.28	1.62	.0.71	20	H	H	H	H
-.	2.85		-0.29	-0.41	-0.44 "	-1.25	1.90"	0.69					
● UGC 2238	29.51:	2.25:	0.30:	-0.20	-0.43:	-1.09		---	—	L	L	L	L
	3.10		0.20:	-0.21	-0.50:	-0.97							
*IR 02 -2122	25.70.	2.13:	0.51:	0.14	-0.47:	-0.81:		---	---	L	L	L	L
	3.10		0.41:	0.13	-0.54:	-0.70:		—					
*UGC 2369	6.92	0.88	-0.35	-0.28	-0.65	-1.70		0.63	a	H	H	H	H
	2.85		-0.40	-0.28	-0.67	-1.65		0.63					

Table la. Observed and **Dereddened** Line Ratios, Densities, Spectral Classification - IRAS Bright Galaxies

Name	H_α / H_β	E(B-V)	[OILI] H_β	[ND] H_α	[S11] H_α	[01] H_α	[OII] [OIII]	6731 / 6716	N_e	Spectral Types [NII]	[SII]	[OI]	Adopted
(1)	(2)	(3)	(4)	(5)	(6)	(7)	(8)	(9)	(lo)	(11)	(12)	(13)	(14)
NGC 1143/44	4.90	0.47	1.13	0.34	0.06	-0.72	—	---	—	S2	S2	S2	S2
	3.10		1.11	0.34	0.04	-0.70	—	—					
* UGC 2403	15.14	1.67	-0.27	-0.27	-0.56	-1.41	—	0.83	240	H	H	H	H
	2.85		-0.35	-0.28	-0.61	-1.33	—	0.83					
NGC 1204	17.38	1.74	-0.38	-0.10	-0.40	-1.19	—	1.17:	1060:	L	L	H	L:
	3.10		-0.47	-0.11	-0.45	-1.10	—	1.17:					
NGC 1266	5.75:	0.62:	0.11:	0.57	0.23	-0.49	—	1.02	640	L	L	L	L
	3.10		0.08:	0.57	0.21	-0.46	—	1.02					
NGC 1377	1.00	—	—	0.59:	0.31:	—	—	0.58	a	—	—	—	—
	3.10		—	—	—		—	—					
IR 03359-1523	5.37	0.65	0.06	-0.46	-0.70	-1.73	-0.10	0.89	370	H	H	H	H
	2.85		0,03	-0.46	-0.72	-1.70	0,18	0.89					
UGC 29S2	18.62	1.89	-0.56	-0.37	-0.45	-1.71	—	0.74	90	H	H	H	H
	2.85		-0.65	-0.38	-0.51	-1.62	—	0.74					
ESO 550-IG025S	9.55	1.13	-0.45	-0.11	-0.42	-1.16	—	0.65	a	L	H	L	L:
	3.10		-0.51	-0.11	-0.45	-1.11	—	0.63					
ESO 550-IG025N	9.12	1.09	-0.17	-0.20	-0.40	-1.04	—	0.74	100	L	L	L	L
	3.10		-0.22	-0.20	-0.44	-0.98	—	0.74					
NGC 1614	7.59	0.99	-0.12	-0.22	-0.69	-1.78	—	1.02	660	H	H	H	H
	2.85		-0.17	-0.22	-0.72	-1.73	—	1.02					
IR 04335-2514	29.51:	2.27:	—	0.04	-0.15	-1.01	—	1.35:	1630:	—	—	—	—
	3.10		—	0.02	-0.22	-0.90	—	1.32:					
ESO 485-G003	5.75	0.71	-0.50	-0.46	-0.53	-1.70	—	0.85	290	H	H	H	H
	2.85		-0.54	-0.46	-0.56	-1.66	—	0.85					
IC 398	1.00			0.00	-0.32	-1.25:		0.60	a		—	—	
	3.10		---	—	—	—	—	—					
NGC 1797	8.71	1.13	-0.80	-0.27	-0.60	-1.61	—	0.98	530	H	H	H	11
	2.85		-0.85	-0.28	-0.63	-1.55	—	0.98					
IR 05186-1017	23.99:	2.05:	0.17:	0.10	-0.17	-0.92	—	—	—	L	L	L	L
	3.10		0.07:	0.09	-0.23	-0.81	—	—					
IR 05189-2524	23.44:	2.03:	1.63:	0.04	-0.66	-1.22	—	0.39	a	S2	S2	S2	S2
	3.10		1.53:	0.03	-0.72	-1.12	—	0.39					
NGC 2388	10.96	1.36	-0.82	-0.24	-0.58	-1.66	—	0.98	510	H	H	H	H
	2.85		-0.89	-0.24	-0.62	-1.59	—	0.95					
IR 08339-5517	4.27	0.40	0.24	-0.58	-0.61	--1.84	0.15:	0.76	110	H	H	H	}1
	2.85		0.22	-0.59	--0.62	-1.82	0.32:	0.76					
NGC 2623	1.00	—	—	-0.01	-0.22	-0.99	—	—			—	—	
	3.10		...				—						
IR 08572.3915	9.12	1.17	0.37	-0.37	-0.35	-1.34	—	0.65	a	H	L	L	1.:
	2.85		0.31	-0.38	-0.39	-1.28		0.65					
NGC 2785	14.79	1.66	-0.29	-0,22	-0.42	-1.31	—	0.85	280	L	H	H	H:
	285		-0.37	-0.23	-0.47	-1.23		0.85					
UGC 4881 SW	12.59	1.50	-0.26	-0.19	-0.49	-1.34	—	.0.81	210	L	H	H	11:
	2.85		-0.33	-0.20	-0.54	-1.26	—	0.81					
UGC 4881 NE	9.55	1.21	70.49:	-0.14	-0.52	-1.31		0.76	110	L	H	H	H:
	2.85		-0.55:	-0.15	-0,56	-1.24	—	0.76					
UGC 5101	23.44	2.04	0.46	0.13	-0.38	-1.05	0.20:	0.41	a	L	L	L	1.
	3.10		0.36	0.12	-0.45	-0.95	1.06:	0.41					
MCG+0818012	8.91	1.15	-0.18	-0.22	-0.54	-1.35	—	0.87:	310:	L	H	H	11:
	2.85		-0.23	-0.23	-0.58	-1.30	—	0.87:					

Table 1a. Observed and **Dereddened Line** Ratios, Densities, Spectral Classification - **IRAS** Bright **Galaxies**

Name	H_α / H_β	E(B-V)	[OILI] / H_β	[NII] / H_α	[SII] / H_α	[OI] / H_α	[011] / [OILI]	6731 / 6716	N_e	Spectral Types [NII]	[SII]	[01]	Adopted
(1)	(2)	(3)	(4)	(5)	(6)	(7)	(8)	(9)	(10)	(11)	(12)	(13)	(14)
NGC 3110	6.92	0.89	-0.91	-0.38	-0.63	-1.62:	—	1.05	690	H	H	H	H
	2.85		-0.95	-0.39	-0.66	-1.57:	—	1.05					
● IK 10565 +2428Main	16.22	1.75	-0.21	-0.31	-0.54	-1.47	—	0.69	a	H	H	H	H
	2.85		-0.30	-0.32	-0.59	-1.38	—	0.68					
*IR 10565+2428SE	1.00	--	—	-0.17	0.09	—	—	—		—	—	-	—
	3.10		. . —	. —	_	— .	—	--					
NG'C 3508S	4.68	0.49	-0.39	-0.45	-0.56	-2.67:	—	0.68	a	H	H	H	H
	2.85		-0.42	-0.45	-0.58	-2.65:	—	0.68					
NGC 3508N	9.12	1.18	-0.60	-0.45	-0.62	-1.72:	—	0.65	a	H	H	H	H
	2.85		-0.65	-0.46	-0.65	-1.66:	—	0.65					
NGC 3597	5.50	0.66	-0.16	-0.37	-0.53	-1.60:	—	0.74	90	H	H	H	H
	2.85		-0.19	-0.37	-0.55	-1.56:	—	0.74					
MCG+0029023	12.30	1.46	0.14	-0.18	-0.51	-1.34	—	—	—	L	H	H	H:
	2.85		0.07	-0.19	-0.55	-1.26	—	--					
● UGC 6436NW	18.20	1.86	-0.44	-0.31	-0.68	-1.63	—	0.81	220	H	H	H	H
	2.85		-0.53	-0.32	-0.74	-1.54	—	0.81					
● UGC 6436SE	21.38	2.03	---	-0.23	-0.63	-1.65:	—	0.93	410	—	—	—	—
	2.85		—	-0.24	-0,69	-1.55:	—	0.91					
● IR 12224-0624	4.17;	0.30;	-0.1 3;	0.05	-0.64	-0.07	—	—	—	L	H	L	L:
	3.10		-0. 14;	0.05	-0.65	-0.06	—	—					
● NGC 4666	7.76	0.91	0.12	0.11,	-0.19	-1.26;	—	0.83	230	L	L	H	L:
	3.10		0.08	0.11	-0.22	-1.21;	—	0.83					
IC 3908	7.59	0.99	-0.31	-0.49	-0.50	-1.29:	—	0.69	a	H	H	H	H
	2.85		-0.36	-0.49	-0.53	-1.24:	—	0.68					
UGC 8058	1.00		—	—.		—.		—	—	S1	S1	S1	S1
	1.00				—	—	--	—					
*NGC 4922	7.08	0.83	0.47	-0.14	-0.47	-1.15	—	0.95	500	L	H	L	L:
	3.10		0.43	-0.14	-0.50	-1.10	—	0.95					
MCG-0233098W	12.30	1.46	-0.13	-0.49	-0.61	-1.18	—	0.41	a	H	H	L	H:
	2.85		-0.20	-0.50	-0.65	-1.11	—	0.41					
MCG-0233098E	6.31	0.79	-0.16	-0.59	-0.52	-1.27:	—	—		H	H	H	H
	2.85		-0.20	-0.59	-0.55	-1.23:	—						
*1C 860	1.00	—	—	0.89	0.62	0.02		—	—	—	—	—	—
	3.10		—.	.	. . _	—	—	—					
*UGC 8335NW	7.94	1.02	0.16	-0.33	-0.43	-1.28	—	0.69	10	H	L	H	H:
	2.85		0.11	-0.34	-0.46	-1.22		0.69					
*UGC 8335SE	6.46	0.83	0.03	-0.39	-0.65	-1.50	-0.02	1.00	590	H	H	H	H
	2.85		-0.01	-0.39	-0.67	-1.45		0.33	1.00				
● UGC 8387	12.30	1.39	-0.10	--0.18	-0.36	-1.01	—	1.23:	1200:	1.	L	L	L
	3.10		-0.16	-0.18	-0.40	-0.94	—	1.23:					
● h'CIC 5104	22.39:	1.99:	0.14:	-0.06	-0.26	-1.14	—	--	-.	L	L	L	L
	3.10		0.04:	-0.07	-0.32	-1.04		—					
*NGC 5218	11.22	1.28	-0.30	-0.06	-0.29	-0.96	—	1.12	850	L	L	L	L
	3.10		-0.36	-0.07	-0.33	-0.89	—	1.10					
*NGC 5256SW	3.89	0.22	0.16	-0.20	-0.33	-0.92	0.07	0.93	410	L	L	L	L
	3.10		0.14	-0.20	-0.33	-0.91	0.17	0.91					
*NGC 5256NE	6.31	0.72	0.6S	-0,25	-0.41	-1.29	-0.61:	0.83	250	S2	S2	S2	S2
	3.10		0.62	-0.25	-0.44	-1.25	-0.30:	0.83					
*NGC 5257	3.24	0.13	-0.12	-0.46	-0.56	--1.68	--	0.85	260	J I	H	H	H
	2.85		-0.12	-0.46	-0.57	-1.67	--	0.85					

Table la. Observed and **Dereddened** Line Ratios, Densities, Spectral Classification - **IRAS** Bright **Galaxies**

Name	H_α / H_β	E(B-V)	[0111] H_β	[NII] H_α	[S11] H_α	[01] H_α	[OII] [0111]	6731 6716	N_e	Spectral Types [NII]	[SII]	[01]	Adopted
(1)	(2)	(3)	(4)	(5)	(6)	(7)	(8)	(9)	(lo)	(ii)	(12)	(13)	(14)
*NGC 5258	1.00	---	---	-0.25	---	---	---	---	---	---	---		---
	2.85		--	- .	—.	---	---	---					
• UGC 8696	9.12	1.07	0.50	0.02	-0.21	-0.90	---	---	---	L	L	L	1.
	3.10		0.45	0.01	-0.24	-0.85	---	---					
* NGC 5430	8.13	1.05	-0.45	-0.30	-0.56	-1.54	---	0.76	120	H	H	ii	H
	2.85		-0.51	-0.31	-0.59	-1.49	---	0.76					
● ZW 247020	12.02	1.44	-0.39	-0.12	-0.64	-1.59	---	1.15	980	L	H	H	H:
	2.85		-0.46	-0.13	-0.69	-1.52	---	1.15					
● NGC 5653W	5.50	0.66	-0.64	-0.42	-0.64	-1.94	---	0.79	160	H	H	H	H
	2.85		-0.68	-0.42	-0.66	-1.90	---	0.78					
● NGC 5653E	9.12	1.16	-0.67;	-0.43	-0.71	-1.74:	---	0.65	a	H	H	H	H
	2.85		-0.73;	-0.44	-0.74	-1.68:	---	0.63					
● NGC 5676	67.61:	3.09:	0.68:	-0.26	-0.63	---	---	---	—	52	52	—.	52
	3.10		0.54:	-0.27	-0.73	---	---	---					
*IR 1434 8-1447SW	12.88	1.43	0.20	-0.22	-0.44	-1.09	---	0.62	a	L	L	L	L
	3.10		0.13	-0.23	-0.48	-1.02	---	0.60					
● IR14348-1447NE	8.51	1.02	0.13	-0.20	-0.48	-0.90	---	0.00	a	L	H	L	L:
	3.10		0.09	-0.21	-0.51	-0.85	---	0.00					
*NGC 5734	9.77	1.15	—	-0.20	-0.54	—	---		—	---	—.	- -	—
	3.10		—	-0.21	-0.57	---	---	---					
*UGC %1S	7.24	0.84	-0.02	-0.08	-0.43	-1.14	—	0.68:	a	L	H	L	L:
	3.10		-0.06	-0.09	-0.46	-1.10	---	0.68:					
Zw 049.057	42.66:	2.73:	-0.71:	-0.54	-0.52	-1.55:	---	---	—.	H	H	H	H
	2.S5		-0.84:	-0,55	-0.60	-1.41:	---						
● IZw107S	17.7s	1.76	0.14	-0.11	-0.29	-1.15	---	0.71	30	L	L	L	L
	3.10		0.06	-0.12	-0.3S	-1.07	---	0.69					
"I Zw 107N	8.13	1.06	0.01	-0.25	-0.56	-1.47	---	0.83	240	H	H	H	H
	2.85		-0.04	-0.26	-0.59	-1.42	---	0.83					
● IR15250-3609	6.61	0.76	0.15	-0.33	-0.43	-1.16	---	0.68	a	ii	L	L	L:
	3.10		0.11	-0.33	-0.45	-1.13	---	0.68					
*NGC 5936	12.59	i .50	-0.55	-0.22	-0.61	-1.62	---	0.98	510	Ii	H	H	H
	2.85		-0.62	-0.22	-0.65	-1.54	---	0.95					
*NGC 5953	7.s9	0.89	0.30	-0.11	-0.37	-1.24	---	0.85	280	1.	L	L	L
	3.10		0.26	-0.11	-0.40	-1.19	---	0.85					
UGC 9913W	1.00			0.29	-0.04	-0.70	---	0.65		---		—.	
	3.10			.	—	- .	---						
UGC 9913E	74.13	3.10	0.95	0.23	-0.07	-0.78		0.51	a	52	52	S2	52
	3.10		0.79	0.22	-0.16	-0.62	---						
*IR 15335-0513	17.78:	1.75:	-0.17:	0.08	-0.29	-0.77	---	---	a	L	L	L	L
	3.10		-0.25:	0.07	-0.34	-0.69							
• NGC 6090	5.01	0.5s	-0.33	-0.48	-0.78	-1.77	---	0.89	350	H	H	H	H
	2.85		-0.35	-0.48	-0.79	-1.74		0.89					
* NGC 6090S	4.68	0.49	0.10	-0.46	-0.64	-1.75	---	0.78	1s0	H	H	H	H
	2.85		0.08'	-0.46	-0.65	-1.73	---	0.78					
● IR 16164-0746	16.60:	1.68:	0.09:	0.01	-0.31	-0.69		- .-	. .	L	L	L	L
	3.10		0.01	0.00	-0.36	-0.61							
*MCG+0142088	12.30	1.47	-0.50	-0.28	-0.47	-1.47	---	1.02:	660:	ii	H	H	H
	2.85		-0.57	-0.29	-0.51	-1.40		1.02:					
● NGC 61S1	6.31	0.80	-0.68:	-0.33	-0.61	. .		0.91	400	H	H		ii
	2.85		-0.72:	-0.33	-0.63		---	0.91					

Table la. Observed and Dereddened Line Ratios, Densities, Spectral Classification - IRAS Bright Galaxies

Name	HO		[0111]	[Nil]	[S11]	[0 1]	[OII]	6 7 3 1		Spectral Types			
	— -	E(B-V)	— — -	~——		———————		·—— ·	N_e				
	H_δ		H_δ	H_α	H_α H_α	[OIII]		6716		[NII]	[SII]	[01]	Adopted
(1)	(2)	(3)	(4)	(5)	(6)	(7)	(8)	(9)	(lo)	(11)	(12)	(13)	(14)
•NGC 6240	15.85	1.65	0.15	0.10	0.09	-0.51	—	—		L	L	L	L
	3.10		0.07	0.09	0.04	-0.43		—					
*NGC 6285/6NW	7.24	0.95	-0.28	-0.32	-0.27	-1.29	—	—		H	H	H	H
	2.85		-0.33	-0.32	-0.29	-1.24	—	—					
* NGC 6285/6SE	10.96	1.26	-0.19	-0.08	-0.18	-0.87	—	—	—	L	L	L	L
	3.10		-0.25	-0.08	-0.22	-0.81	—	—					
● IR 17132+5313W	1.00	—	—	0.47	-0.22	—	--	0.71	40	—	—	—	—
	3.10		—	-		—.	—	—					
*IR 17132 +5313E	4.90	0.55	-0.36	-0.35	-0.49	-1.66	—·	0.93	450	H	H	H	H
	2.85		-0.38	-0.35	-0.50	-1.63	—	0.93					
● IR 17138-1017	1.00		—·	-0.30	-0.44	-1.43:	--	0.74	70	—	—	—	—
	2.85		—		—	—	—	—					
● IR 17208-0014	18.20	1.87	-0.05	-0.40	-0.59	-1.39	—	0.71	20	H	H	H	H
	2.85		-0.14	-0.41	-0.64	-1.30	—	0.69					
● NGC 6621	11.22	1.30	-0.37	-0.22	0.44	-1.35	—	—	—	H	H	H	H
	3.10		-0.43	-0.22	0.40	-1.28	—	—					
● IR 18293-3413	16.60	1.76	-0.53	-0.33	-0.57	-1.56	—	0.83	250	H	H	H	H
	2.85		-0.62	-0.34	-0.62	-1.47	—	0.83					
*NGC 6670W	18.20	1.8S	-0.83:	-0.42	-0.63	-1.65	--	0.71	40	H	H	H	H
	2.85		-0.92:	-0.43	-0,68	-1.56	—	0.71					
•NGC 6670E	19.50	1.94	-0.04	-0.42	-0.53	-1.47	--	0.85	280	H	H	H	H
	2.85		-0.14	-0.43	-0.59	-1.37	--	0.85					
● NGC 6701	10.00	1.26	-0.07	-0.12	-0.46	-1.29	—	0.89	360	L	H	H	H:
	2.85		-0.13	-0.13	-0.50	-1.23	--	0.89					
● ESO 593-IG008S	2.95	0. 04	-0.19	0.45;	-0.23	-1.00	—	—·	—	L	L	L	L
	3.10		-0.19	0.45;	-0.23	-1.00	—.	—					
● ESO 593-IG008N	9.12	1.16	-0.15	-0.31	-0.48	-1.50	—	0.65	a	H	H	H	H
	2.85		-0.21	-0.31	-0.52	-1.44	—	0.63					
● IR 19297-0406	13.80	1. 5-1	-0.16	-0.25	-0.47	-1.18	--	0,81	200	H	H	L	H:
	2.85		-0.23	-0.26	-0.52	-1.10	—·	0.79					
● NGC 6926	15.85:	1. 63:	0.88:	0.12	-0.11	-0.48	—		—	S2	S2	S2	S2
	3.10		0.80:	0.11	-0.16	-0.40	—	—					
*ZW 448.020Main	3.89	0.31	0.31	-0.67	-0.77	-1.67	—	0.83	230	H	H	H	H
	2.85		0.30	-0.67	-0.78	-1.66	--	0.83					
*Zw 448. 020NW	7.08	0.92		-0.23	-0.46	-1.08	—	0.69	10	—	—	—	—
	2.85		--	-0.23	-0.49	--1.03	—·	0.69					
*ESO 286- IG019	8.91	1.07	-0.06	-0.41	-0.40	-1.21	--	0.65	a	L	L	H	L:
	3.10		--0.11	-0.41	-0.44	-1.16	--	0.63					
*ESO 343-IGO13s	5.01	0.57	-0.38	-0.26	-0.39	-1.28		0.71	20	H	L	H	H:
	2.85		-0.41	-0.27	-0.41	-1.25	---	0.69					
*ESO 343-IG013N	8.13	1.04	-0.33	-0.29	-0.40	-1.37	-·	0.69	10	H	H	H	H
	2.85		-0.38	-0.29	-0.43	-1.31	--	0.69					
*IC 5135	234.42	4.43	0.44	-1.46	--1.71	-2.07	· · ·	(s.66	a	L	L	L	L
	2.85		0.22	-1.48	-1.84	-1.85	·—·	0.63					
● IC 5179	9.12	1.18	-0.63:	-0.51	-0.63	-1.43	--	0.98:	510:	H	H	H	H
	2.85		-0.69:	-0.52	-0.67	-1.37	---	0.95:					
• ESO 602-G025	10.72	1.24	0.02	-0.18	-0.67	-1.23		0.72	60	L	H	L	L:
	3.10		-0.04	-0.18	-0.70	-1.17	---	0.72					
*ESO 534-G009	5.75:	0.63:	0.30:	0.30	0.06	-0.42	--	0.79	180	L	L	L	L
	3.10		0.27:	0.30	0.04	-0.39	—	0.79					

Table la. Observed and Dereddened Line Ratios, Densities, Spectral Classification - IRAS Bright Galaxies

Name	H_α / H_β	E(B-V)	[OIII] / H_β	[NII] / H_α	(SII) / H_α	[OI] / [OIII]	[OII] / [OIII]	6731 / 6716	N_e	Spectral Types [NII]	[SII]	[OI]	Adopted
(1)	(2)	(3)	(4)	(5)	(6)	(7)	(8)	(9)	(10)	(11)	(12)	(13)	(14)
*UGC 12150	19.50	1.93	-0.46	-0.17	-0.48	-1.47	---	—		L	H	H	H:
	2.85		-0,55	-0.18	-0.54	--1.37		—					
*IR 22491-1808	**6.46**	0.81	-0.15	-0.37	-0.60	-I .28	0.28	0.68	a	H	H	H	H
	2.85		-0.19	-0.37	-0.62	-1,24	0.62	0.66					
*NGC 7469	**2.82**	-0.01	-0.28	--0.74	-1.34	-2.02	—	0.93	430	S1	S1	S1	S1
	2.85		-0.28	-0.74	-1.34	-2.02	--	0.93					
*Zw 453.062	**10.96**	1.27	0.09	0.09	-0.28	-0.91	—	0.81:	620:	L	L	L	L
	3.10		0.03	0.08	-0.32	-0.84	—	0.79:					
● 7,w 475.0S6	**9.55**	1.13	0.67	-0.02	-0.56	-1.32	--	1.02	190	S2	S2	S2	S2
	3.10		0.62	-0.02	-0.59	-1.26	---	1.00					
*NGC 7591	12.30	1.39	0.10	-0.01	-0.37	-1.05	-.	0.71	40	L	L	L	L
	3.10		0.04	-0.02	-0.41	-0.98	---	0.71					
*NGC 7592W	6.31	0.71	0.55	-0.14	-0.39	-1.00	--	0.93	450	S2	S2	S2	S2
	3.10		0.51	-0.15	-0.41	-0.96	---	0.93					
● NGC 7592E	4.37	0.42	-0.12	-0.49	-0.63	-1.61	---	0.74	100	H	H	H	H
	2.85		-0.14	-0.50	-0.64	-1.59	---	0.74					
*NGC 7674	3.89	0.23	1.07	-0.11	-0.55	-0.97	-1.25	1.10	790	S2	S2	S2	S2
	3.10		1.06	-0.11	-0.56	-0.95	-1.16	1.10					
*NGC 7679	17.38	1.73	0.68	-0.23	-0.53	-1.23	---	0.79	160	S2	S2	S2	S2
	3.10		0.60	-0.24	-0.58	-1.14	—	0.78					
*NGC 7714	3.55	0.21	0.19	-0.43	-0.71	-1.75	—	1.00	590	H	H	H	H
	2.85		0.18	-0.43	-0.72	-1.74	—	1.00					
IR 23365+3604	7.41	0.88	-0.26	-0.18	-0.35	-1.18	0.38	0.74	90	L	L	L	L
	3.10		-0.30	-0.18	--0.37	-1.13	0.75	0.74					
*NGC 7771 Main	21.38	2.03	0.02	-0.32	-0.38	-1.35	---	1.05	690	H	H	H	H
	2.85		-0.08	-0.33	-0.44	-1.25		1.02					
*NGC 7771S	5.25	0.61	-0.17	-0.44	-0.57	- 1.98;	—	0.74	80	H	H	H	H
	2.85		-0.20	-0.44	-0.59	-1 .95;	--	0.74					
*Mrk 331	8.32	1.09	-0.41	-0.27	-0.57	-1.60	—	0.98	510	H	H	H	H
	2.85		-0.46	-0.27	-0.60	-1.55	---	0.98					

Note: The uncertainty on the emission line ratios is typically 10% and 25% for the entries with a colon(:).
a: unreasonable physical input (low density limit): 6716/6731 > 1.45
*: object observed under photometric conditions

Table lb. Observed and Dereddened Line Ratios, Densities, **Spectral** Classification - **Warm** IRAS **Galaxies**

Name	H_α / H_β	E(B-V)	[orII] / 113	[NII] / HO	[sII] / H_α H_α	[OI] [OII] / [0111]		6731 / 6716	N_e	Spectral Types [NII]	[SII]	[0 1]	Adopted
(1)	(2)	(3)	(4)	(5)	(6)	(7)	(8)	(9)	(lo)	(11)	(12)	(13)	(14)
● NGC 985	1.00	—	—	0.31:	0.23:	-0.83:	—	—	—	—	—	—	—
	3.10		—			—		—					
● IR 02433+1544	15.85	1.73	-0.62	-0.21	-0.71	-1.68:	—			H	H	H	H
	2.85		-0.70	-0.22	-0.76	-1.59:	—						
MCG+0310045	7.24	0.93	-0.19	-0.49	-0.51	-1.62	—	0.74	90	H	H	H	H
	2.85		-0.23	-0.50	-0.54	-1.58	—	0.74					
*1R 04259-0440	7.94;	0.95;	0.27;	-0.13	-0,26	-0,91		—		L	L	L	L
	3.10		0.22;	-0.14	-0.29	-0.86	—						
IR 07599-6508	1.00	—	—	—	—	—	—	—	—	S1	S1	S1	S1
	—					—	—	—					
IR 09209-3943	6.92	0.89	-0.48	-0.34	-0.56	-1.53	0.55	0.74	100	H	H	H	H
	2.85		-0.53	-0.35	-0.59	-1.48	0.92	0.74					
IR 09218-3428	6.17	0.78	-0.18	-0.36	-0.53	-1.57	0.32	0.72	50	H	H	H	H
	2.85		-0.21	-0.37	-0.56	-1.53	0.65	0.72					
IR 09245-3517	11.22	1.36	-0.08	-0.25	-0.57	-1.34:	0.00	—	—	H	H	H	H
	2.85		-0.14	-0,26	-0.61	-1.27:	0.58	—					
IR 09245-3300	1.00		0.09	---	--	—	0.58	—		—	—	—	—
	2.85				—	—	—	—					
IR 09252-3124	15.49	1.62	0.27	-0.22	-0.44	-1.13	—	—	—	L	L	L	L
	3.10		0.20	-0.23	-0.49	-1.05	—	—					
IR 09268-2808	7.59	0.99	-0.59	-0.35	-0.61	-1.47	—	0.91	390	H	H	H	H
	2.85		-0.63	-0.35	-0.64	-1.42	—	0.91					
Zw 238.066	9.33	1.10	0.26	-0.09	-0.40	-1.18	-0.05:	0.87	310	L	L	L	L
	3.10		0.20	-0.09	-0.43	-1.13	0.42:	0.87					
IR 09303-2736	15.85:	1.72:	-0.45:	-0.36	-0.41	-1.68:		0.72	60	H	H	H	H
	2.85		-0.53:	-0.37	-0.46	-1.60:	—	0.72					
IR 09338+3133	5.62	0.69	-0.76	-0.38	-0.61	-1.61	0.88	0.72	60	H	H	H	H
	2.85		-0.79	-0.38	-0.63	-1.57	1.17	0.72					
IR 09339-X35	7.08	0.91	-0.30	-0.35	-0.56	-1.42	0.37	0.78	140	H	H	H	H
	2.85		-0.34	-0.36	-0.58	-1.38	0.75	0.78					
IR 09399+2830	7.94	0.95	0.23	-0.32	-0.46	-1.22	0.23:	0.79	180	H	L	L	L:
	3.10		0.19	-0.33	-0.49	-1.18	0.63:	0.79					
Zw 182.010	7.94	1.02	-0.59	-0.30	-0.62	-1.66	0.45:	0.81	200	H	H	H	H
	2.85		-0.64	-0,30	-0.65	-1.60	0.88:	0.81					
IR 09425-1751	5.89	0.64	1.09	-0.25	-0.61	-1.03	-0.73	—		S2	S2	S2	S2
	3.10		1.05	-0,25	-0.63	-1.00	-0.46						
IR 09427+1929	4.37:	0.43:	-0.37:	-0.41	-0,47	-1.57:	0.49			H	H	H	H
	2.85		-0.39:	-0.41	-0.48	-1.55:	0.67						
IR 09433+1910	1.00		—	0.63	0.05	-0.34:	—	0.59	a	—	—	—	—
	3.10		—	—	—	—	—						
*IK 10210-752S	5.37	0.63	-0.01	-0.34	-0.65	-1.55:	0.11			H	H	H	H
	2.85		-0.04	-0.34	-0.67	-1.51:	0.37						
IR 11571+3004	13,49:	1.47:		-0.20	-0.63	—	—		—	—	—	—	—
	3.10		—	:0.21'	-0.67	—							
● IR 12071-0444	14.45	1.55	0.77	-0.51	-0.23	-1.16	-0.59	—	—	S2	S2	S2	S2
	3.10		0.70	-0.51	-0.28	-1.08	0.07						
● 7,W 041.073	8.71	1.12	-0.58	-0.40	-0.66	--1.84		—		H	H	H	H
	2.85		-0.63	-0.40	-0.69	-1.78	---	—					
IR 12450+3401	3.24;	0.05;	0.07:	0.10;	0.21;	-0,41;	0.57	2.14;	19460;	L	L	L	L
	3.10		0.07:	0.10;	0.21;	-0.41;	0.59	2.14;					

Table lb. Observed and Dereddened Line Ratios, Densities, Spectral Classification - Warm IRAS Galaxies

Name	H_α / H_β	E(B-V)	[0111] / H_β	[NII] / H_α	[S11] / H_α	[01] / H_α	[OII] / [0111]	6731 / 6716	N_e	Spectral Types [NII]	[S11]	[01]	Adopted
(1)	(2)	(3)	(4)	(5)	(6)	(7)	(8)	(9)	(10)	(11)	(12)	(13)	(14)
IR 13349 -243s	1.00									S1	S1	S1	S1
	1.00												
● ZW 10:956	6.31	0.81	0.11	-0.40	-0.66	-1.74				H	H	H	H
	2.85		0.07	-0.40	-0.69	-1.70							
*IR 13446- 1121	14.13	1.52	0.69	-0.49	-0.71	-1.42				S2	H	S2	S2:
	3.10		0.62	-0.49	-0.76	-1.35							
IR 14229-1425	5.50	0.56	0.83	-0.16	-0.24	--1.04	-0.31	1.05	710	S2	S2	S2	S2
	3.10		0.80	-0.16	-0.26	-1.01	-0.07	1.05					
IR 14341 -3017NW	7.76	0.92	0.06	-0.28	-0.27	--1.12	0.30:	0.93	430	H	L	L	L:
	3.10		0.02	-0.28	-0.30	-1.07	0.69:	0.93					
IR 14341 -3017SE	5.37	0.64	-0.58	-0.30	-0.58	--1.64	0.48:	0.85	260	H	H	H	H
	2.85		-0.61	-0.31	-0.60	-1.61	0.75:	0.85					
IR 14416-6618	5.62	0.67	0.31	-0.50	-0.60	-1.39	-0.09	0.76	100	H	H	H	H
	2.85		0.28	-0.50	-0.62	-1.36	0.19	0.76					
IR 15206-3342	5.25	0.61	0.45	-0.66	-0.74	--1.44	-0.24	0.78	150	H	H	H	H
	2.85		0.42	-0.66	-0.76	-1.41	0.02	0.78					
*IR 15304-3017	5.50	0.57	1.17	-0.01	-0.32	-0.86	-1.23	0.87	310	S2	S2	S2	S2
	3.10		1.14	-0.01	-0.33	-0.83	-0.99	0.87					
*IR 15312-4236	7.08	0.91	-0.05	-0.35	-0.43	-1.69:		0.83	240	H	H	H	H
	.2.85		-0.09	-0.35	-0.45	-1.64:		0.83					
*IR 15324-3203	10.72	1.34	-0.30	-0.31	-0.52	-1.26:	0.22	0.72	50	H	H	H	H
	2.85		-0.36	-0.32	-0.56	-1.19:	0.79	0.71					
● IR 1535S.3831	1.00			-0.09	-0.32	-1.05:		1.07	740				
	3.10												
*IR 15359-3139	10.00	1.27	-0.27	-0.22	-0.57	--1.41	0.60:	0.85	270	L	H	H	H:
	2.85		-0.34	-0.22	-0.61	-1.35	1.14:	0.83					
● IR15364-3320	3.98	0.33	-0.48	-0.43	-0.64	-1.62:		0.87	330	H	H	H	H
	2.85		-0.50	-0.43	-0.65	-1.60		0.87					
● IR15384-3841	7.24	0.95	-0.35	-0.46	-0.92	-1.55	0.40:			H	H	H	H
	2.85		-0.39	-0.47	-0.95	-1.51	0.80:						
● IR 15391-3214SW	8.32	1.08	-0.60	-0.31	-0.64	-1.61	0.82	0.91	370	H	H	H	H
	2.85		-0.65	-0.31	-0.68	-1.56	1.28	0.89					
● IR15391-3214NE	8.51	1.09	-0.83	-0.38	-0.61	-1.41		0.72	60	H	H	H	H
	2.85		--0.88	-0.39	-0.65	-1.35		0,72					
● IR15394-3532	4.07	0.36	-0.25	-0.50	-0.61	-1.68	0.46	0.72:	60:	H	H	H	H
	2.85		-0.27	-0.51	-0.62	-1.66	0.61	0.72:					
● IR15404-3228	15.85	1.64	0.19	-0.23	-0.64	-1.11	0.49	0.62	a	L	H	L	L:
	3.10		0.11	-0.24	-0.69	-1.03	1.18	0.62					
● IR15414-3238	7.24	0.94	-0.19	-0.25		-1.40	0.47:			H		H	H
	2.85		-0.24	-0.25		-1.35	0.87:						
● IR15418-3938	12.30	1.47	-0.57	-0.42	-0.49	-1.70				H	H	H	H
	2.85		-0.64	-0.43	-0.54	-1.62							
● IR 15415-2840	4.57	0.38	0.99	-0.09	-0.40	-0.95	-1.12	0.98	510	S2	S2	S2	S2
	3.10		0.97	-0.10	-0.41	-0.93	-0.96	0.98					
● IR 15440-2834	6.61	0.84	-0.25	-0.50	-0.49	-1.51		0.71	30	H	H	H	H
	2.85		-0.29	-0.51	-0.51	-1.47		0.71					
● IR 15445-3312	6.03	0.67	-0.07	-0.06:	-0.25	-0.66	0.78	0.79	160	L	L	L	L
	3.10		-0.10	-0.06:	-0.28	-0.63	1.07	0.78					
● IR 15463-4131	4.90	0.54	-0.64	-0.37	-0.62	-1.47		0.76	110	H	H	H	H
	2.85		-0.67	-0.37	-0.64	-1.44		0.76					

Table lb. Observed and Dereddened Line Ratios, Densities, Spectral Classification - Warm IRAS Galaxies

Name	H_α / H_β	E(B-V)	[oIII] / H_β	[NII] / H_α	[s11] / H_α	[01] / [0111]	[OII]	6731 / 6716	N_e	Spectral Types [NH]	[S11]	[01]	Adopted
(1)	(2)	(3)	(4)	(5)	(6)	(7)	(8)	(9)		(10)	(11)	(12)	(13)	(14)
*IR 15469+2853	17.38:	1.73:	0.20:	-0.22	-0.48	---	---	0.76	130	L	H	---	L:
	3.10		0.12:	-0.23	-0.54			0.76					
*IR 15481+2920	6.61	0.76	0.35	-0.07	-0.75	-1.30		0.74:	70:	L	H	L	L
	3.10		0.31	-0.08	-0.78	-1.26		0.72:					
*IR 15483+4227	4.47	0.44	-0.41	-0.43	-0.53;	-1.59	---	---	---	H	H	H	H
	2.85		-0.43	-0.44	-0.54;	-1.57		---					
*IR 15514+3330	6.61	0.85	-0.19	-0.35	-0.52	-1.50	---	0.85	280	H	H	H	H
	2.85		-0.23	-0.36	-0.55	-1.46	---	0.85					
● IR 15519+3537	10.47	1.31	-0.12	-0.28	-0.66	-1.14	0.36	0.66	a	11	H	L	H:
	2.85		-0.19	-0.29	-0.70	-1.08	0.92	0.65					
● IR 15534+3004	1.00	---	---	0.04	-0.27:	-0.79:	---	---	---	---	---	---	---
	3.10		---	---		---	---	---					
*IR 15534+3519	3.63	0.25	-0.28	-0.37	-0.56	-1.03	0.07:		---	H	H	L	H:
	2.85		-0.29	-0.37	-0.57	-1.02	0.17:						
*IR 15535+2854	8.32	1.08	-0.65:	-0.32	-0.79	-1.67:	---	0.74	90	H	H	H	H
	2.85		-0.70:	-0.33	-0.82	-1.62:	---	0.74					
● IR 15543+4158NW	7.24	0.94	-0.12	-0.25	-0.57:	-1.21	0.22	---		H	H	L	H:
	2.85		-0.17	-0.26	-0.60:	-1.16	0.61						
*IR 15543+4158SE	5.25	0.61	-0.07	-0.43	-0.36:	-1.27	0.21	---	---	H	L	H	H:
	2.85		-0.10	-0.44	-0.38:	-1.24	0.47	---					
● IR 15543+3013	3.31	0.16	0.31	-0.68	-0.74	-1.61	4.05	0.76	110	H	H	H	H
	2.85		0.30	-0.68	-0.75	-1.60	0.02	0.76					
*IR 15545+4000	4.90	0.55	-0.14	-0.21	-0.66:	-1.59	1.17	0.95:	480;	L	H	H	H:
	2.85		-0.16	-0.21	-0.68:	-1.56	1.41	0.95:					
*IK 15549+4201	4.57	0.48	0.13	-0.33	-0.53	-1.44	0.29	0.89	330	H	H	H	H
	2.85		0.11	-0.33	-0.55	-1.41	0.49	0.87					
*IK 15569 +2807W	9.55	1.14	--0.13:	-0.15	-0.39	-1.02:		0.69	a	H	H	H	H
	3.10		-0.19:	-0.16	-0.43	-0.96:		0.68					
*IR 15569+2807E	5.62:	0.59:	1.04:	-0.07	-0.31	-0.84		0.87	290	S2	S2	S2	S2
	3.10		1.01:	-0.07	-0.33	-0.81	---	0.85					
*IK 15577-3816	1.00		1.07	--	---	---	-0.87	---	---	---	---	---	---
	2.85		---	---		---	---						
● IR 15589+4121	3.16	0.02	0.50	-0.79	-0.40:	-0.90:	-0.32:	---	---	11	S2	S2	S2:
	3.10		0.50	-0.79	-0.40:	-0.90:	-0.31:	---					
*IR 15597-3133	1.00	---	---	-0.30	-0.20	-0.55	---	0.87	310	---	---	---	---
	3.10		---	---			---	---					
*IR 16007 +3743	10.47	1.21	0.00	-0.29		-1.14	0.50	---		H	---	L	L:
	3.10		-0.06	-0.29		-1.07	1.02	---					
IR 16130-2725	5.89	0.74	0.10	-0.46	-0.70	-1.66:	---	---	---	H	H	H	H
	2.85		0.06	-0.46	-0.72	-1.62:		---					
Zw 052.015	7.94	1.03	-0.32	-0.40	-0.47	-1.71		0.79	170	H	H	H	H
	2.85		-0.37	-0.41	-0.50	-1.66	---	0.79					
● IR 21479-1305	1.00	---	---	-0.14	-0.13	-1.04:		1.07	740		---	---	---
	3.10		---					---					
*IR 214 84-1314	13.18	1.54	0.02:	-0.41	-0.62:	-1.51		---	---	H	H	H	H
	2.85		-0.05:	-0.42	-0.66:	-1.43		---					
● 1R 21549-1206NW	4.68	0.41	0.13	-0.48	-0,37	-1.18		0.76	120	11	L	L	L:
	3.10		0.11	-0.48	-0.38	-1.16	---	0.76					
● IR 21519 -1206SE	4.07	0.36	0.02	-0.45	-0.47	-1.36	0.12:	0.78	150	11	H	H	H
	2.85		0.00	-0.45	-0.48	-1.34	0.27:	0.78					

Table 1 b. Observed and Dereddened Line Ratios, Densities, Spectral Classification - Warm IRAS Galaxies

Name	H_α / H_β	E(B-V)	[OIII] 5007 / H_β	[NII] 6583 / H_α	[SII] 6716,6731 / H_α	[OI] 6300 / H_α	[OIII] 5007 / [OIII] 4959	[OIII] 5007 / [OIII] 4363	N_e	Spectral Types [NII]	[SII]	[OI]	Adopted
(1)	(2)	(3)	(4)	(5)	(6)	(7)	(8)	(9)	(10)	(11)	(12)	(13)	(14)
● IR 22114-1109	5.50	0.58	0.62	-0.21	-0.42	-1.11	-0.65	0.95	480	S2	S2	S2	S2
	3.10		0.59	-0.21	-0.44	-1.08	-0.40	0.95					
*IR 22152-0227	7.76	0.92	0.90	-0.17	-0.32	-0.90	-0.68	--	---	S2	S2	S2	S2
	3.10		0.86	-0.18	-0.35	-0.85	-0.29	---					
*IR 22191-1400	9.33	1.19	-0.52	-0.28	-0.65	-1.30	—			H	H	H	H
	2.85		-0.58	-0.28	-0.68	--1.24	---	--					
*IR 22193-1217	6.61	0.85	-0.55	-0.33	-0.75	-1.38	—	0.83	240	H	H	H	H
	2.85		-0.59	-0.34	-0.78	-1.34	—	0.83					
IR 22199-0345	6.17	0.69	0.62	-0.21	-0.53	-1.20	-0.61	1.00	570	S2	S2	S2	S2
	3.10		0.58	-0.21	-0.55	-1.17	-0.32	1.00					
*IR 22204-0214NW	10.47	1.30	-0.05	-0.27	-0.51:	-1.22	0.47	--		H	H	H	H
	2.85		-0.12	-0.27	-0.55:	-1.15	1.02	—					
*IR 22204-0214SE	7.24	0.95	-0.57	-0.36	-0.83:	---	0.55	--	—	H	H	---	H
	2.85		-0.61	-0.36	-0.86:	—	0.95	--					
	2.85		-0.54:	-0.35	-0.60	-1.42	--	0.76					
*IR 222200S25	7.59	0.98	-0.53	-0.20	-0.50	-1.39	0.16:	0.83	230	L	H	H	H:
	2.85		-0.58	-0.20	-0.53	-1.34	0.57:	0.83					
● IR 22215-0645	8.71	1.11	-0.32	-0.27	-0.61	-1.37	—	1.32	1510	H	H	H	H
	2.85		-0.37	-0.27	-0.64	-1.31	—	1.32					
*IR 22279-1112NW	6.46	0.82	0.27	-0.55	-0.66	-1.16	0.09	0.81	220	H	H	L	H:
	2.85		0.23	-0.56	-0.68	--1.12	0.44	0.81					
● IR 22279-1112SE	14.79:	1.57:	0.31:	-0.09	-0.22	-0.46:	—	0.76	110	L	L	L	L
	3.10		0.23:	-0.10	-0.27	-0.38:	--	0.74					
*IR 222 S3-1439	15.85	1.72	-0,39:	-0.16	--0.50	--1.28	--	0.76	110	L	H	H	H:
	2.85		-0.47:	-0.17	-0.55	-1.19	—	0.76					
*IR 22338-1015	8.91	1.14	-0.01	-0.23	-0.53	-1.54	—	1.41	1950	L	H	H	H:
	2.85		-0.07	-0.23	-0.56	-1.48	--	1.41					
*IR 22343-0840	1.00	—	--	-0.12	-0.48	-0.75:	---	1.10:	790:	---	---	---	---
	3.10			—	---	—	—	---					
*IR 22381-1337	5.01	0.57	0.27	-0.61	-0.70	-1.64	-0.26	0.72	50	H	H	H	H
	2.85		0.24	-0.61	-0.71	-1.61	-0.02	0.71					
IR 22472+3439	5.50	0.66	-0.02	-0.39	-0.36	-1.25	—	--		H	L	H	H:
	2.85		-0.05	-0.39	-0.38	--1.22	—	---					

Note: The uncertainty on the emission line ratios is typically 10% and 25% for the entries with a colon (:).
a: unreasonable physical input (low density limit): 6716/6731 > 1.45
*: object observed under photometric conditions

Table 2. Observed and Dereddened Red Line Ratios, Red-Line Spectral Classification

Name	H_α / H_β	E(B-V)	[0111] / $1l_\beta$	[s11] / H_α	[011] / H_α	[SIII] / H_α	Spectral Types [oIII]	[s11]	[s111]	Tab 1
(1)	**(2)**	**(3)**	**(4)**	**(5)**	**(6)**	**(7)**	**(8)**	**(9)**	(10)	(11)
BGSs Objects										
IR 03359-1523	**5.25**	**0.61**	**0.06**	-0.70	-1.82	- -	H	H	—	H
	2.85		0.03	-0.72	1.900	—				
NGC 1614	**7.59**	**0.99**	-0.12	-0.69	-1.77	—	H	H	—	H
	2.85		-0.17	-0.72	-1.90	—				
IR 08339+6517 "	**4.27**	0.40	0.24	-0.61	-2.05	—	H	H		H
	2.85		0.22	-0.62	-2.10	—				
MCG-0233098W	**12.30**	1.46	-0.13	-0.61	—	0.08	—	—	H/L	H:
	2.85		-0.20	-0.65	—	-0.71				
*UGC 8335 SE	**6.46**	0.83	0.03	-0.65	-1.74	—	H	H	- -	H
	2.85		-0.01	-0.67	-1.85	—				
*NGC 5256SW	**3.89**	0.22	0.16	-0.33	-1.28	- -	L	L	—	L
	3.10		0.14	-0.33	-1.31	—				
*NGC 5256NE	**6.31**	0.72	0.65	-0.41	-1.92	—	H	H/S2	—	S2
	3.10		0.62	-0.44	-2.01	—				
* NGC 7674	**3.89**	0.23	1.07	-0.55	-1.24	—	S2	S2	—	S2
	3.10		1.06	-0.56	-1.27	—				
● NGC 7714	**3.55**	0.21	0.19	-0.71	-1.66	—	H	H	—	H
	2.85		0.18	-0.72	-1.69	—				
WGSs Objects										
*IR 10210+7528	**5.37**	0.63	-0.01	-0.65	—	-0.81	—	—	H	H
	2.85		-0.04	-0.67	—	-1.28				
*IR 15300+3017	**5.50**	0.57	1.17	-0.32	-1.11	—	S2	S2		S2
	3.10		1.14	-0.33	-1.18	—				

Note: The uncertainty on the emission line ratios is typically 10% and 25% for the entries with a colon (:).
*: object observed under photometric conditions

Table 3. Spectral Classifications

$\log (L_{ir}/L_{\odot})$	< 11	11-12	≥ 12	All
# objects	**54**	**123**	**24**	201
Ambiguous (%)	9	**8**	13	9
AGN (%)	28	39	54	38
H II (%)	63	**52**	33	53
Sey 1 (%)	o	1	13	2
Sey **2 (%)**	**6**	*14*	17	12
LINER (%)	22	*24*	25	24
Sey1 +2/AGN (%)	2 0	*38*	54	37
LINER/AGN (%)	8 0	*62*	46	63

Table 4a. H_α Luminosities - IRAS Bright Galaxies

Name	$F(H_\alpha)$	cz (km s-l)	E(B-V)	log $L(H_\alpha)$	$EW(H_\alpha)$
(1)	(2)	{3)	(4)	(5)	(6)
*NGC 23	0.25E-12	4557	0.74	41.79	33.8
*NGC 34	0.10E-12	5860	2.08	42.93	27.8
*MCG-0201051 s	0.14E-12	8173	0.90	42.21	186.7
*MCG-020105 1 N	0.18E-13	8082	0.40	40.81	72.0
*NGC 232	0.67 E- 13	6775	1.31	42.13	30.5
*UGC 556	0.14E-13	4626	1.15	40.95	14.4
*IC 1623N	0.16E-12	6103	0.32	41.43	64.0
● IC1623SE	0.44E-12	5837	0.20	41.72	366.7
*MCG-0304014	0.99E-13	10473	1.10	42.48	90.0
*MCG+0204025	0.40E-13	9529	1.12	42,02	125.0
*UGC 903	0.16E-13	2439	1.18	40.48	13.3
*NGC 520	0.18E-13	2569	2.37	41.75	12.9
*IR 01364-1042	0.19E-14	14518	1.27	41.22	14.6
*NGC 660	0.46E-13	822	1.69	40.49	14.8
*111 Zw 35s	0.99E-14	8442	1.18	41.36	10.0
*III Zw 35N	0.16E-13	8305	0.31	40.70	88.9
*NGC 695	0.36E-13	9497	1.03	41.88	32.7
● NGC 873	0.97E-13	3986	1.13	41.64	48.5
NGC 1050	0.21E-12	4130	0.77	41.65	65.6
NGC 1056	0.19E-12	1846	0.85	40.98	24.7
*NGC 1068	0.44E-11	1320	0.68	41.89	91.7
*NGC 1083	0.29E-13	7684	1.73	42.29	38.7
*UGC 2238	0.1413-13	6477	2.25	42.33	28.0
● IR 02438+2122	0.60E-14	7204	2,13	41.94	9 . 7
*UGC 2369	0.12E-12	9511	0.88	42.26	131.9
NGC 1143/44	0.22E-13	8638	0.47	41.03	8.5
*UGC 2403	0.43E-13	4340	1.67	41.90	39.1
NGC 1204	0.32E-13	4486	1.74	41.87	21.3
NGC 1266	0.14E-13	2019	0.62	39.70	5.0
IR 03359+1523	0.86E-13	10643	0.63	41.97	256.2
UGC 2982	0.33E-13	5368	1.89	42.19	27.5
ESO 550-IG025S	0.12E-13	9593	1.13	41.51	17.6
ESO 550-IG025N	0.12E-13	9721	1.09	41.48	32.4
NGC 1614	0.10E-11	4746	0.99	42.67	147.1
IR 04335-2514	0.75E-14	4959	2.27	41.85	8,5
ESO 485-GO03	O.1OE-I2	4554	0.71	41.36	83.3
NGC 1797	0.12E-12	4563	1.13	41.85	50.0
IR 05186-1017	0.26E-14	8506	2.05	41.65	7.4
IR 05189-2524	0.29E-13	12767	1.93	42.94	34.1
IR 08339+6517	0.51E-12	5728	0.40	41.96	124.4
IR 08572+3915	0.19E-14	17482	1.17	41.29	47.5
NGC 2785	0.2411-13	2672	1.66	41.21	26.7
UGC 4881SW	0.35E-13	11795	1.50	42.53	37.2
UGC 4881NE	0.3213-13	11854	1.21	42.21	24.6
UGC 5101	0.38E-13	11795	2.04	43.10	30.9
MCG+0818012	0.19E-13	7775	1.,15	41.54	32.8
NGC 3110	0.72E-13	5062	0.89	41.49	48.0
*IR 10565 +2428Main	0.53E-13	13156	I .75	43.05	85.S
NGC 3508S	0.49E-13	3878	0,49	40.69	59.0
NGC 3508N	0.49E-13	3856	1.18	41.36	44,5

Table 4a. H_α Luminosities - IRAS Bright Galaxies

Name	F(H_α)	Cz (km s-l)	E(B-V)	log L(H_α)	EW(H_α)
(1)	(2)	(3)	(4)	(5)	(6)
NGC 3597	0.31E-13	3504	0.66	40.57	77.5
MCG+0029023	0.48E-13	7515	1.46	42.22	32.0
*UGC 6436NW	0.34 E-13	10237	1.86	42.74	100.0
*UGC 6436SE	0.16E-13	10324	2.03	42.59	32.0
*IR 12224-0624	0.34E-14	2147	0.30	38.82	2.6
*NGC 4666	0.25E-13	1585	0.91	40.03	3.5
IC 3908	0.17E-13	1284	0.99	39.75	40.5
*NGC 4922	0.63E-13	6825	0.83	41.63	140.0
MCG-0233098W	0.44E-13	5016	1.46	41.83	163.0
MCG-0233098E	0.30E-13	5162	0.79	41.02	100.0
*UGC 8335NW	0.24E-13	9378	1.02	41.68	44.4
*UGC 8335SE	0.17E-12	9228	0.83	42.33	274.2
*UGC 8387	0.28E-13	6711	1.39	41.82	50.0
● NGC 5104	0.14E-13	5154	1.99	41.88	12.7
*NGC 5218	0.19E-13	2832	1.28	40.78	12.7
*NGC 5256SW	0.11E-12	8360	0.22	41.45	127.9
*NGC 5256NE	0.72E-13	8410	0.72	41.77	101.4
*NGC 5257	0.36E-13	6491	0.13	40.65	97.3
*UGC 8696	0.67E-13	11585	1.07	42.37	101.5
*NGC 5430	0.78E-13	3106	1.05	41.25	25.2
*Zw 247.020	0.56E-13	7758	1.44	42.30	50.9
*NGC 5653W	0.56E-13	3632	1.16	41.35	19.3
*NGC 5653E	0.17E-12	3444	0.66	41.29	193.2
*NGC 5676	0.12E-13	2206	3.09	42.15	3.3
*IR 14348 -1447SW	0.141? -13	24796	1.43	42.74	87.5
*IR 14348 -1447NE	0.49E-14	24654	1.02	41.88	44.5
*NGC 5734	0.281? -13	4107	1.15	41.15	9.0
*UGC 9618	0.55E-14	10233	0.84	40.94	17.2
Zw 049.057	0.72E-13	3516	2.73	42.98	55.4
*I Zw 107S	0.12E-13	11795	1.76	42.32	63.2
*I Zw 107N	0.78E-13	11818	1.06	42.44	147.2
*IR 15250+3609	0.19E-13	16217	0.76	41.82	51.4
*NGC 5936	0.89E-13	4052	1.50	41.98	55.6
*NGC 5953	0.18E-12	2069	0.89	41.10	27.3
*IR 15335-0513	0.46E-14	8035	1.75	41.55	12.4
*NGC 6090NW	0.31E-12	8707	0.5.8,	42.29	206.7
*NGC 6090SE	0.10E-12	8743	0.49	41.72	156.2
*IR 16164-0746	0.44E-14	6286	1.68	41.24	15.2
*MCG+0142088	0.53E-13	7432	1.47	42.27	48.2
*NGC 6181	0.48E-13	2512	0.80	40.60	13.0
*NGC '6240	0.85E-13	7371	1.65	42.64	100.0
● NGC 6285/6 NW"	0.22 E- 13	5582	0.95	41.12	41.5
*NGC 6285/6SE	0.67E-14	5619	1.26	40.91	12.9
*IR 17132 +5313E	0.21E-13	15102	0.55	41,59	77.8
*IK 17208-0014	0.16E-13	12814	1.87	42.63	69.6
*IR 18293-3413	0.93E-13	5400	1.76	42.51	84.5
*NGC 6670W	0.16E-13	8492	1.85	42.24	69.6
*NGC 6670E	0.53E-13	8538	1.94	42.85	82.8
*NGC 6701	O.1OE-12	3878	1.26	41.76	30.3
*ESO 593-IG008S	0.33 E- 14	13024	-0.04	40.07	34.4

Table 4a. H_α Luminosities - IRAS Bright Galaxies

Name	$F(H_\alpha)$	Cz (km s^{-1})	E(B-V)	log $L(H_\alpha)$	$EW(H_\alpha)$
(1)	(2)	(3)	(4)	(s)	(6)
*ESO 593-IGO08N	O. 17 E- 13	13097	1.16	41.97	**85.0**
● IR 19297-0406	0.66E-14	25143	1.49	42.49	**89.2**
*NGC 6926	0.34E-14	5760	1.63	41.00	**11.3**
*ZW 448.020Main	0.25E-12	10635	0.31	42.11	**287.4**
*Zw 448.020NW	0.91 E-14	10772	0.92	41.29	**32.5**
● ESO 286-IG019	0.50E-13	12901	1.07	42.34	**75.8**
*ESO 343-IG013S	0.70E-14	5550	0.57	40.24	**15.2**
*ESO 343-IG013N	0.32E-13	5792	1.04	41.40	**52.5**
*IC 5135	0.21E-12	4321	1.04	41.96	**66.7**
*IC 5179	0.44E-13	4987	1.18	41.54	**29.3**
*ESO 602-G025	0.54E-13	7455	1.24	**42.05**	**49.1**
*ESO 534-GO09	0.46E-14	3323	0.63	**39.66**	**2.7**
*UGC 12150	0.41E-13	6670	1.93	42.51	**29.3**
*IR 22491-1808	0.23E-13	23262	0.81	**42.29**	**76.7**
*NGC 7469	0.29E-11	4902	0.01	**42.17**	**263.6**
*Zw 453.062	0.12E-13	7556	1.27	**41.44**	**26.7**
*Zw 475.056	0.54E-13	8155	1.13	**42.02**	**31.8**
*NGC 7591	0.24E-13	4968	1.39	**41.49**	**17.1**
● NGC 7592W	0.82E-13	7318	0.42	**41.40**	**106.5**
*NGC 7592E	0.75E-13	7382	0.71	**41.66**	**84.3**
*NGC 7674	0.22E-12	8746	**0.23**	41.80	**137.5**
*NGC 7679	0.19E-12	4806	**1.73**	42.69	**32.8**
● NGC 7714	0.98E-12	2805	**0.21**	41.43	**171.9**
IR 23365+3604	0.16E-13	19364	**0.88**	42.03	**34.8**
● NGC 777 1Main	0.59E-13	4363	**2.03**	42.39	**25.7**
*NGC 7771S	0.73E-13	3993	**0.61**	41.01	**89.0**
*Mrk 331	0.18E-12	5486	**1.09**	42.15	**62.1**

Table 4b. H_α Luminosities - Warm IRAS Galaxies

Name	F(H_α)	Cz (km S-')	E(B-V)	log L(H_α)	EW(H_α)
(1)	(2)	(3)	(4)	(5)	(6)
*IR 02433+1544	0.70E-13	3947	0.65	41.02	70.0
MCG+0310045	0.24E-12	1110	0,93	40.72	50.0
*IR 04259-0440	0.14E-13	4763	0.95	40.78	17.3
IR 09209+3943	0.15E-13	27669	0.89	42.34	65.2
IR 09218+3428	0.18E-13	20310	0.78	42.02	105.9
IR 09245+3517	0.14E-13	41694	1.36	43.17	73.7
IR 09252+3124	0.46E-14	23914	1.62	42.41	35.4
IR 09268+2808	0.12E-13	13088	0.99	41.65	48.0
Zw 238.066	0.23E-13	10207	1.10	41.82	30.3
IR 09303+2736	0.23E-14	12718	1.72	41.63	16.4
IR 09338+3133	0.29E-13	22946	0.69	42.26	72.5
IR 09339+2835	0.15E-13	35769	0.91	42.61	115.4
IR 09399+2830	0.16E-13	15962	0.95	41.92	57.1
Zw 182.010	0.29E-13	12324	1.02	42.01	52.7
IR 09425+1751	0.54E-13	38423	0.64	42.96	317.6
IR 09427+1929	0.33E-14	44736	0.43	41.69	52.4
IR 09433+1910	0.93E-15	15947	0.00	39.75	1.6
*IR 10210+7528	0.79E-13	8175	0.63	41.69	79.8
IR 11571+3004	0.47E-14	15163	1.55	41.93	36.2
*IR 12071-0444	0.33 E- 13	38513	1.64	43.74	173.7
*Zw 041.073	0.25E- 12	5531	1.12	42.33	75.8
IR 12450+3401	0.59E-15	47621	0.05	40.63	12.0
*Zw 102.056	0.26E-12	6404	0.81	42.17	108.3
*IR 13446+1121	0.28E-12	6912	1.52	42.97	140.0
IR 14229+1425	0.15E-13	17974	0.65	41.70	53.6
IR 14341+3017NW	0.16E-13	10313	1.00	41.57	33.3
IR14341+3017SE	0.34E-13	10369	0.64	41.55	79.1
IR 14416+6618	0.76E-13	11300	0.67	42.01	135.7
IR 15206+3342	0.11E-12	37539	0.61	43.22	333.3
*IR 15304+3017	0.22E-13	19483	0.57	41.87	73.3
*IR 15312+4236	0.21E-13	5988	0.91	41.12	30.4
*IR 15324+3203	0.83E-14	32772	1.34	42.69	63.8
*IR 15359+3139	0.78E-14	16061	i .27	41.93	43.3
*IR 15364+3320	0.14E-13	6743	0.33	40.48	29.8
*IR 15384+3841	0.89E-14	20204	0.95	41.88	22.2
*IR 15391+3214NE	0.661-14	15775	1.09	41.66	66.0
● IR 15391 +3214SW	0.29E-13	15981	1.08	42.31	145.0
*IR 15394+3532	0.77E-14	37208	0.36	41.81	108.5
*IR 15404+3228	0.79E-14	20794	1.64	42.54	31.6
*IR 15414+3238	0.37E-14	60926	0.94	42.55	94.9
*IR 15418+3938	0.63E-14	19423	1.47	42.21	30.0
*IK 15418+2840	0.43E-13	9888	0,38	41.35	50.6
*IR 15440+2834	0.27E-13	9867	0.84	41.60	49.1
● IR15445+3312	0.12E-14	46713	0.67	41.53	52.2
*IR 15469+2853	0.73E-14	9798	1.73	41.91	18.7
● IR15463+4131	0.13E-13	9954	0.54	41.00	29.5
● IR15481+2920	0.15E-13	25000	0.76	42.12	25.4
● IR 15483+4227	0.22E-13	6304	0.44	40.72	44.9
● IR15514+3330	0.15E-13	16525	0.85	41.82	57.7
*IR 15519+3537	0.14E-13	25567	1.31	42.65	45,2

Table 4b. H_α Luminosities - Warm IRAS Galaxies

Name	F(H_α)	Cz (km s^{-1})	E(B-V)	log L(H_α)	EW(H_α)
(1)	(2)	(3)	(4)	(5)	(6)
*IR 15534+3519	0.33E-14	25682	0.25	40.98	2.4
*IR 15535+2854	0.95E-14	23354	1.08	42.17	36.5
*IR 15543 +4158NW	0.91E-14	40294	0.61	42.21	126.4
*IR 15543 +4158SE	0.68E-14	40437	0.94	42.41	69.4
*IR 15543+3013	0.59E-13	36364	0.16	42,48	347.1
*IR 15545+4000	0.40E-13	21347	0.55	42.19	121.2
*IR 15549+4201	0.61E-13	10489	0.48	41.66	46.9
*IR 15569 +2807W	0.32E-14	15506	0.59	40.84	18.8
*IR 15569 +2807E	0.17E-14	15693	1.14	41.12	17.3
*IR 15589+4121	O.1OE-14	28661	0.02	40.34	19.2
*IR 16007+3743	0.27E-14	55412	1.21	42.59	64.3
IR 16130+2725	0.56E-13	12977	0.74	42.07	186.7
Zw 052.015	0.85E-13	1426	1.03	40.58	47.2
*IR 21484-1314	0.90E-14	23038	1.54	42,59	42.9
*IR 21549-1206NW	0.33E-14	15102	0.41	40.65	27.5
*IR 21549-1206SE	0.7013-14	15267	0.36	40.94	46.7
*IR 22114-1109	0.28E-13	16358	0.58	41.82	121.7
*IR 22152-0227	0.25E-13	27880	0.92	42.60	89.3
*IR 22191-1400	0.71E-14	23234	1.19	42.15	37.4
*IR 22193-1217	0.1913-13	23917	0.85	42.27	79.2
IR 22199-0345	0.37E-13	18111	0.69	42.14	137.0
*IR 22204 -0214NW	0.31 E-14	41836	0.95	42.11	64.6
*1R 22204 -0214SE	0.22E-14	41808	1.30	42.31	57.9
*IR 22213-0238	0.19E-13	16906	1.41	42.50	105.6
*IR 22220-0825	0.77E-14	18062	0.98	41.74	36.7
*IR 22225-0645	0.75E-14	26765	1.11	42.23	44,1
*IR 22279 -1112NW	0.69E-14	26048	0.82	41.88	75.0
*IR 22279 -1112SE	0.16E-14	26276	1.57	41.99	11.4
*IR 22283-1439	0.69E-14	18579	1.72	42.45	75.0
*IR 22338-1015	0.18E-13	18510	1.14	42.29	78.3
*IR 22381-1337	0.39E-13	32968	0.57	42.61	390.0
JR 22472+3439	0.11E-13	7122	0.66	40.74	52.4

Table 5. Electron Temperatures

l'.lamc	$\frac{[OIII](\lambda_{4959} + \lambda_{5007})}{[O\ III]\lambda_{4363}}$	T_e (K) $N_e = 10^3$ (c m^{-3})	T_e (K) $N_e = 10^6$ (c m^{-3})	Spectral Type
(1)	(2)	(3)	(4)	(5)
BGSs Objects				
IC 1623N	51	17140	9260	HII
IC 1623SE	233	9790	6440	HII
IIIZw 35N	44	18650	9520	HII
NGC 1614	78	14090	8280	HII
UGC 8335S13	163	10950	6810	HII
NGC 5256NE	59	16210	8760	S2
NGC 7592E	37	20860	10070	HII
NGC 7592W	153	10950	7000	S2
NGC 7674	97	12960	7830	S2
NGC 7714	70	14900	8510	}111
WGSs Objects				
IR 09425+1751	106	12600	7610	S2
IR 14229+1425	80	14090	8050	S2
IR 15206+3342	137	11580	7200	HII
IR 15304+3017	80	14090	8050	S2
IR 15418+2840	58	16210	8760	S2
IR 22114-1109	57	16210	9000	S2
IR 22152-0227	137	11580	7200	S2
IR 22199.0345	103	12600	7610	S2

Table 6. Long-Slit Sample"

Number	Name	cz (km/s)	log(L_{ir}) (LO)	Spectral Type
(1)	(2)	(3)	(4)	(5)
1	NGC 34	5860	11.43	S2
2	NGC 660	822	10.37	L
3	NGC 1204	4486	10.91	L
4	Zw 102.056	6404	10.94	HII
5	IR 15414+3238	60926	12.02	HII
6	IR 22220-0825	18062	11.39	HII
7	UGC 8696	11585	12.11	L
8	IR 15250+3609	16217	11.98	L
9	ESO 286-IG019	12901	11.99	L
10	IC 5135	4321	11.22	L
11	Zw 453.062	7556	11.32	L
12	NGC 7679	4806	11.05	HII
13	Zw 247.020	7758	11.25	HII
14	IR 18293-3413	5400	11.71	HII
15	ESO 602-G025	7455	11.28	S2
16	NGC 7591	4968	11.00	L
17	MCG-0304014	10473	11.61	HII
18	IR 15304+3017	19483	11.18	S2
19	NGC 5953	2069	10.40	L
20	IR 22114-1109	16358	11.21	S2
21	Zw 475.056	8155	11.53	S2
22	NGC 7674	8746	11.51	S2
23	Mrk 331	5486	11.44	HII

" Mixed list of objects from the CBGSs and WGSs, not in RA order

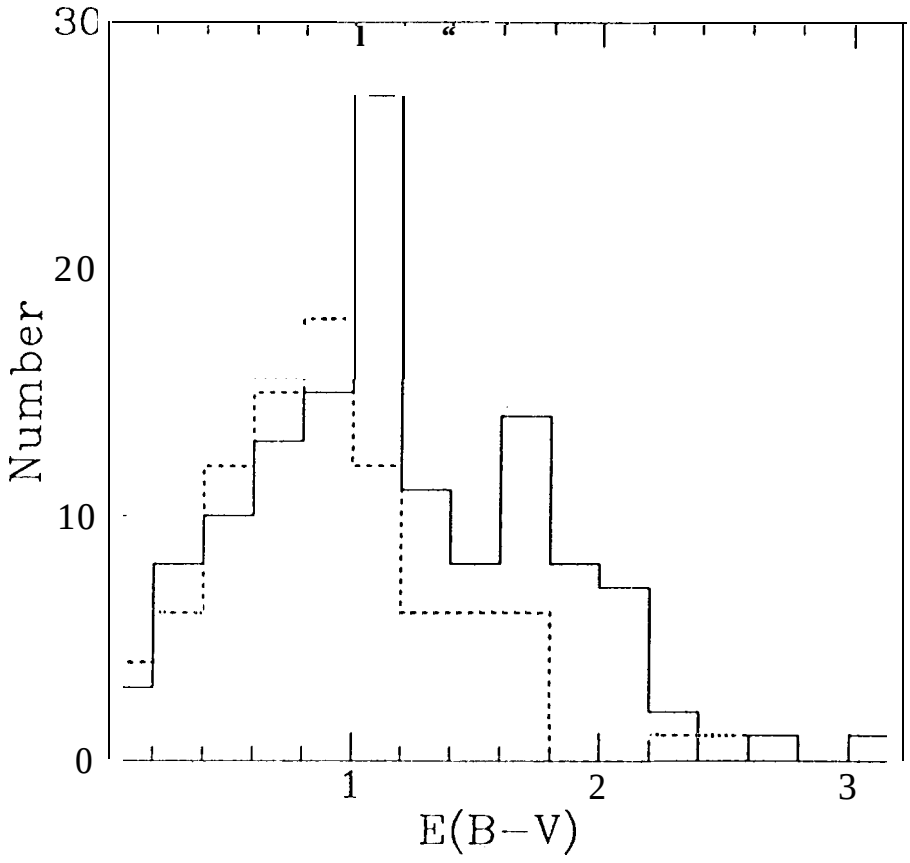
30
20
10
0
Number
1
2
3
E(B−V)

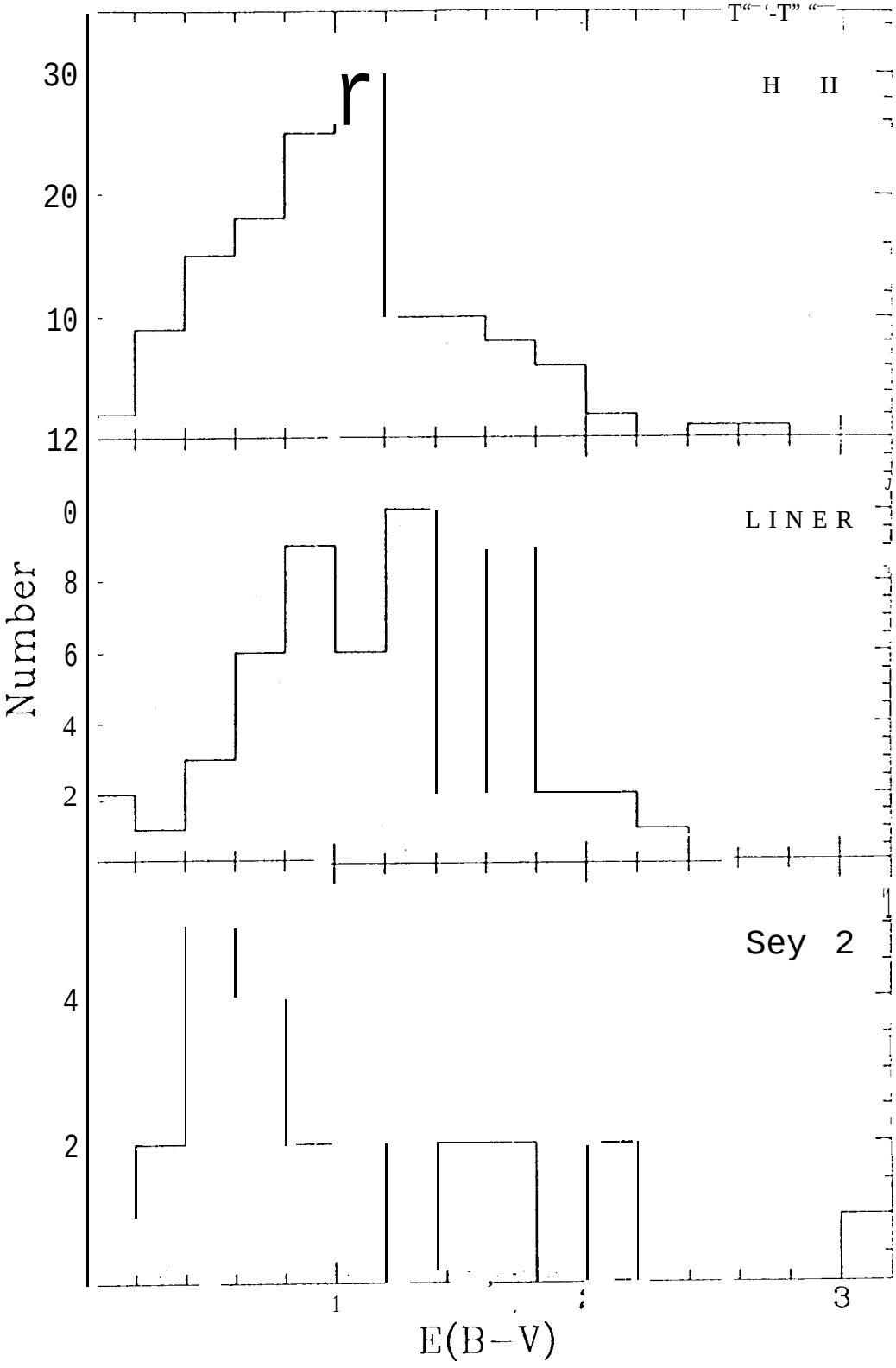
H II
LINER
Sey 2
Number
E(B−V)
30
20
10
12
0
8
6
4
2
4
2
1
3

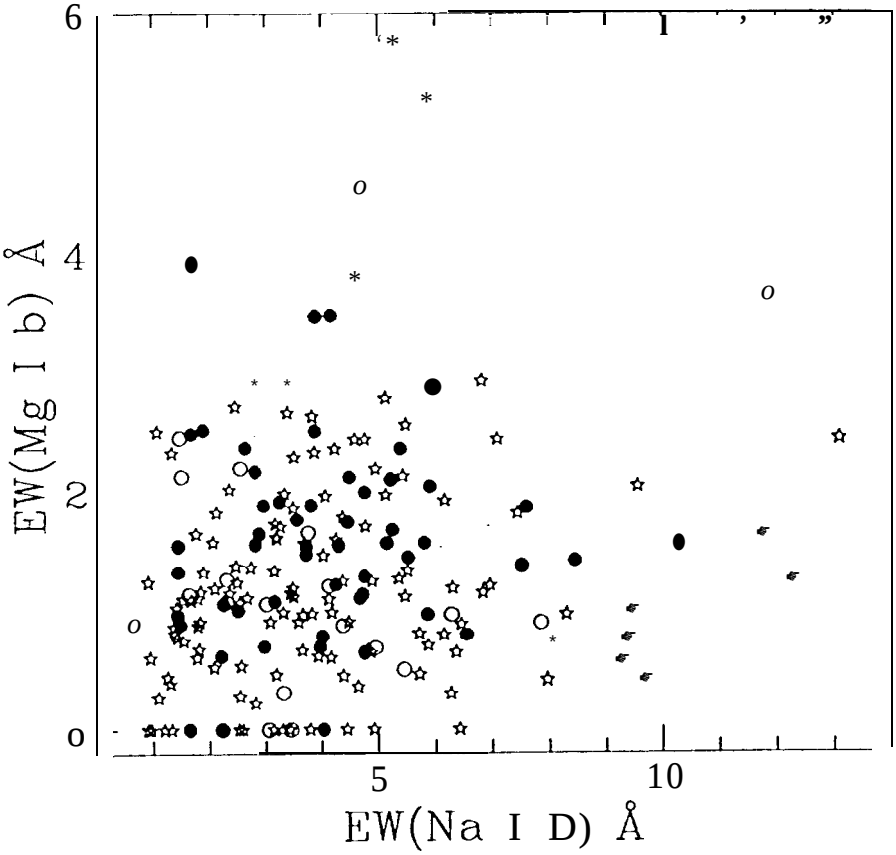
6
4
2
0
EW(Mg I b) Å
5
10
EW(Na I D) Å

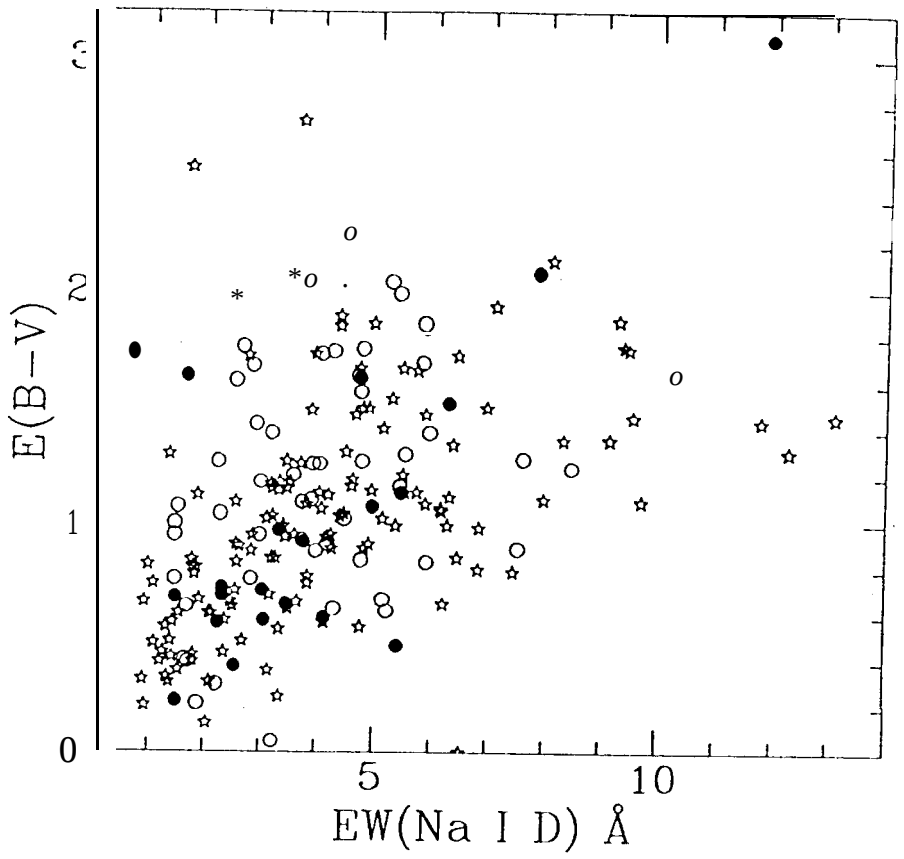
E(B−V)
0
1
2
5
10
EW(Na I D) Å

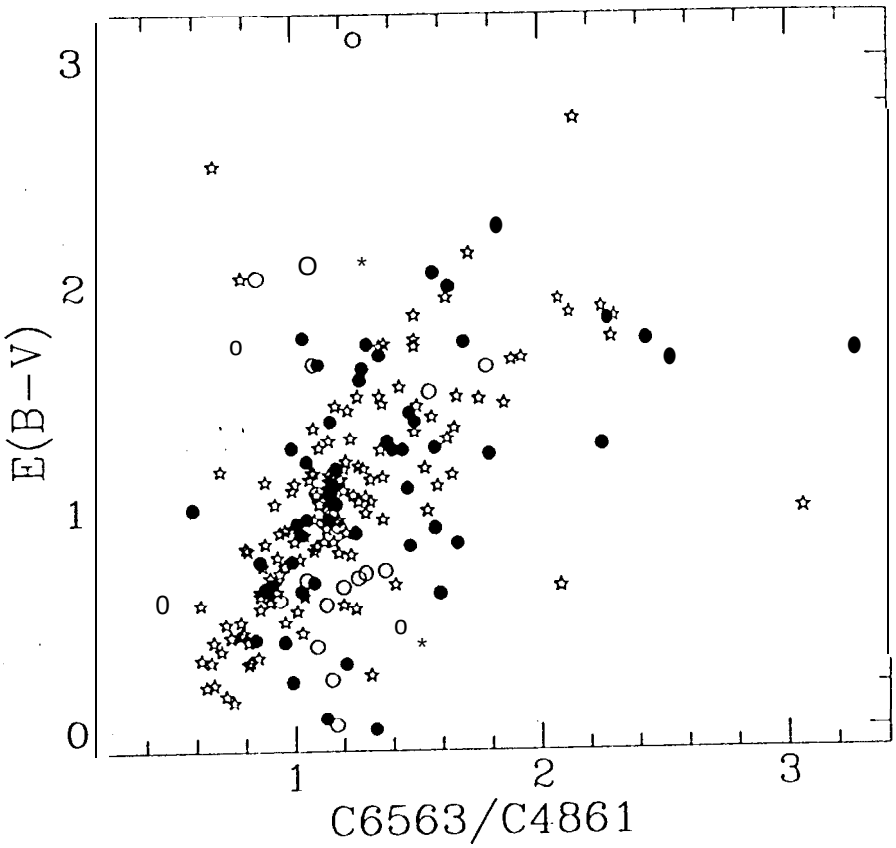
E(B−V)
C6563/C4861
0
1
2
3
1
2
3

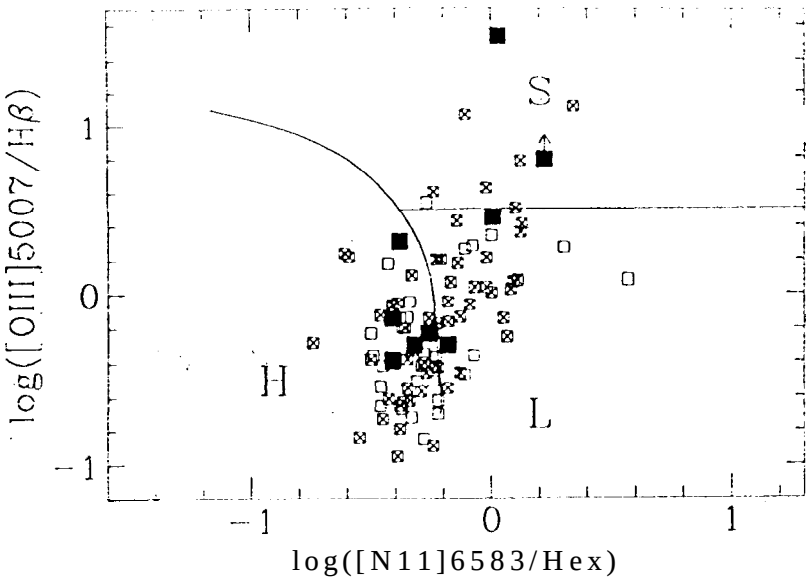
S
H
L
log([OIII]5007/Hβ)
log([N11]6583/Hex)

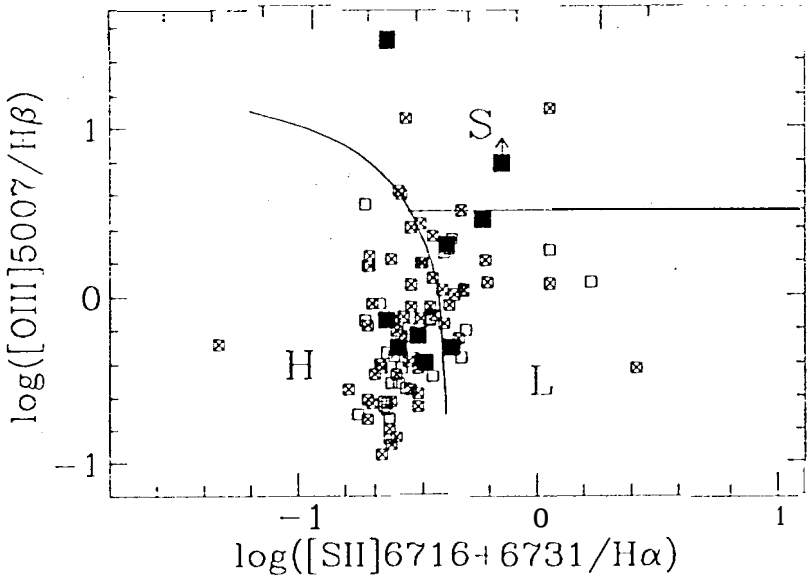
S
H
L
log([OIII]5007/Hβ)
log([SII]6716+6731/Hα)

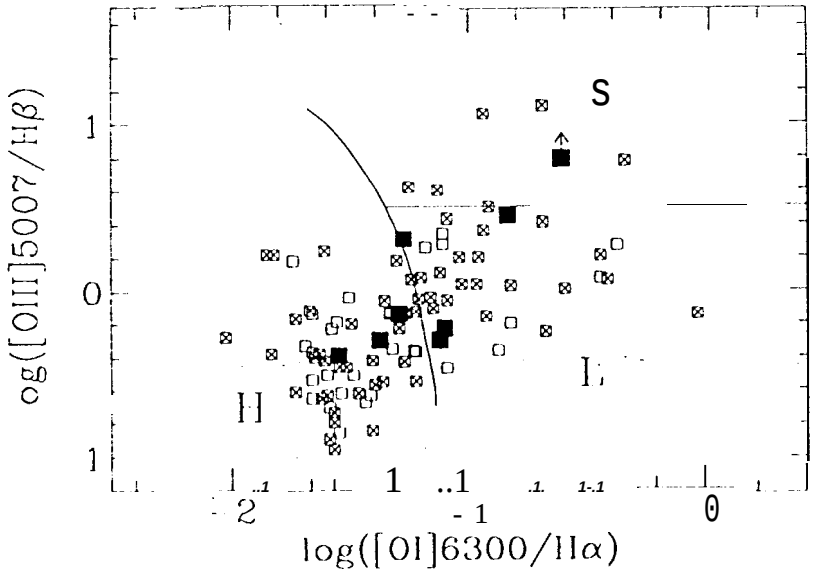
S
H
L
log([OIII]5007/Hβ)
log([OI]6300/Hα)

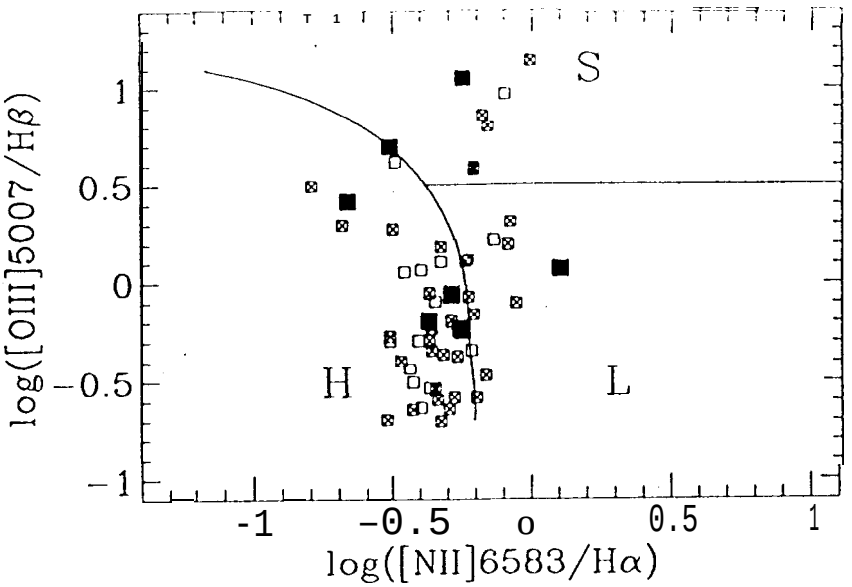
S
H
L
log([OIII]5007/Hβ)
log([NII]6583/Hα)
1
0.5
0
−0.5
−1
-1
-0.5
o
0.5
1

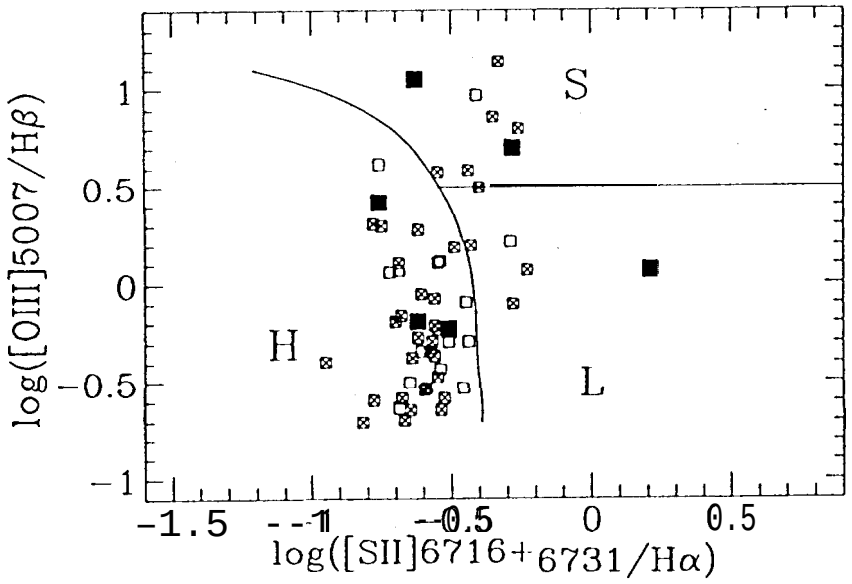
S
H
L
log([OIII]5007/Hβ)
log([SII]6716+6731/Hα)
1
0.5
0
−0.5
−1
-1.5
-1
-0.5
0
0.5

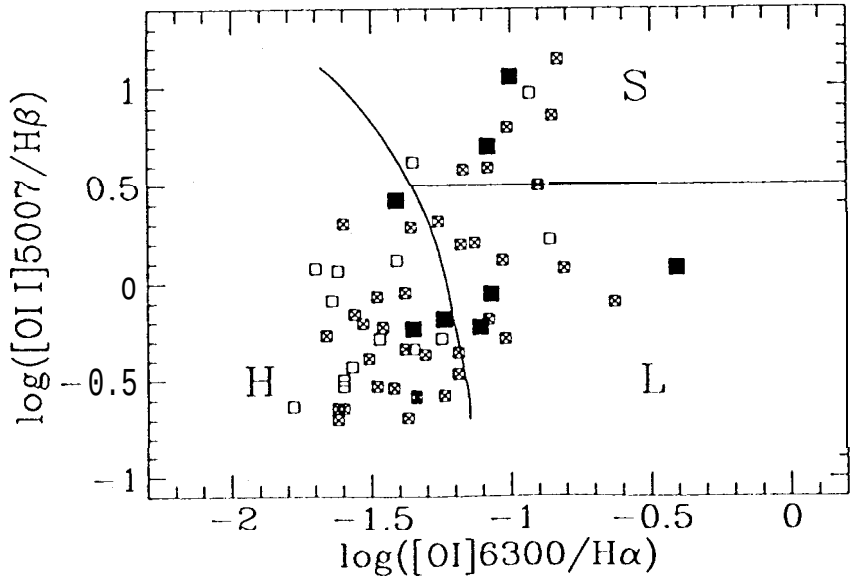
S
H
L
log([OI]5007/Hβ)
log([OI]6300/Hα)
1
0.5
0
−0.5
−1
−2
−1.5
−1
−0.5
0

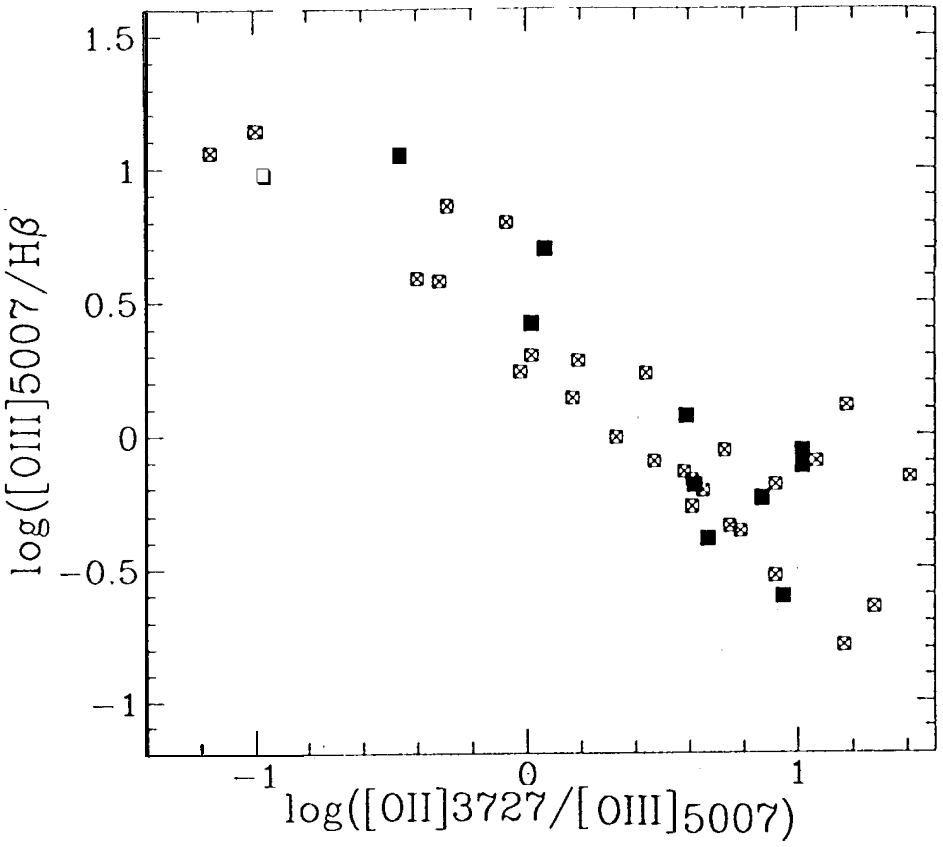
1.5
1
0.5
0
−0.5
−1
−1
0
1
log([OII]5007/Hβ
log([OII]3727/[OIII]5007)

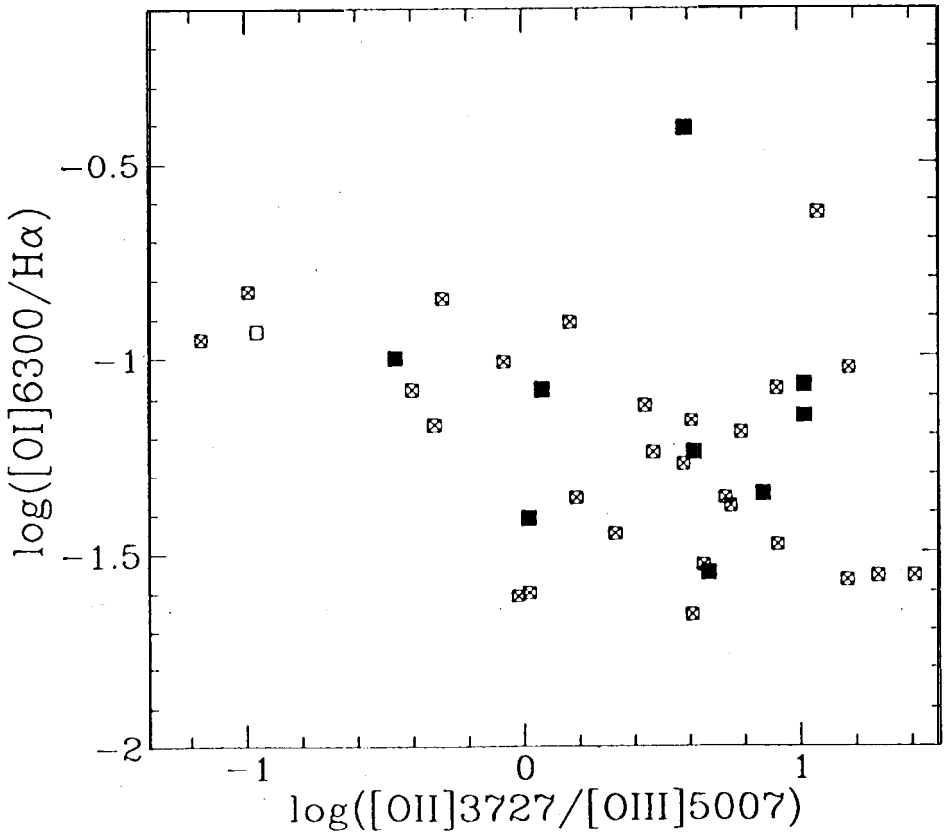
−0.5
−1
−1.5
−2
−1
0
1
log([OI]6300/Hα)
log([OII]3727/[OIII]5007)

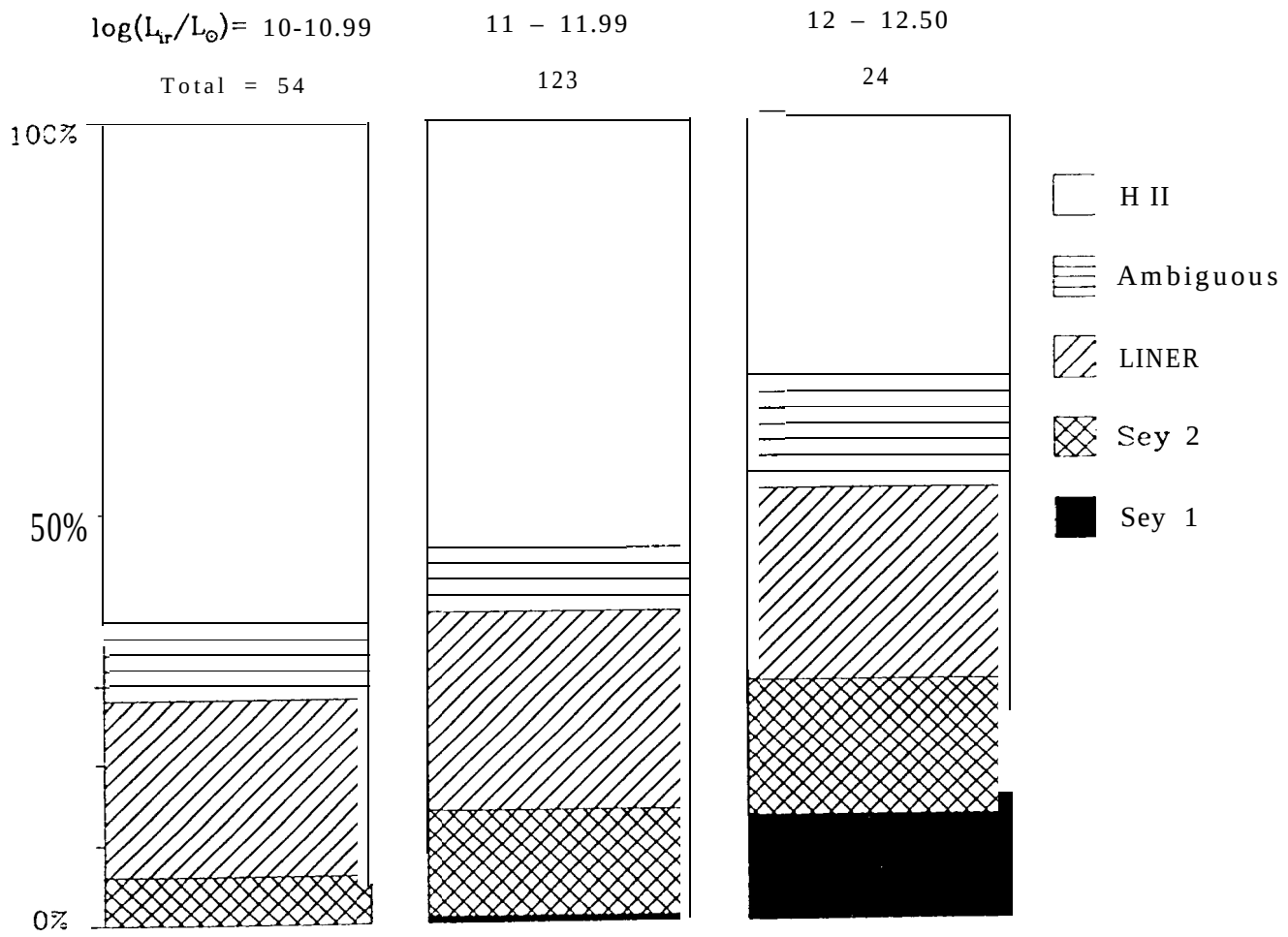
log(L_ir/L_⊙)= 10-10.99
11 – 11.99
12 – 12.50
Total = 54
123
24
100%
50%
0%
H II
Ambiguous
LINER
Sey 2
Sey 1

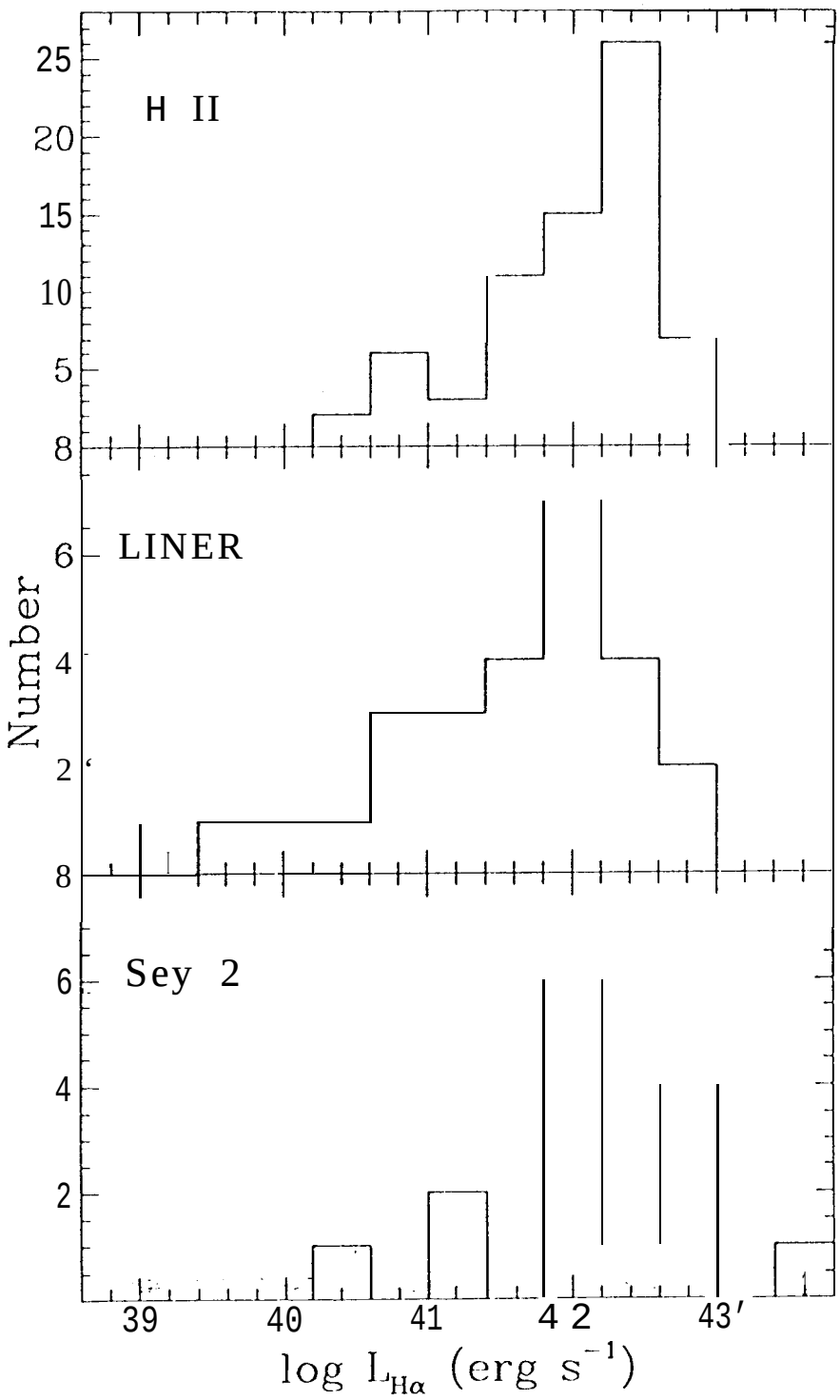
H II
LINER
Sey 2
Number
25
20
15
10
5
8
6
4
2
8
6
4
2
39
40
41
4 2
43′
log $L_{H\alpha}$ (erg s^{-1})

G

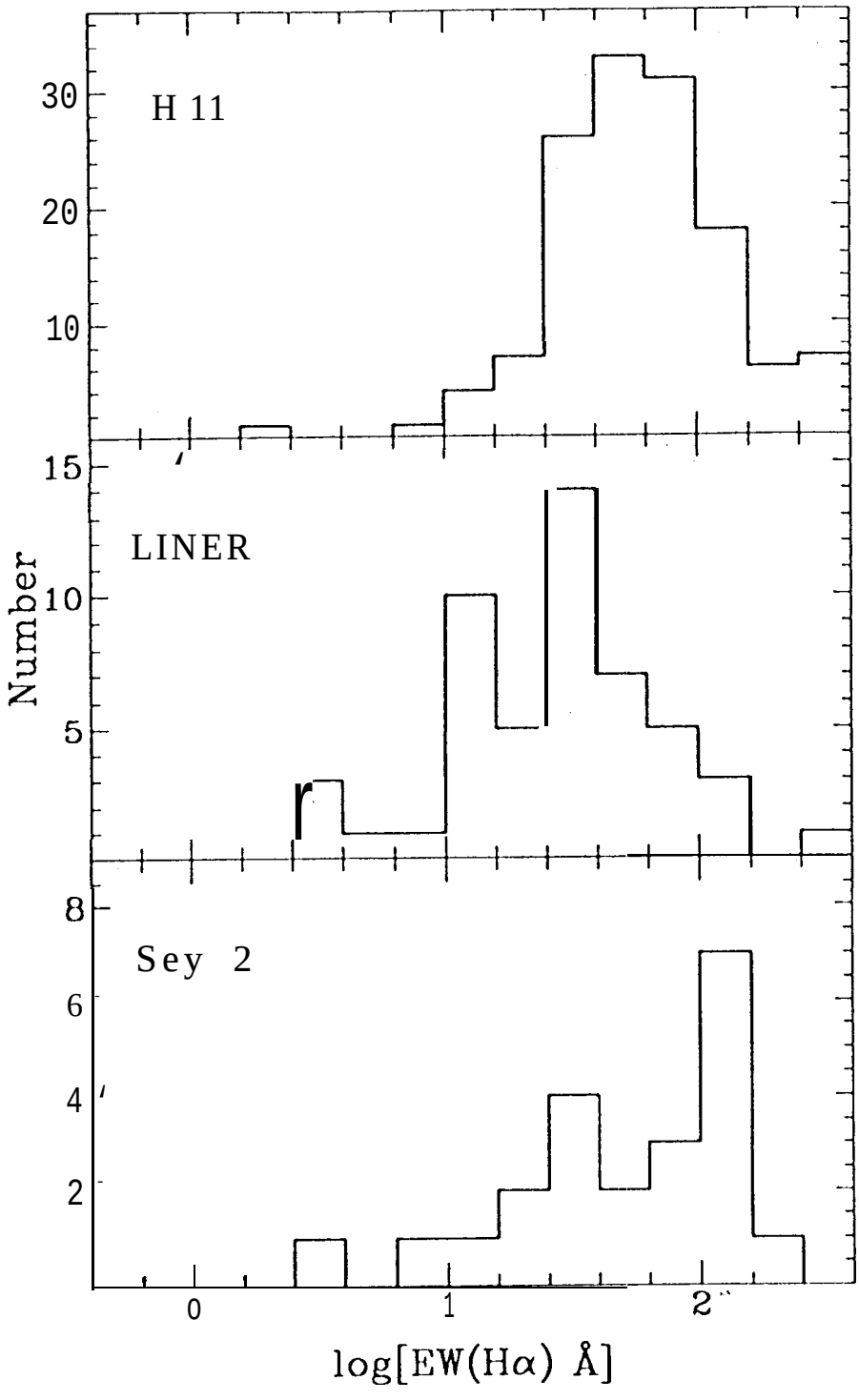
H 11
LINER
Sey 2
Number
log[EW(Hα) Å]
30
20
10
15
10
5
8
6
4
2
0
1
2

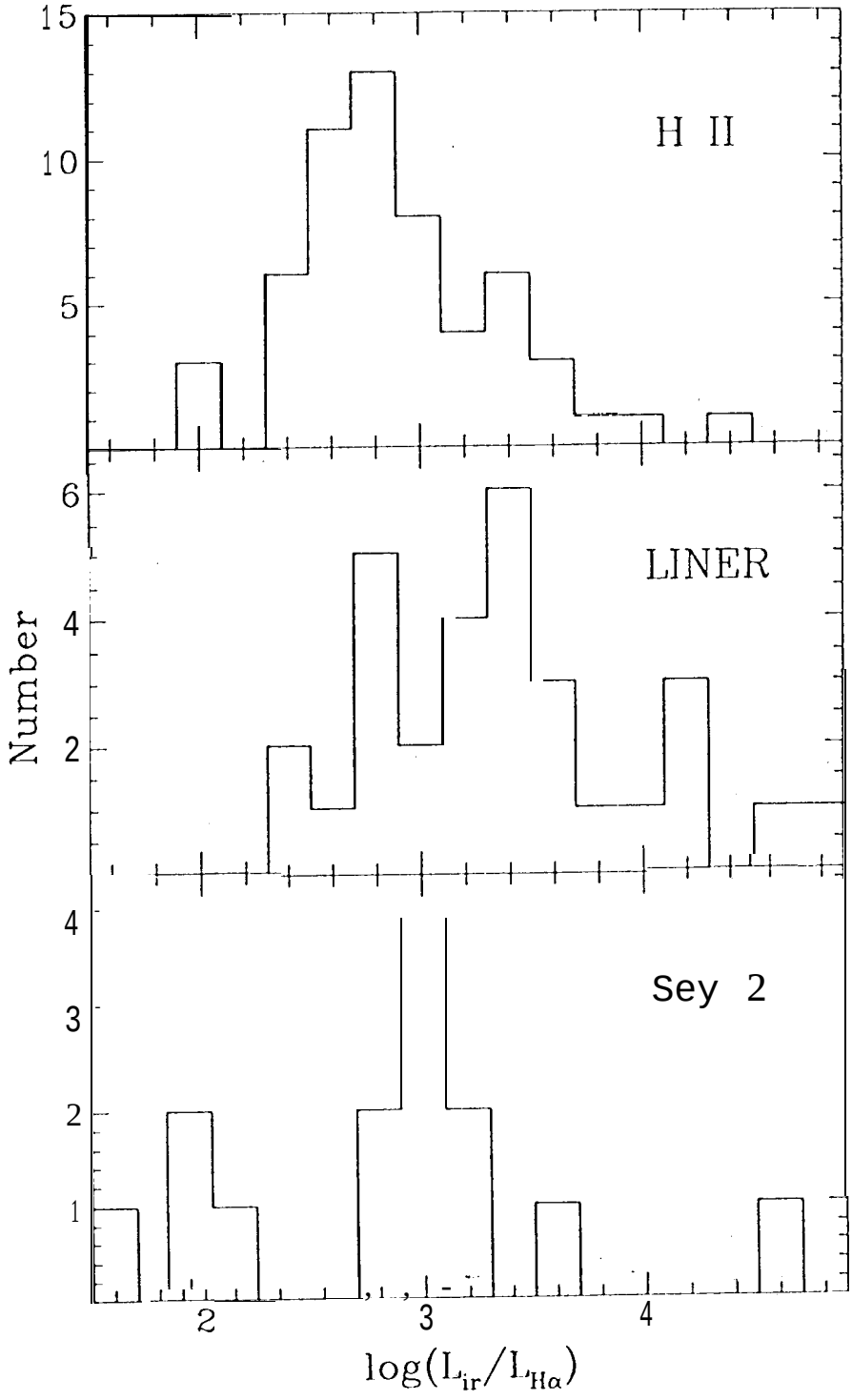
H II
LINER
Sey 2
Number
log(L_ir/L_Hα)

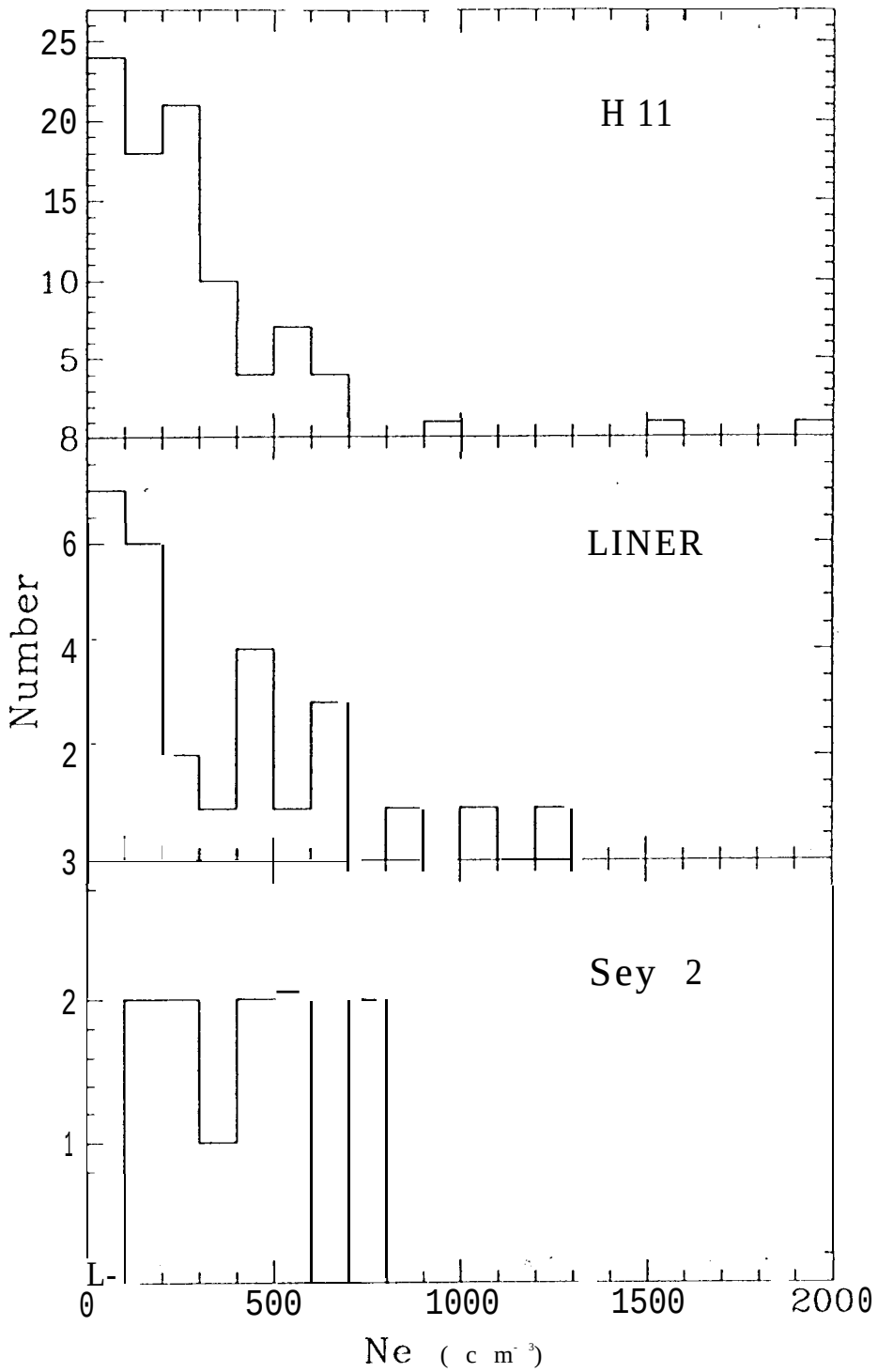
H 11
LINER
Sey 2
Number
Ne (c m⁻³)
25
20
15
10
5
8
6
4
2
3
2
1
L-
0
500
1000
1500
2000

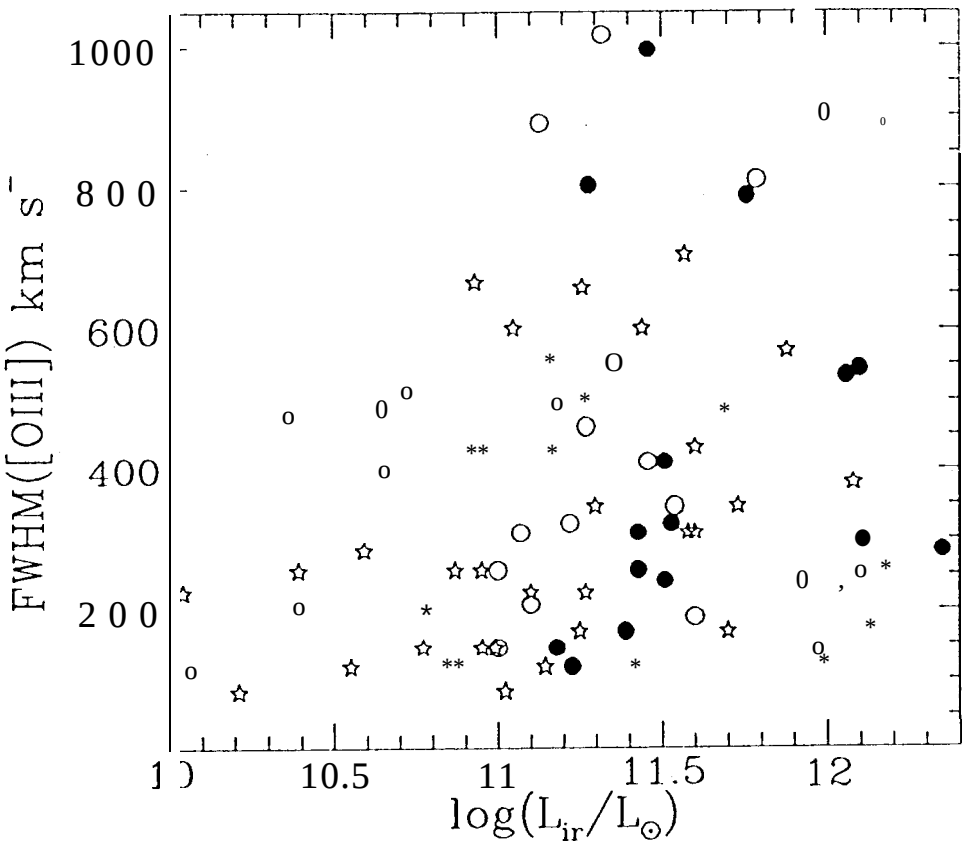
1000
800
600
400
200
FWHM([OIII]) km s⁻
10
10.5
11
11.5
12
log(L_ir/L_⊙)

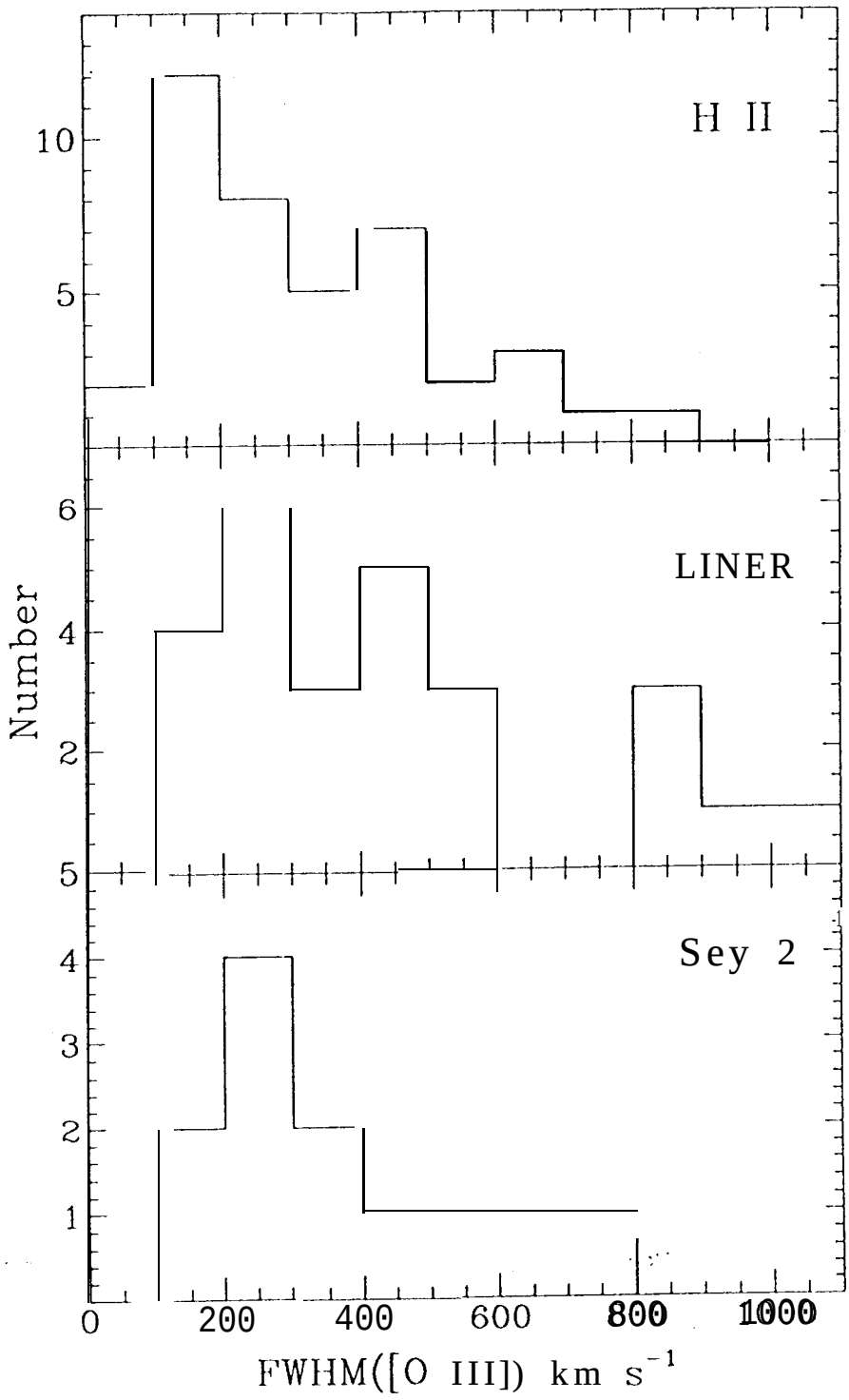
H II
LINER
Sey 2
Number
FWHM([O III]) km s^{-1}
0
200
400
600
800
1000
10
5
6
4
2
5
4
3
2
1

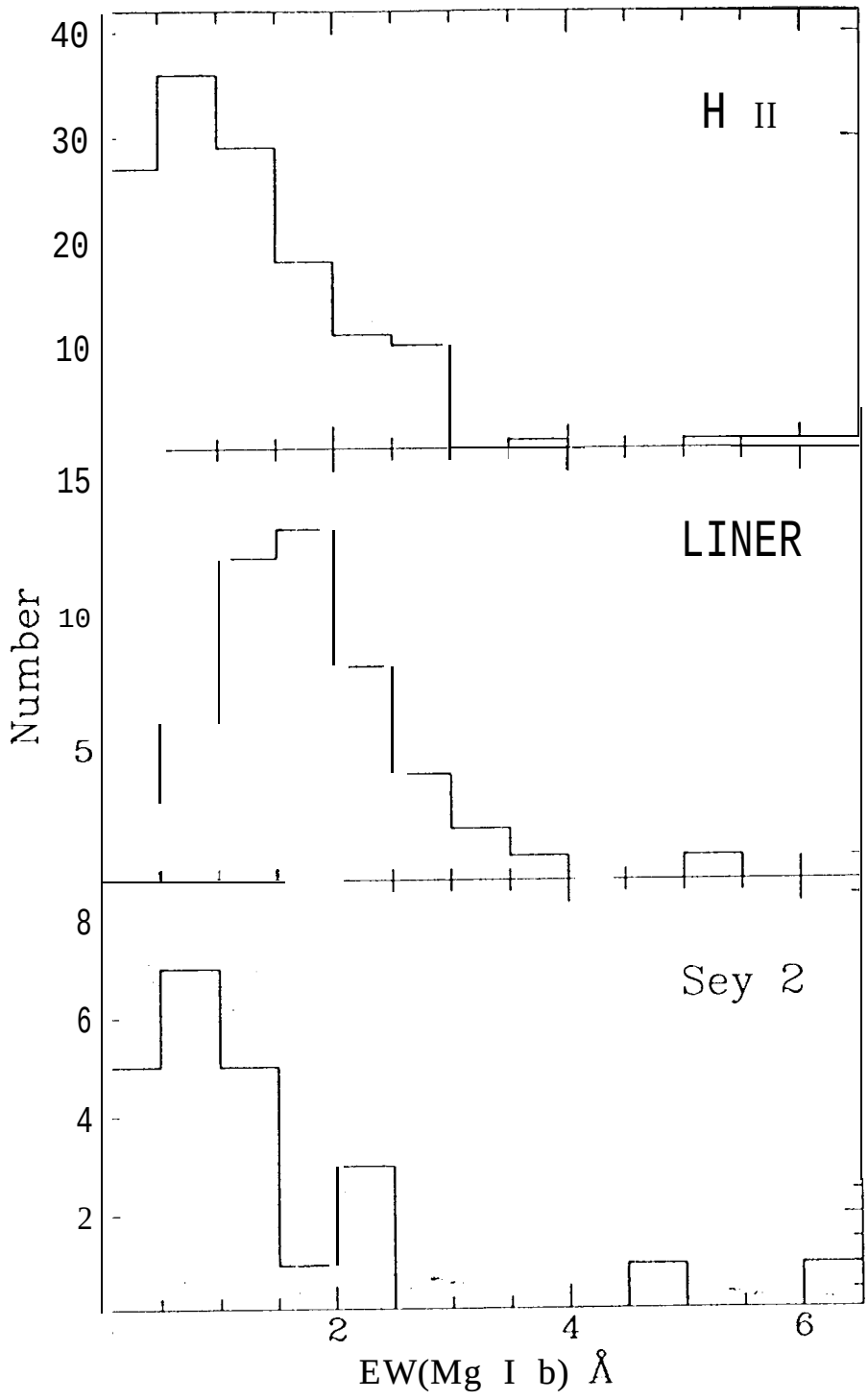
H II
LINER
Sey 2
Number
EW(Mg I b) Å
40
30
20
10
15
10
5
8
6
4
2
2
4
6

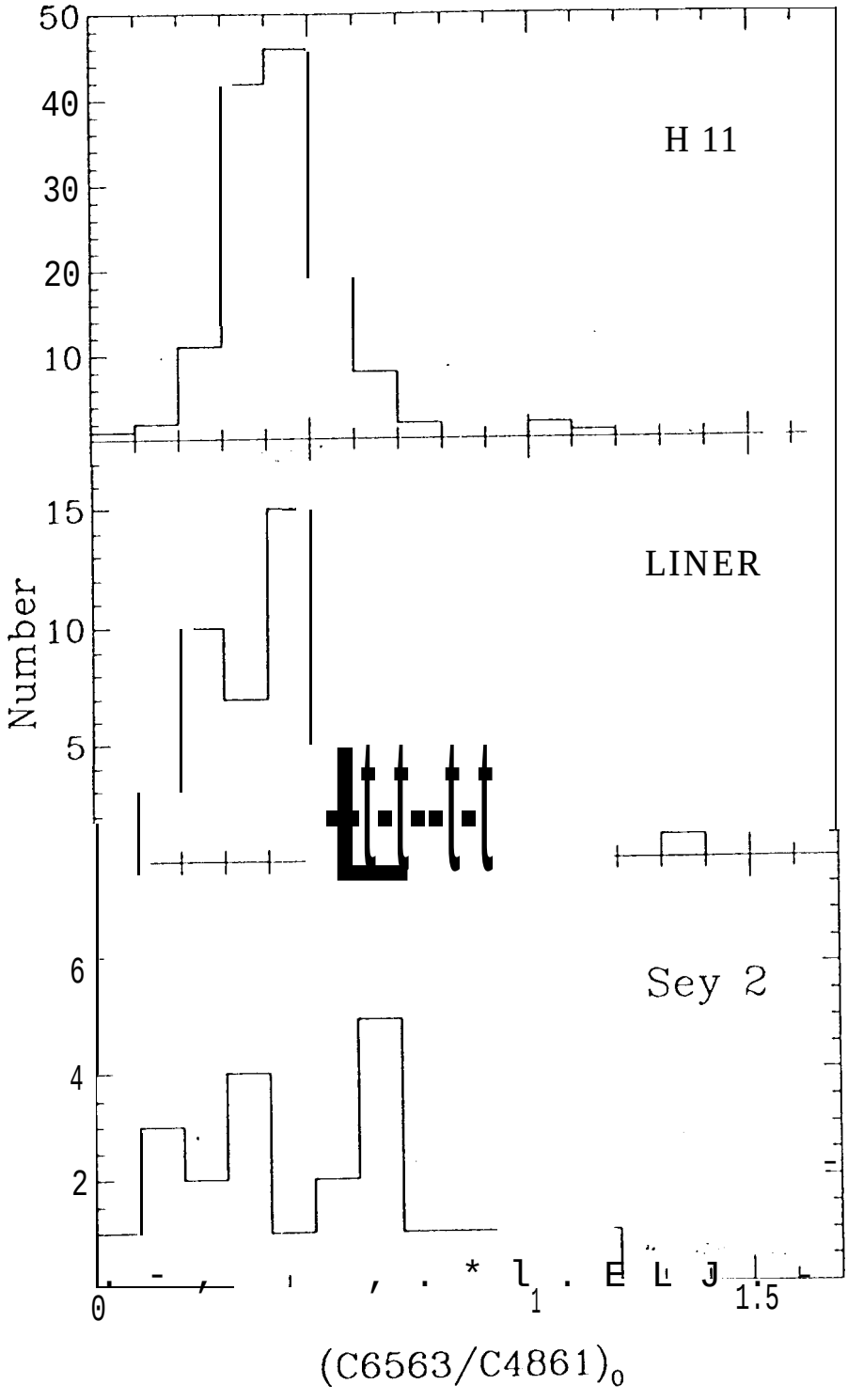
H 11
LINER
Sey 2
Number
50
40
30
20
10
15
10
5
6
4
2
0
1
1.5
(C6563/C4861)0

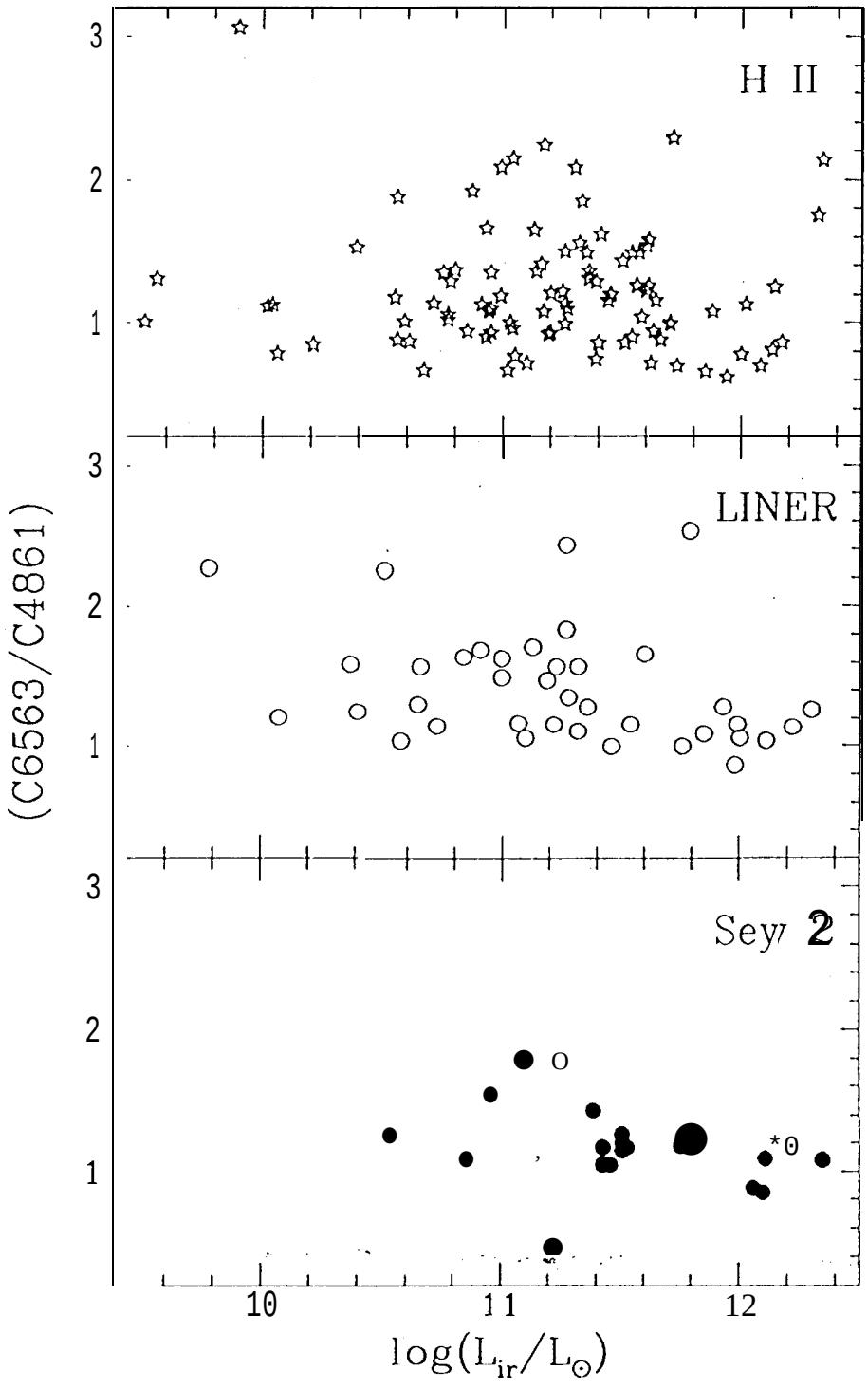
H II
LINER
Sey 2
(C6563/C4861)
log(L_ir/L_⊙)
3
2
1
10
11
12
o
*o

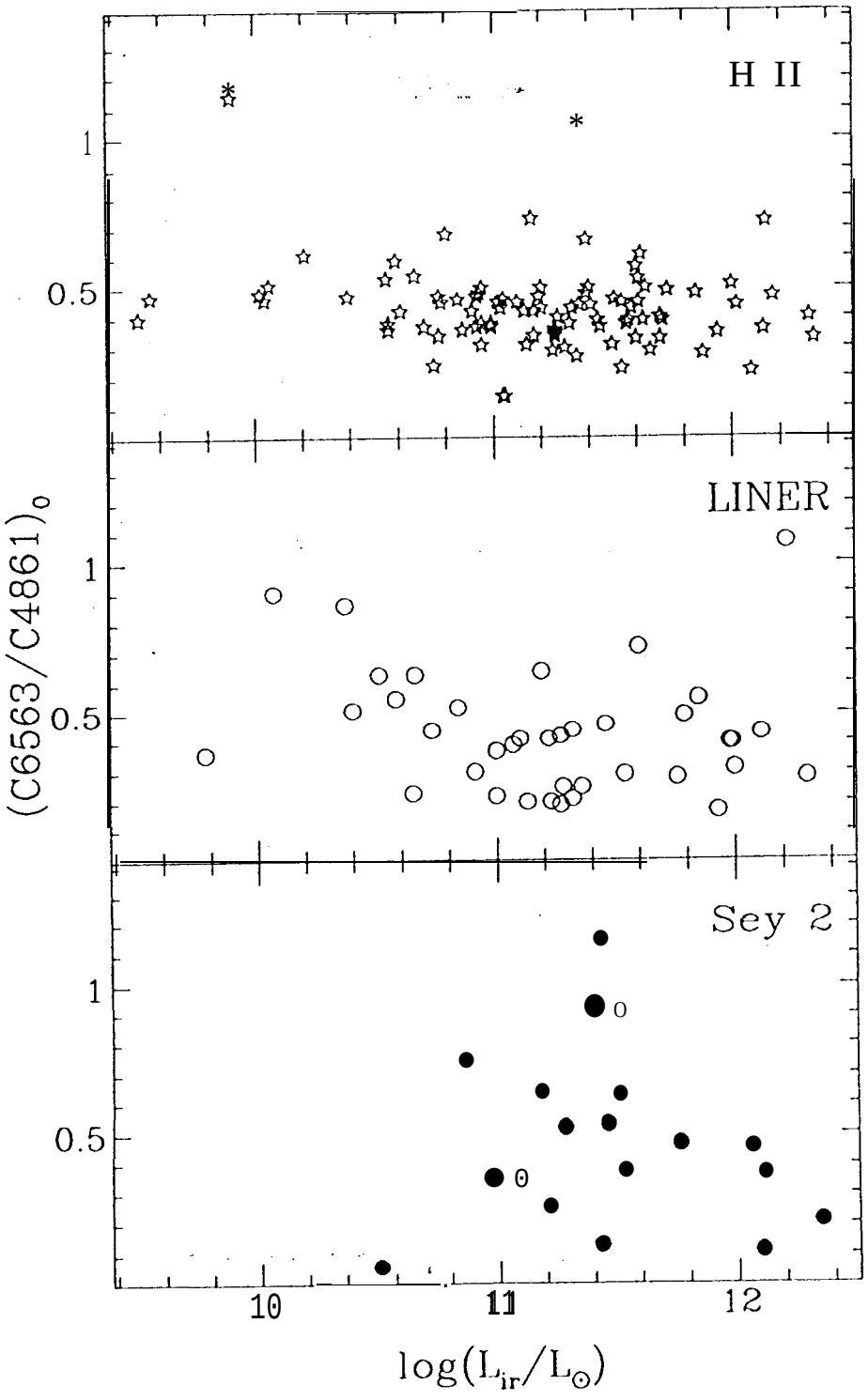
H II
LINER
Sey 2
1
0.5
1
0.5
1
0.5
10
11
12
(C6563/C4861)$_o$
log(L$_{ir}$/L$_\odot$)

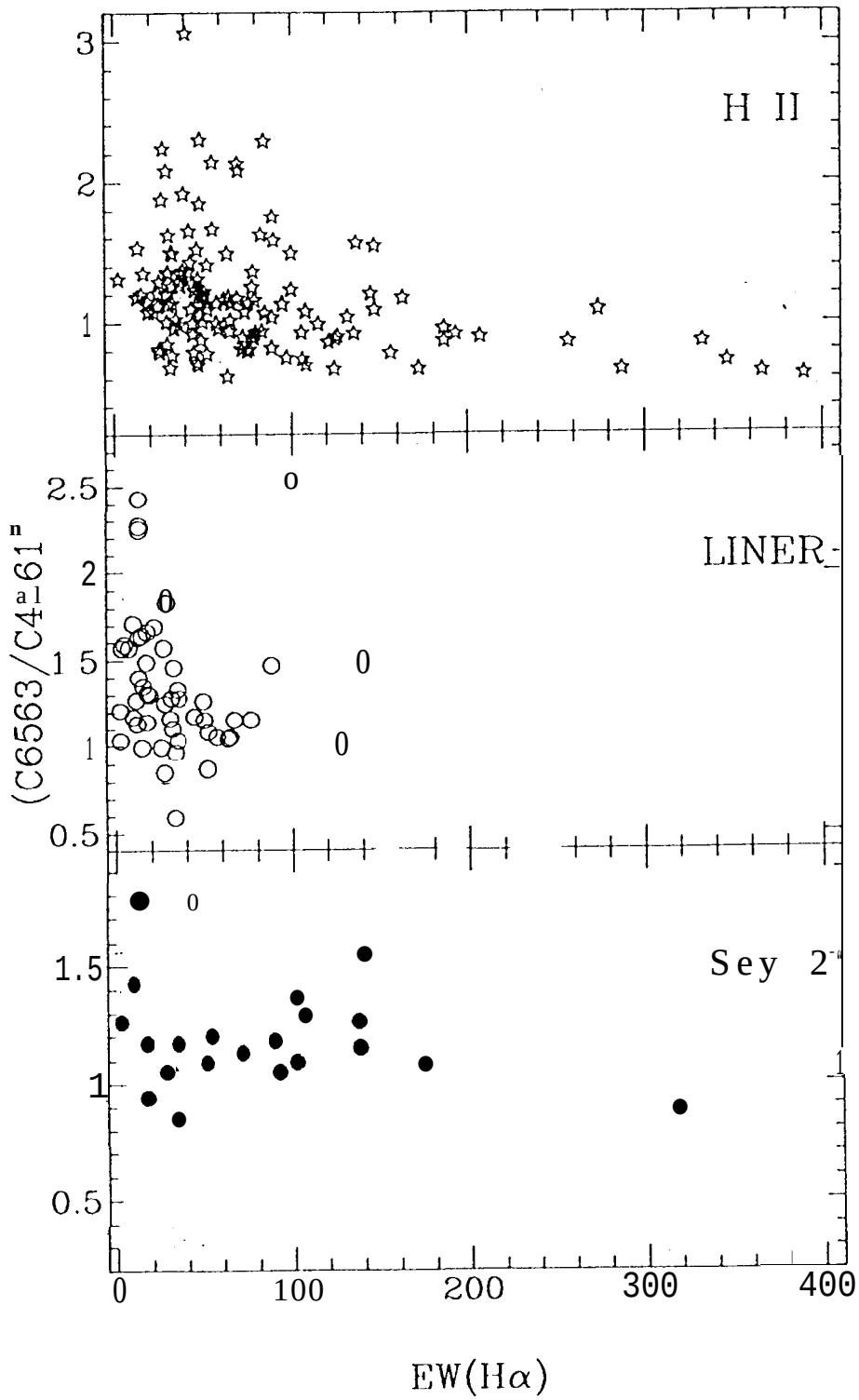
H II
LINER
Sey 2
(C6563/C4861)
EW(Hα)
3
2
1
2.5
2
1.5
1
0.5
1.5
1
0.5
0
100
200
300
400

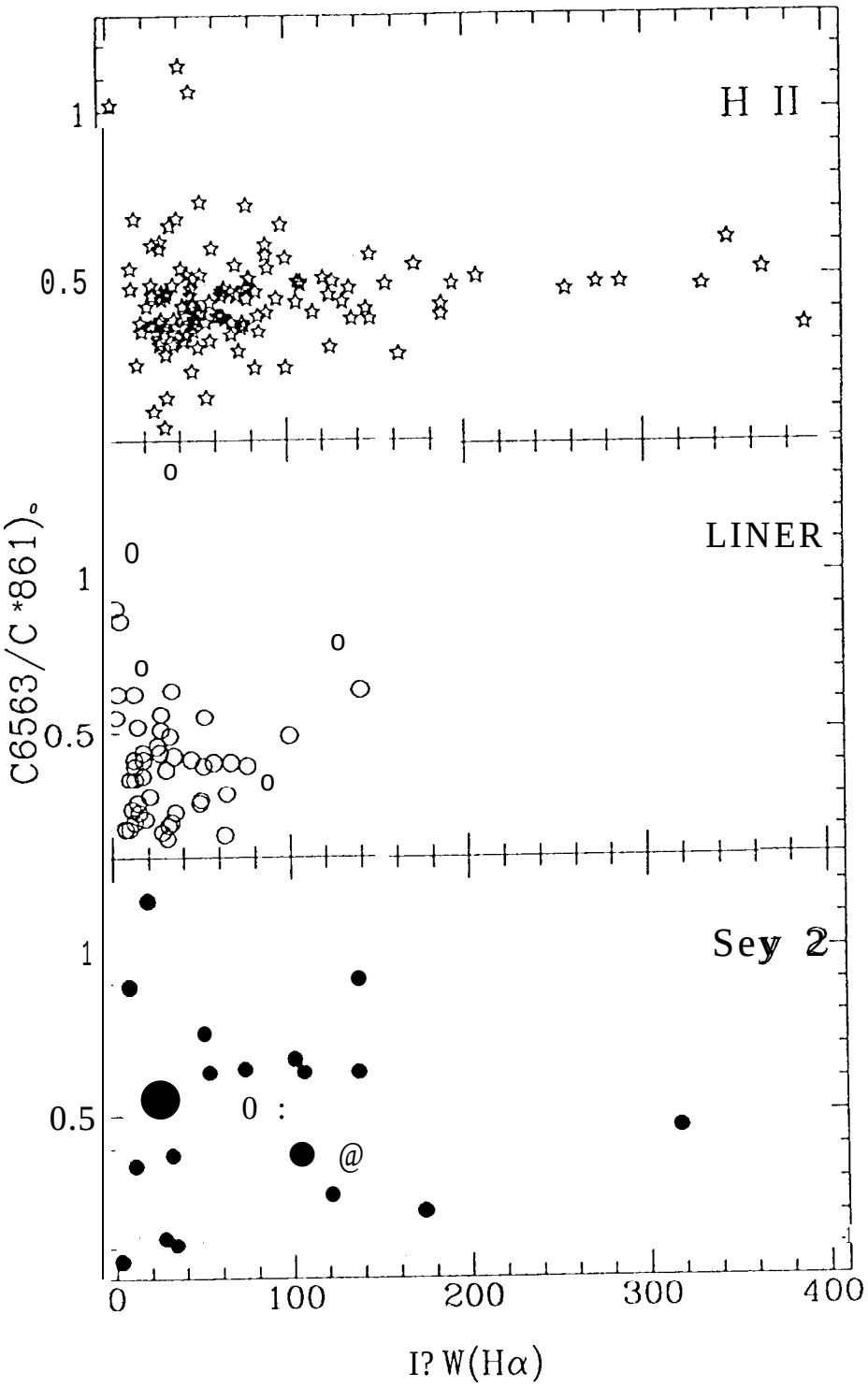
H II
LINER
Sey 2
1
0.5
1
0.5
1
0.5
C6563/C*861)o
0
100
200
300
400
I? W(Hα)

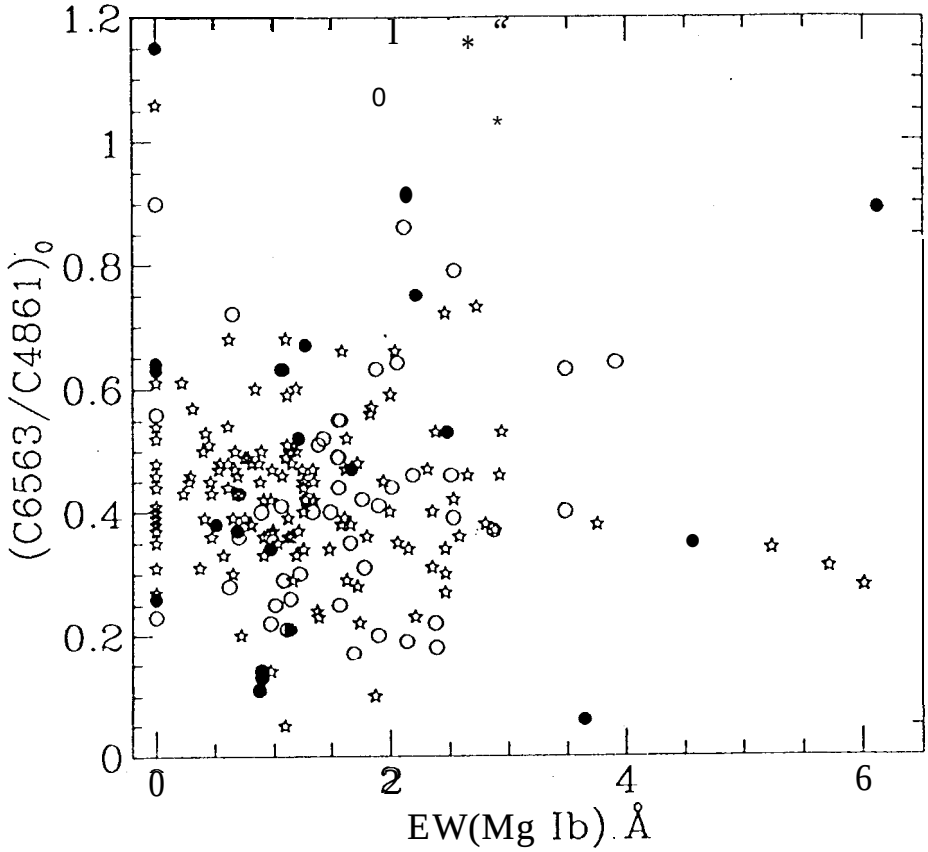
1.2
1
0.8
0.6
0.4
0.2
0
$(C6563/C4861)_0$
0
2
4
6
EW(Mg Ib) Å

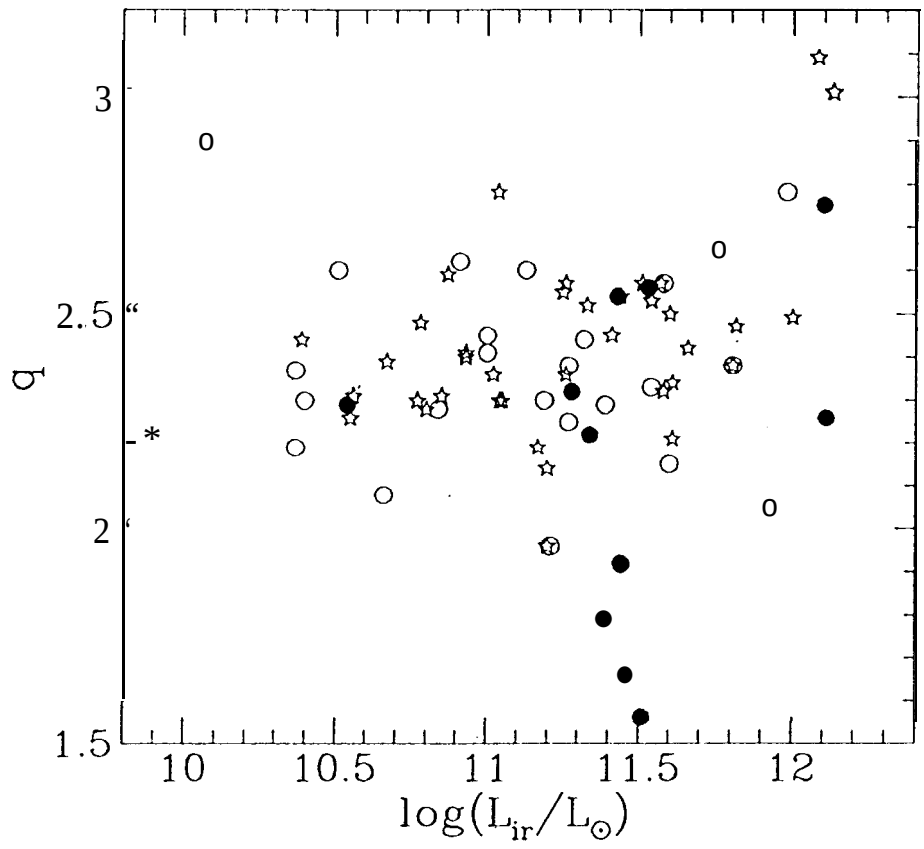
3
2.5
2
1.5
q
10
10.5
11
11.5
12
log(L_ir/L_⊙)

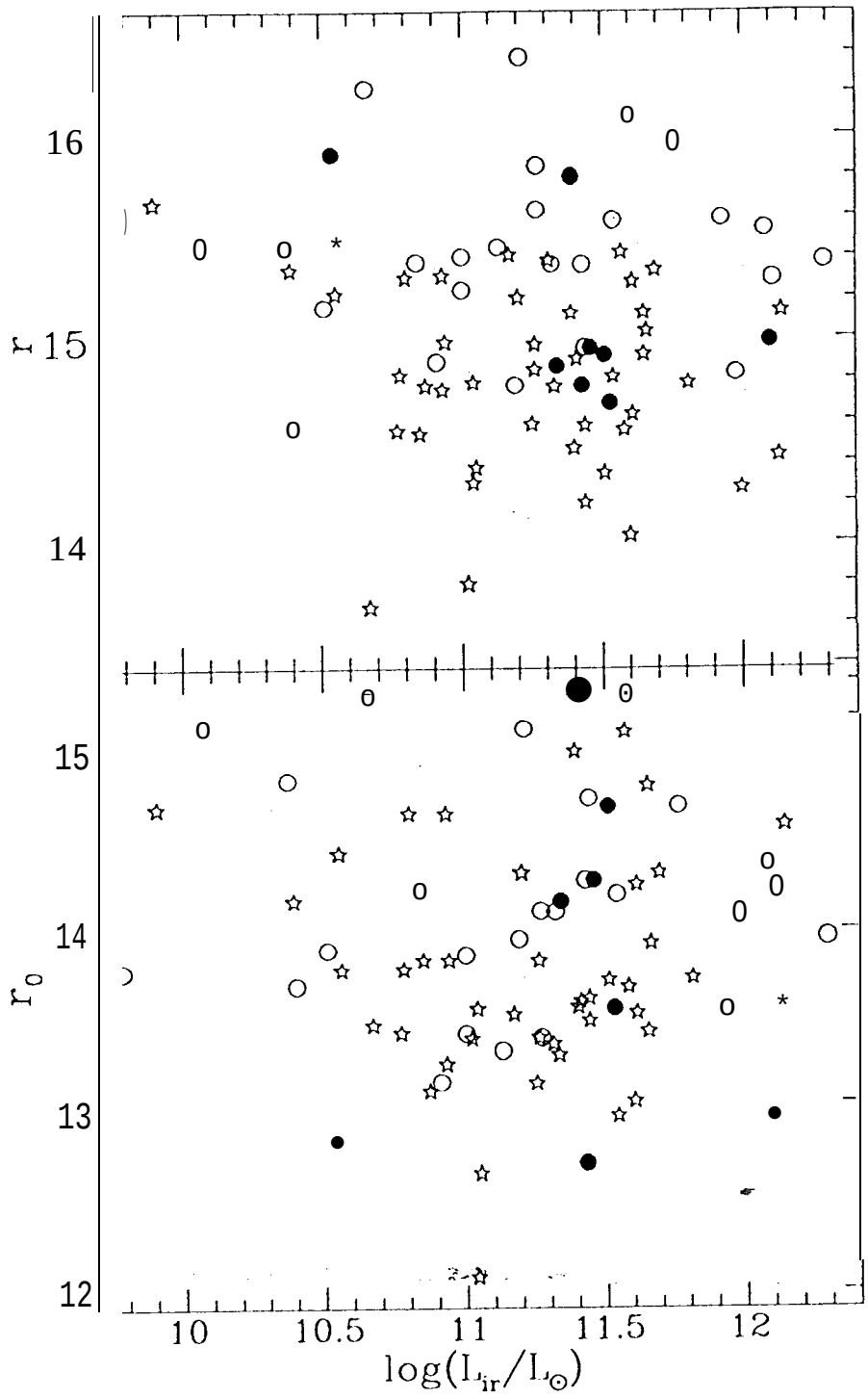
16
15
14
15
14
13
12
r_o
10
10.5
11
11.5
12
$\log(L_{ir}/L_\odot)$

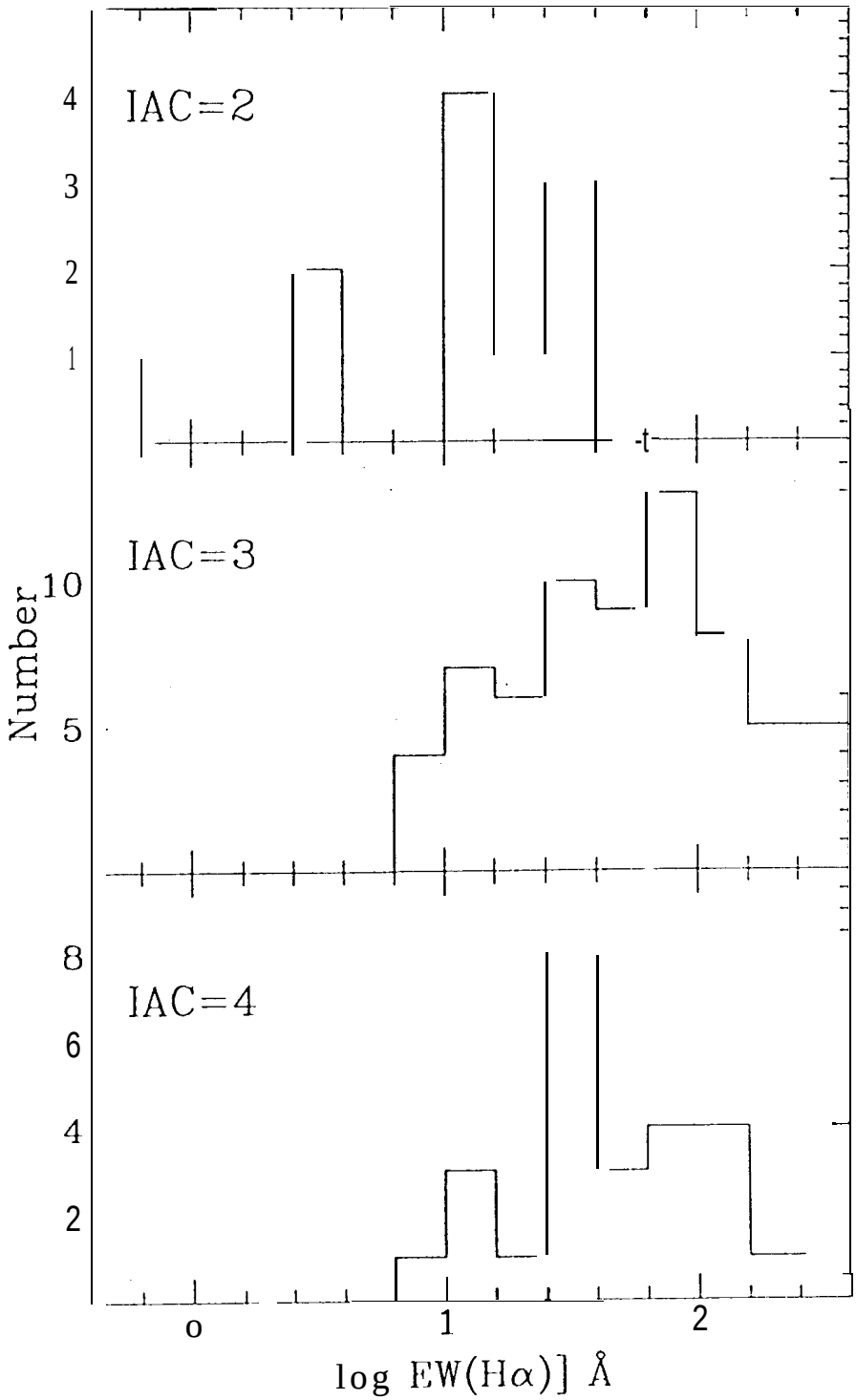
IAC=2
IAC=3
IAC=4
Number
4
3
2
1
10
5
8
6
4
2
0
1
2
log EW(Hα)] Å

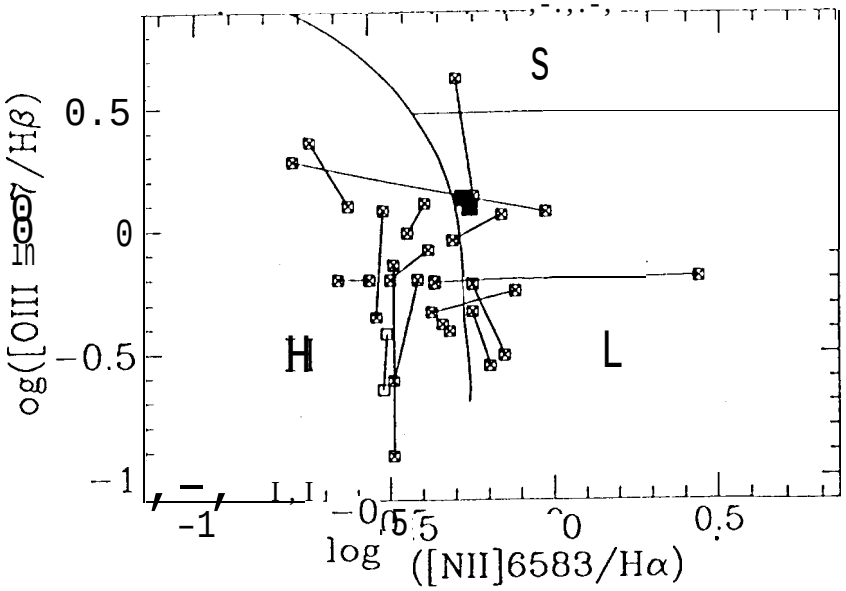
S
H
L
0.5
0
−0.5
−1
log([OIII]5007/Hβ)
log([NII]6583/Hα)

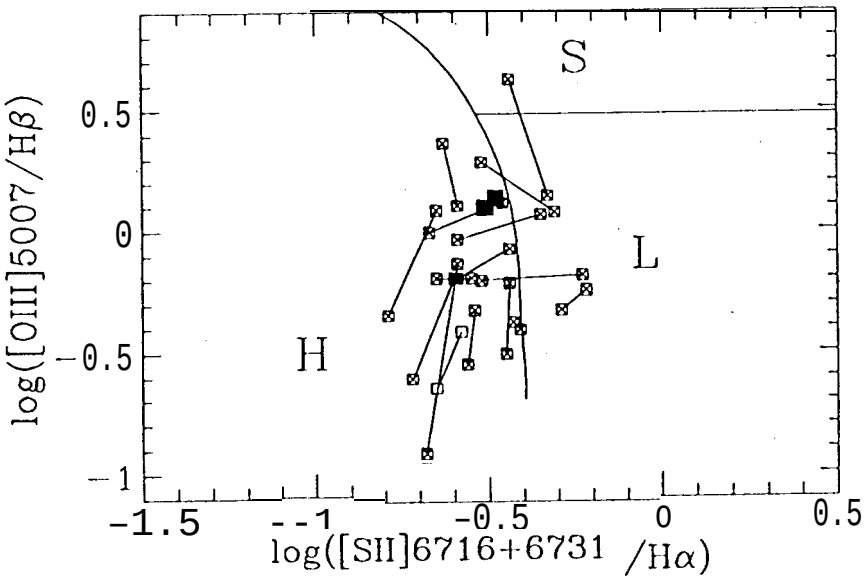
S
L
H
0.5
0
−0.5
−1
−1.5
log([OIII]5007/Hβ)
log([SII]6716+6731 /Hα)

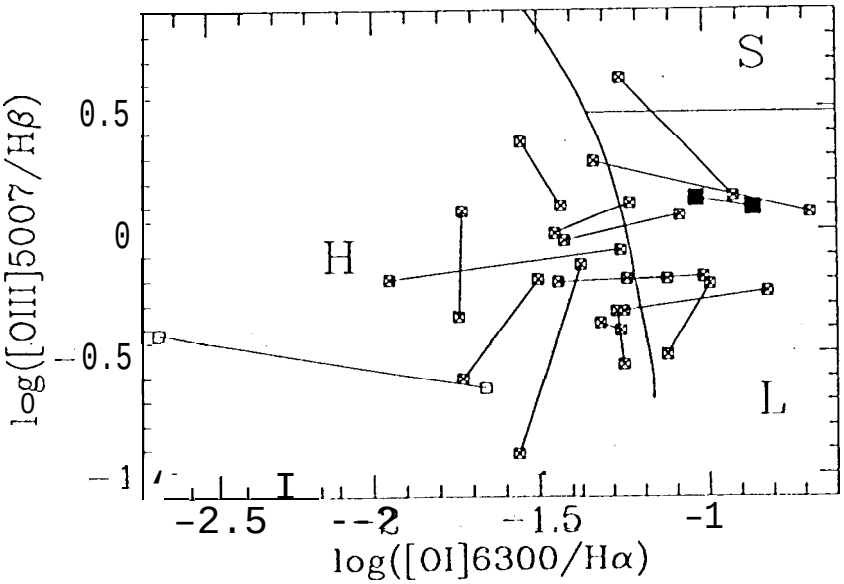
S
H
L
0.5
0
−0.5
−1
−2.5
−2
−1.5
−1
log([OIII]5007/Hβ)
log([OI]6300/Hα)

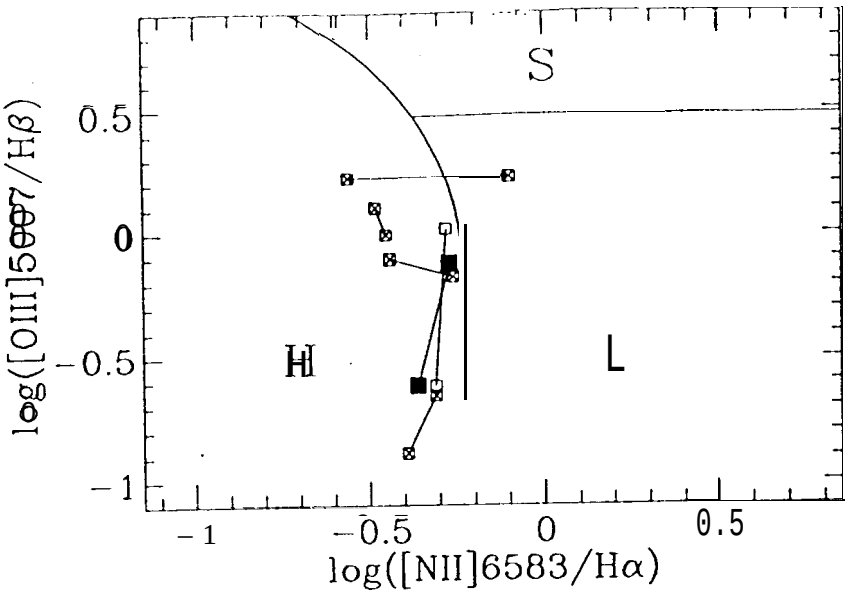
S
H
L
0.5
0
−0.5
−1
−1
−0.5
0
0.5
log([NII]6583/Hα)
log([OIII]5007/Hβ)

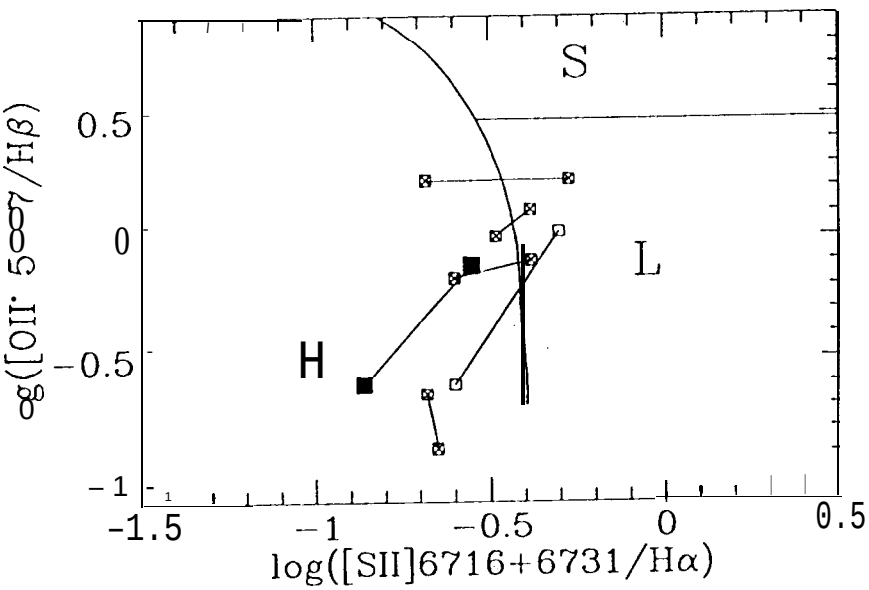
S
H
L
0.5
0
−0.5
−1
-1.5
−1
−0.5
0
0.5
log([SII]6716+6731/Hα)
log([OIII 5007/Hβ)

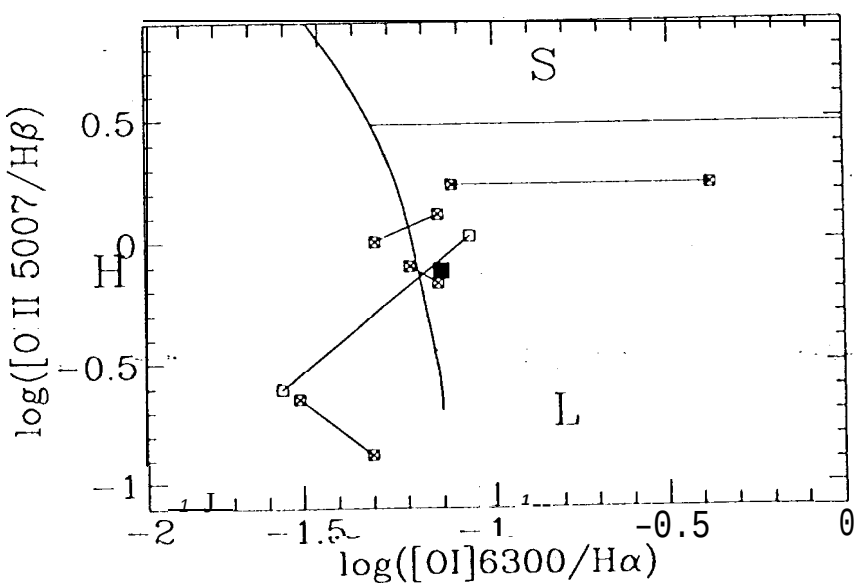
S
H
L
0.5
0
−0.5
−1
−2
−1.5
−1
-0.5
0
log([OI]6300/Hα)
log([O II 5007/Hβ)

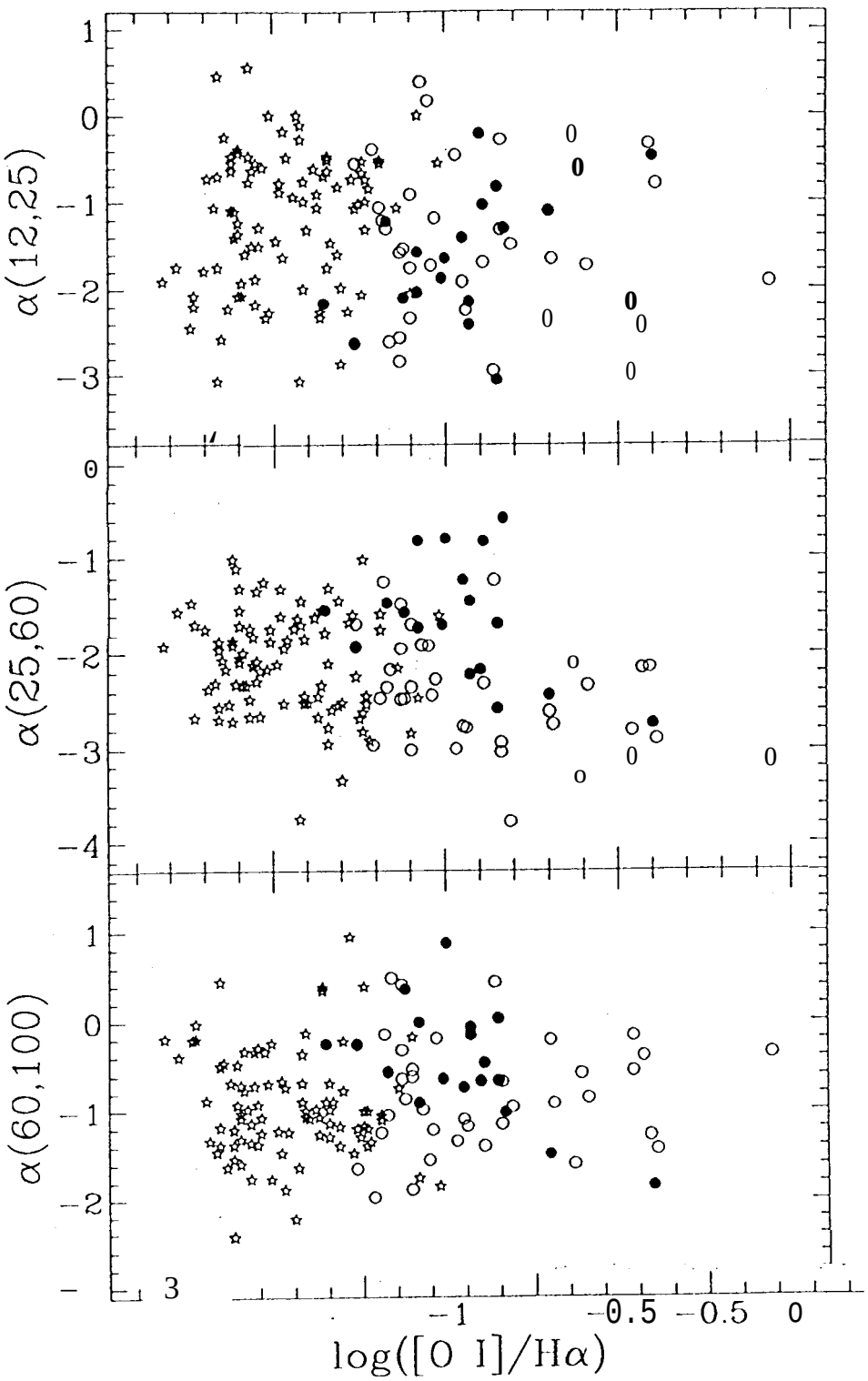
α(12,25)
α(25,60)
α(60,100)
log([O I]/Hα)
1
0
−1
−2
−3
−4
−0.5
−0.5
0

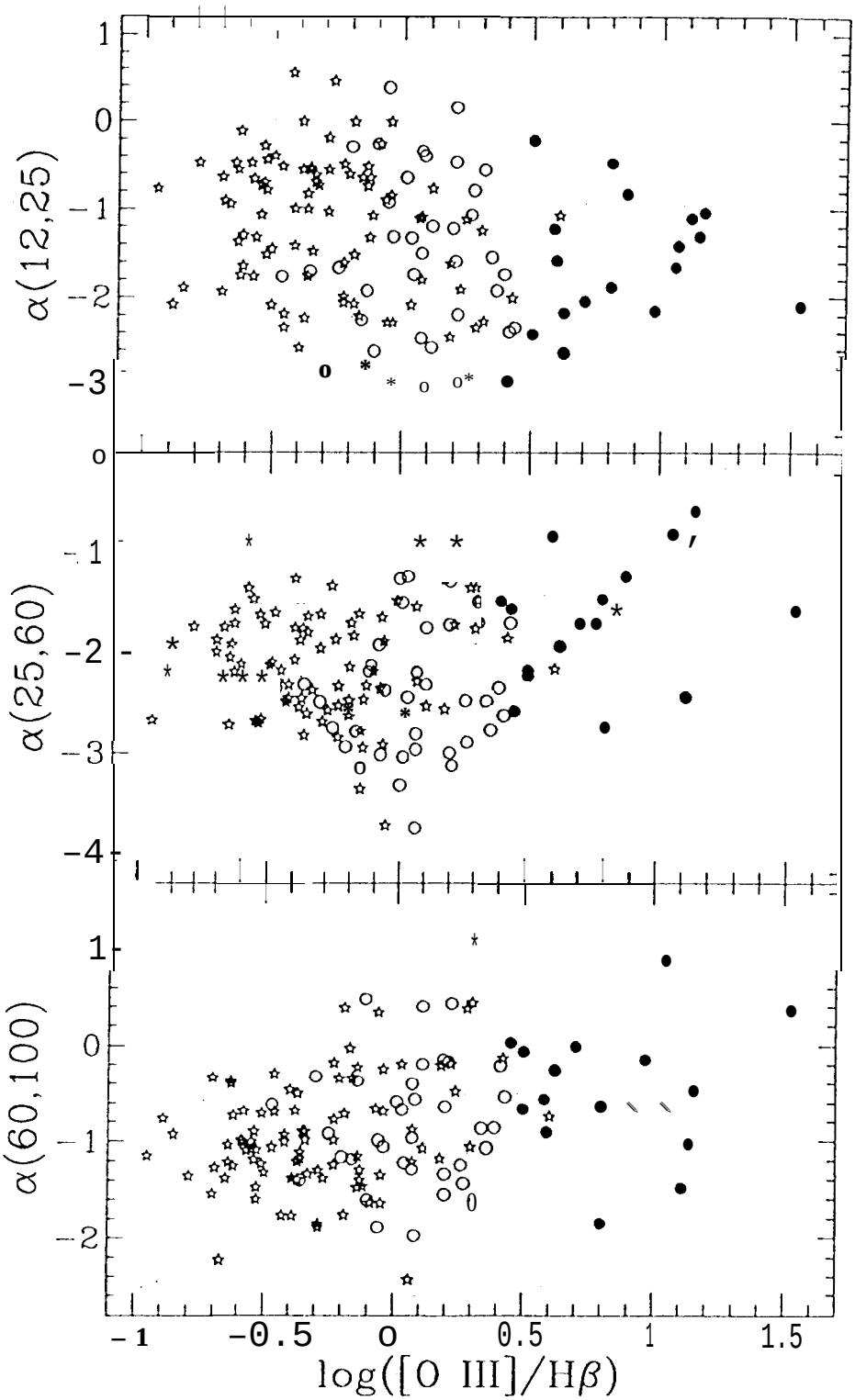
α(12,25)
α(25,60)
α(60,100)
log([O III]/Hβ)
1
0
−1
−2
−3
−4
−1
−0.5
0
0.5
1
1.5

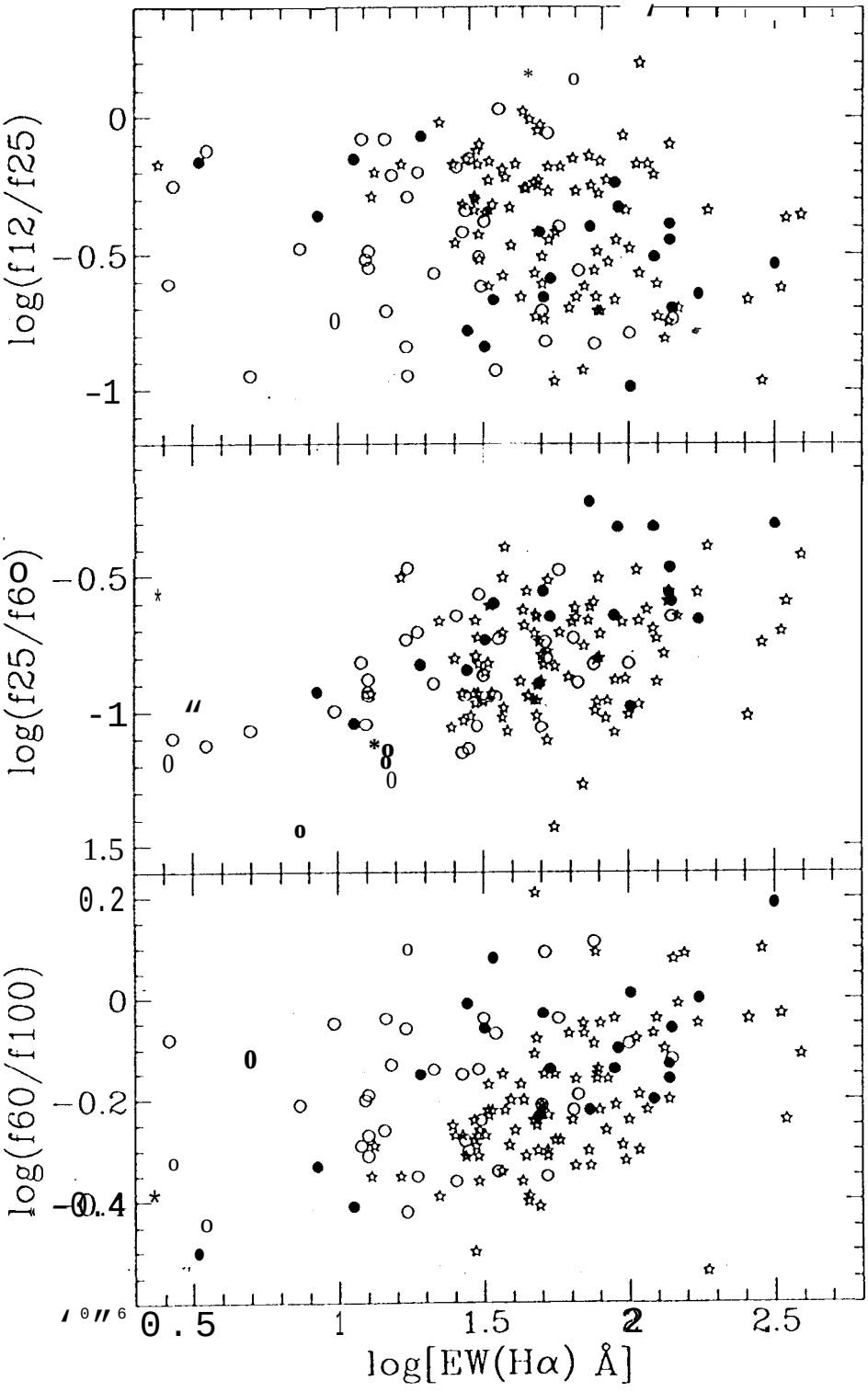
log(f12/f25)
log(f25/f60)
log(f60/f100)
log[EW(Hα) Å]
0
-0.5
-1
1.5
0.2
-0.2
-0.4
0.5
1
1.5
2
2.5

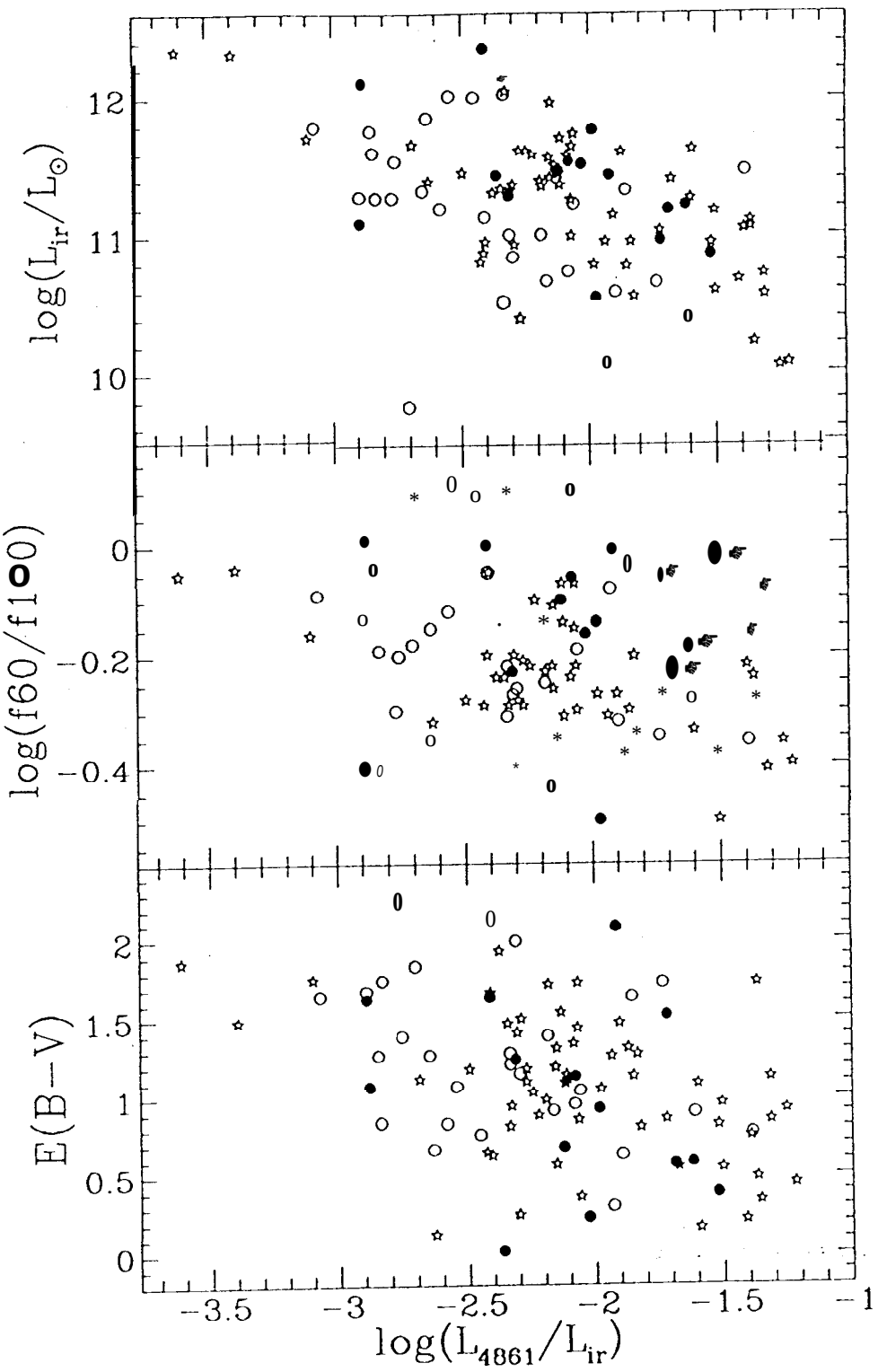
log(L_ir/L_⊙)
12
11
10
log(f60/f100)
0
−0.2
−0.4
E(B−V)
2
1.5
1
0.5
0
−3.5
−3
−2.5
−2
−1.5
−1
log(L_4861/L_ir)

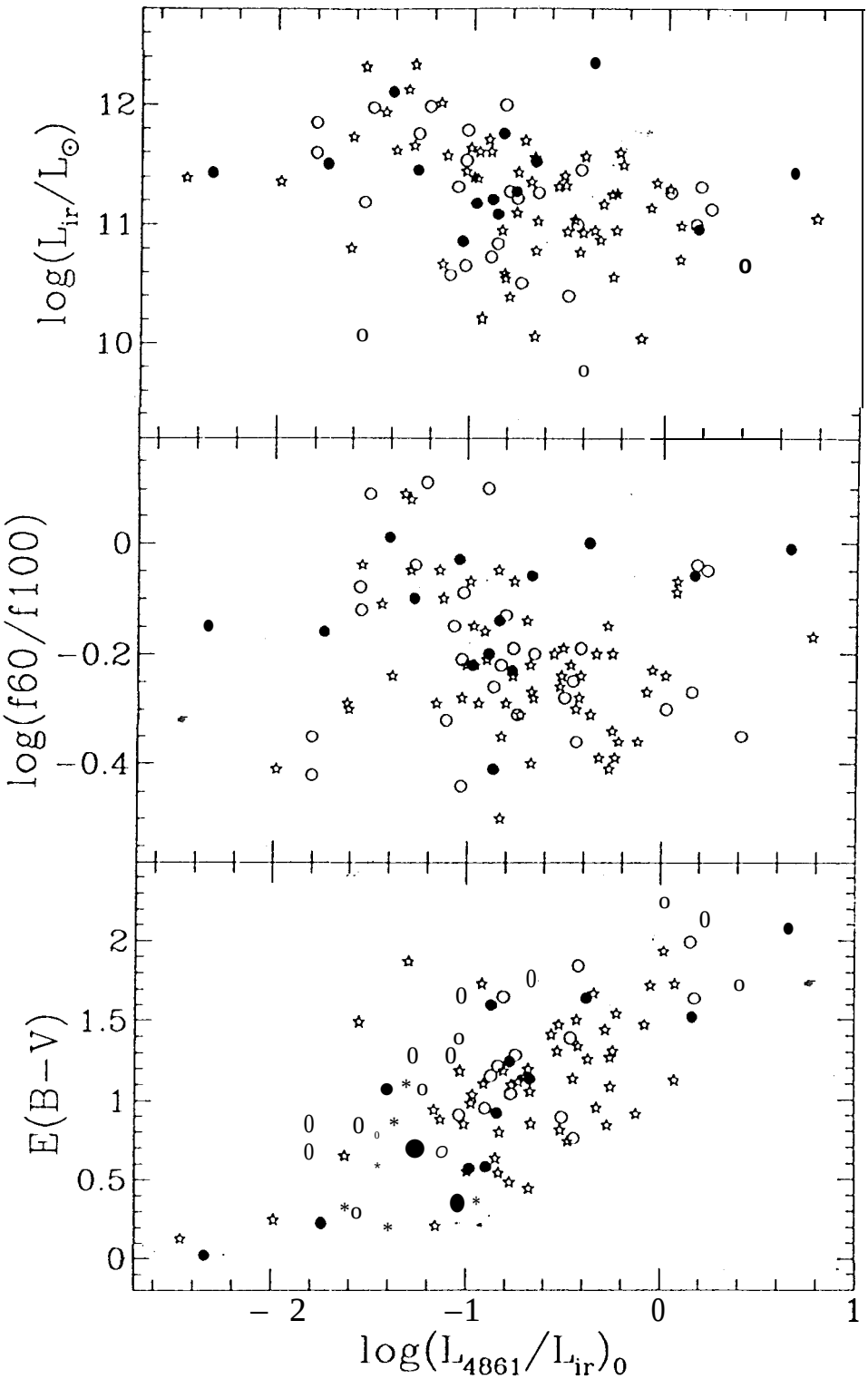
log(L_ir/L_⊙)
12
11
10
log(f60/f100)
0
−0.2
−0.4
E(B−V)
2
1.5
1
0.5
0
−2
−1
0
1
log(L_4861/L_ir)_0

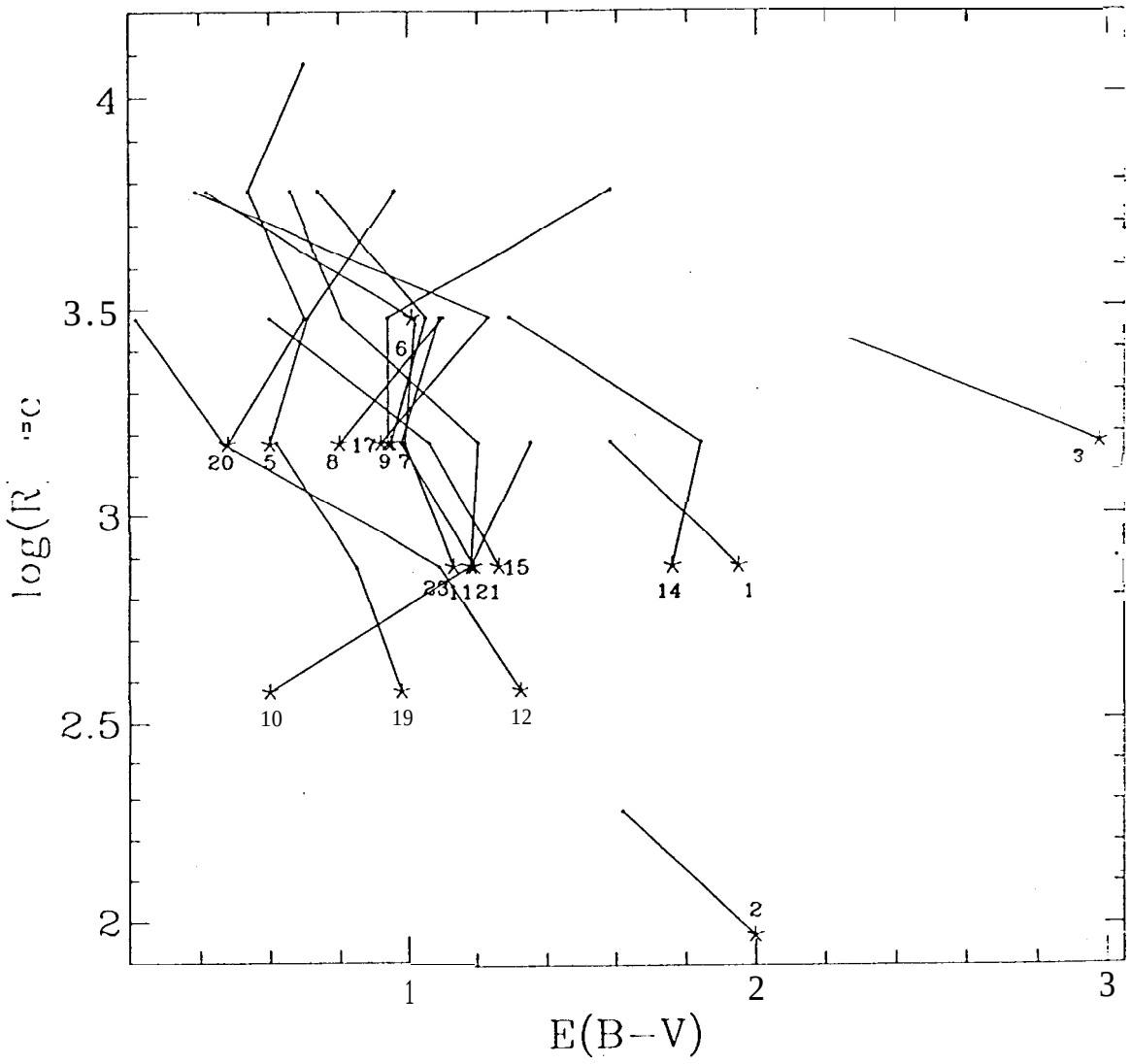
4
3.5
3
2.5
2
1
2
3
E(B−V)
log(R
20
5
8
17
9
7
6
15
23
1
12
21
14
1
3
10
19
12
2

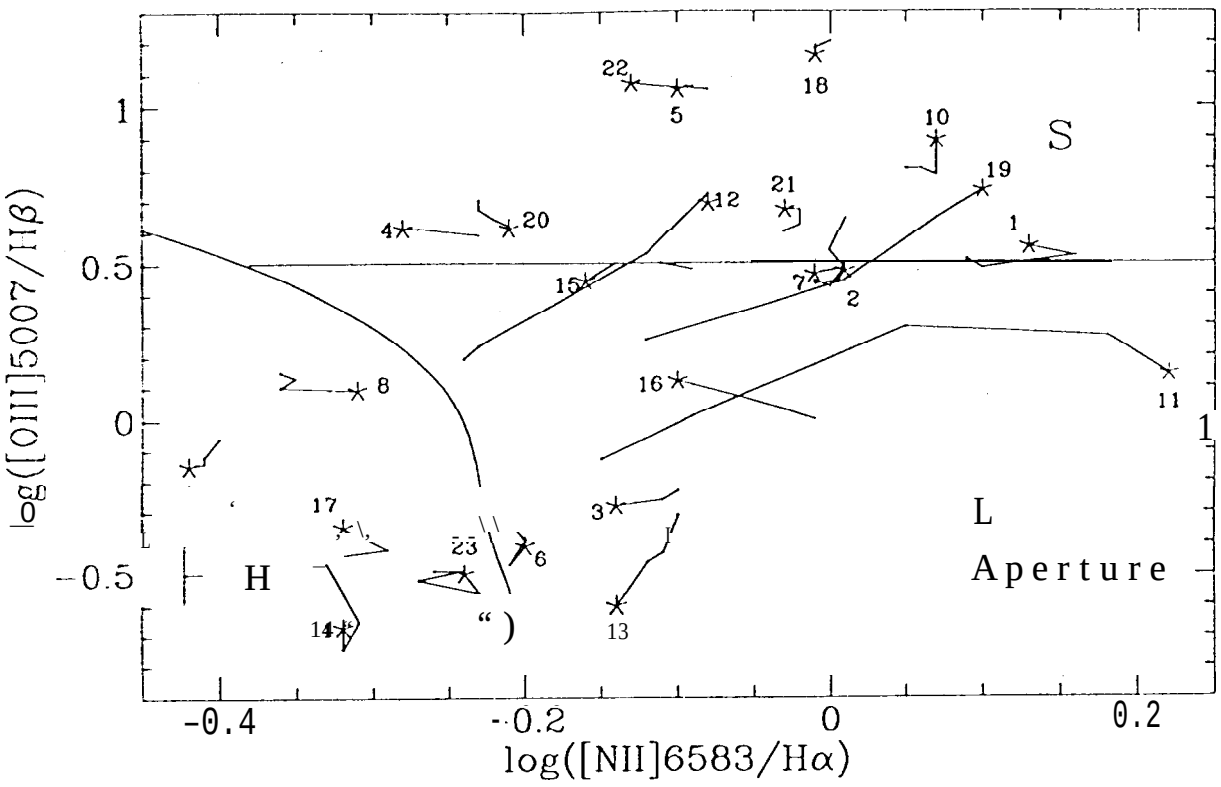
log([OIII]5007/Hβ)
log([NII]6583/Hα)
S
L
H
Aperture
1
0.5
0
-0.5
-0.4
-0.2
0
0.2
22
5
18
10
19
21
12
4
20
1
15
7
2
8
16
11
17
3
23
6
14
13

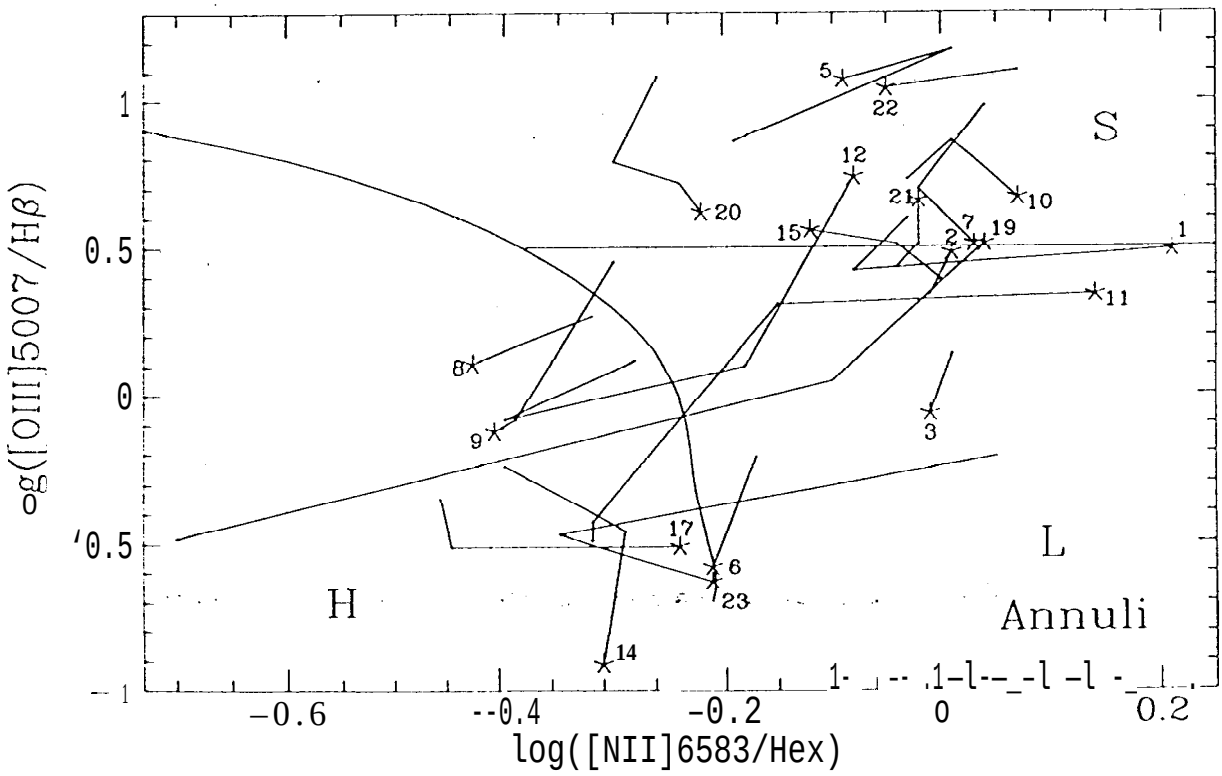
log([OIII]5007/Hβ)
log([NII]6583/Hex)
S
L
H
Annuli
1
0.5
0
-0.5
-1
-0.6
-0.4
-0.2
0
0.2
5
22
12
20
21
10
15
7
19
2
1
11
8
9
3
17
6
23
14

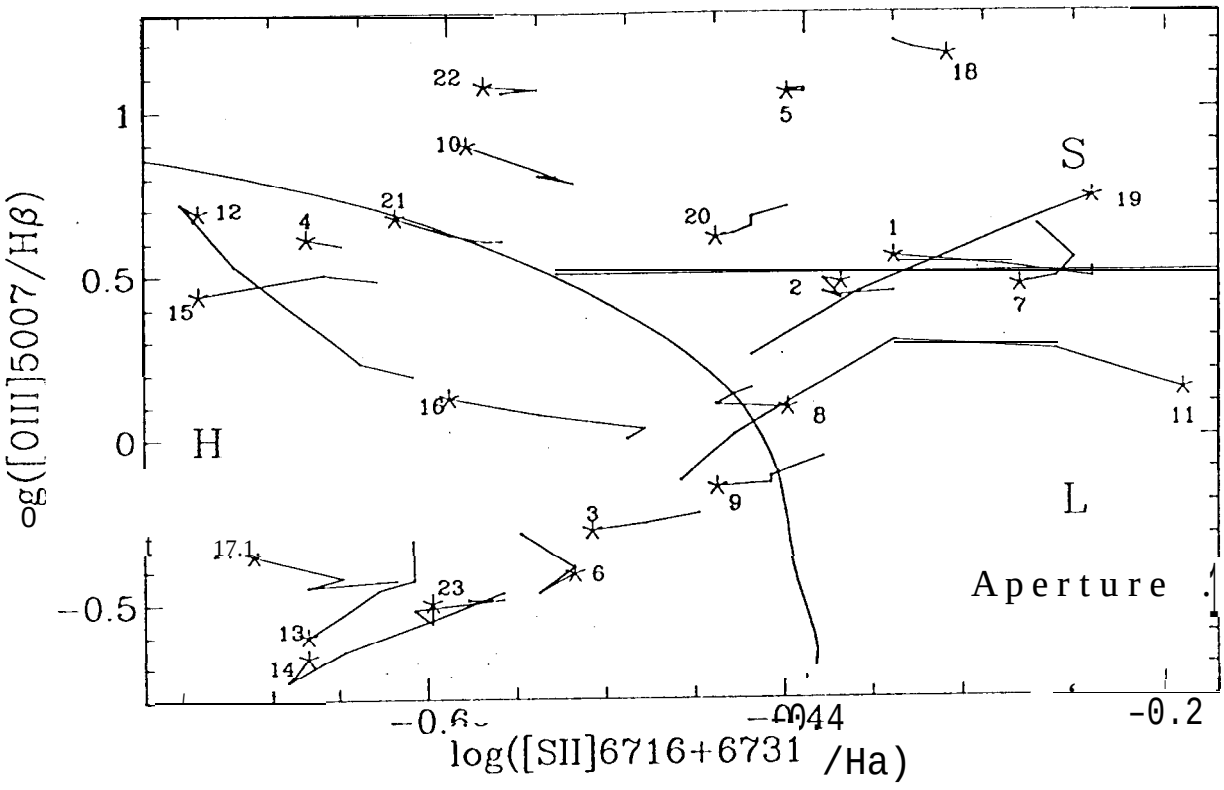
S
H
L
Aperture
log([SII]6716+6731 /Ha)
-0.2

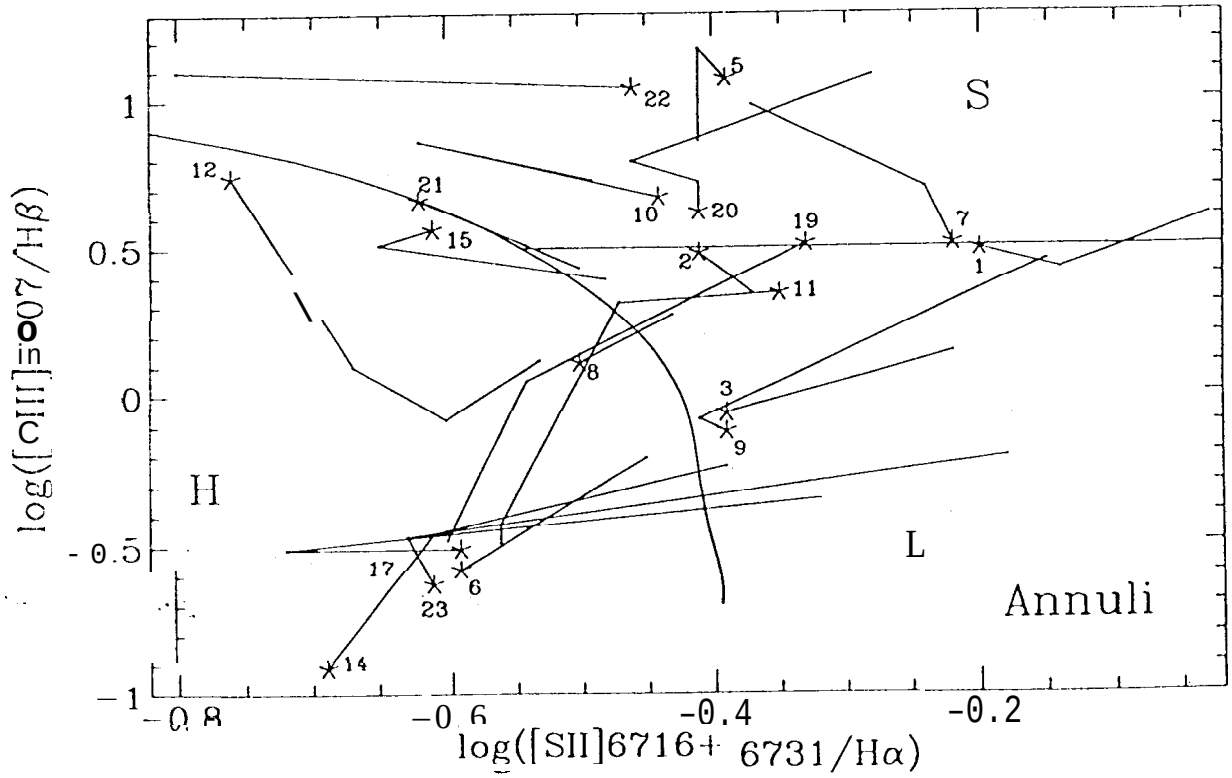
S
H
L
Annuli
log([SII]6716+ 6731/Hα)
-0.4
-0.2

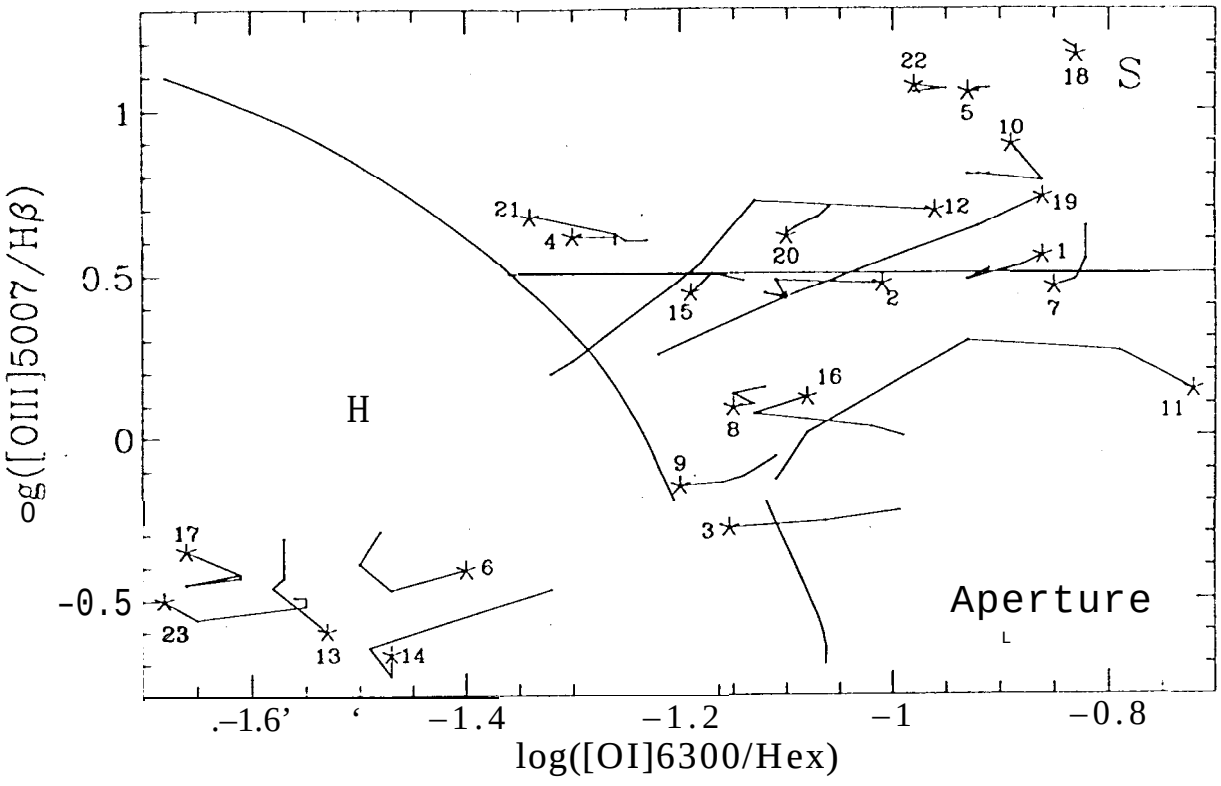
S
H
Aperture
1
0.5
0
-0.5
-1.6
-1.4
-1.2
-1
-0.8
log([OI]6300/Hex)
og([OIII]5007/Hβ)

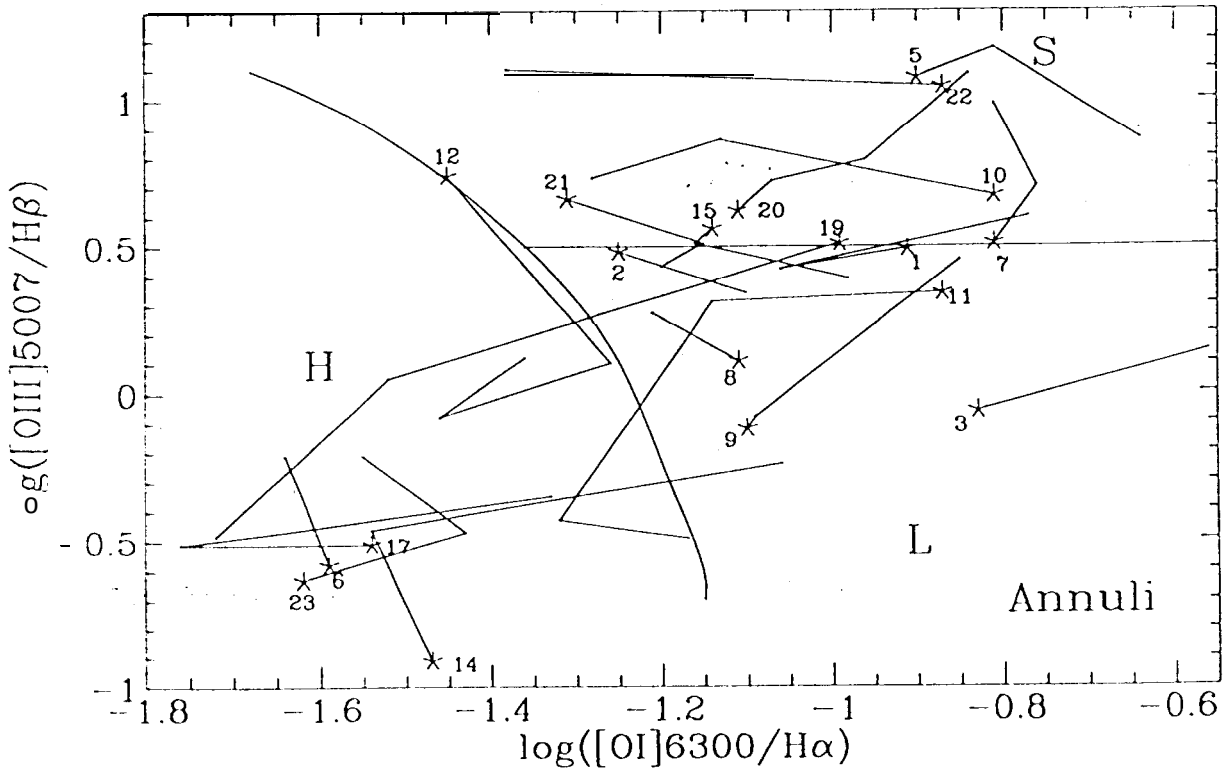
S
H
L
Annuli
1
0.5
0
- 0.5
-1
-1.8
-1.6
-1.4
-1.2
-1
-0.8
-0.6
log([OI]6300/Hα)
og([OIII]5007/Hβ)

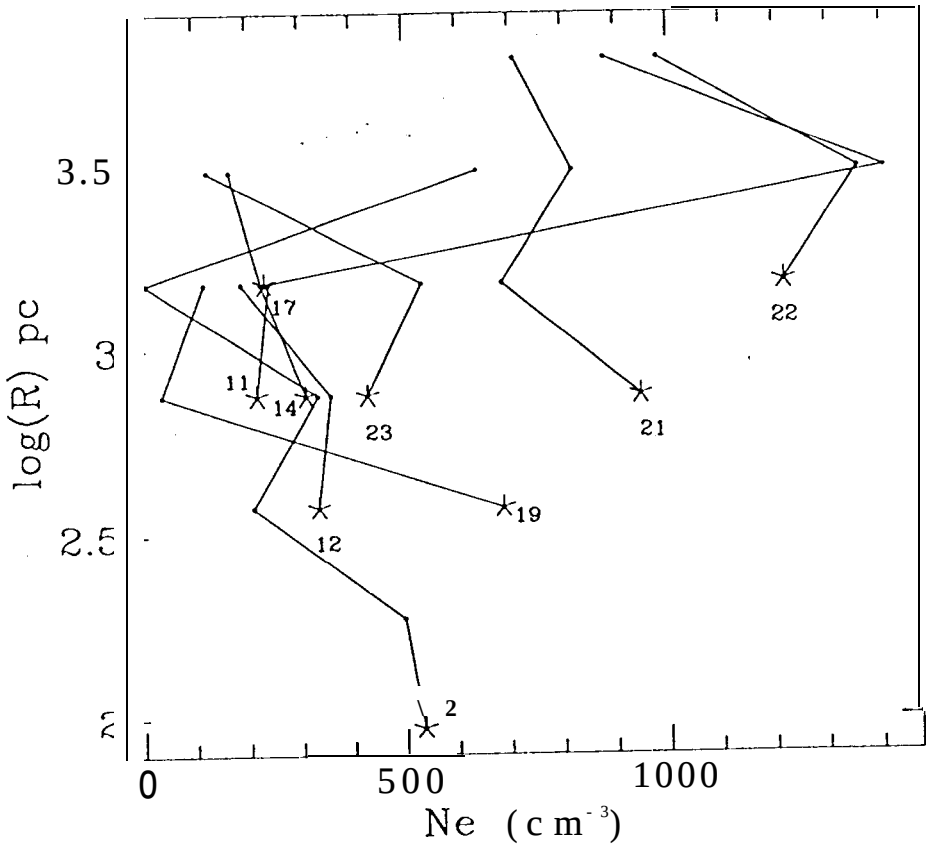
3.5
3
2.5
log(R) pc
0
500
1000
Ne (cm⁻³)
17
11
14
23
21
22
19
12
2

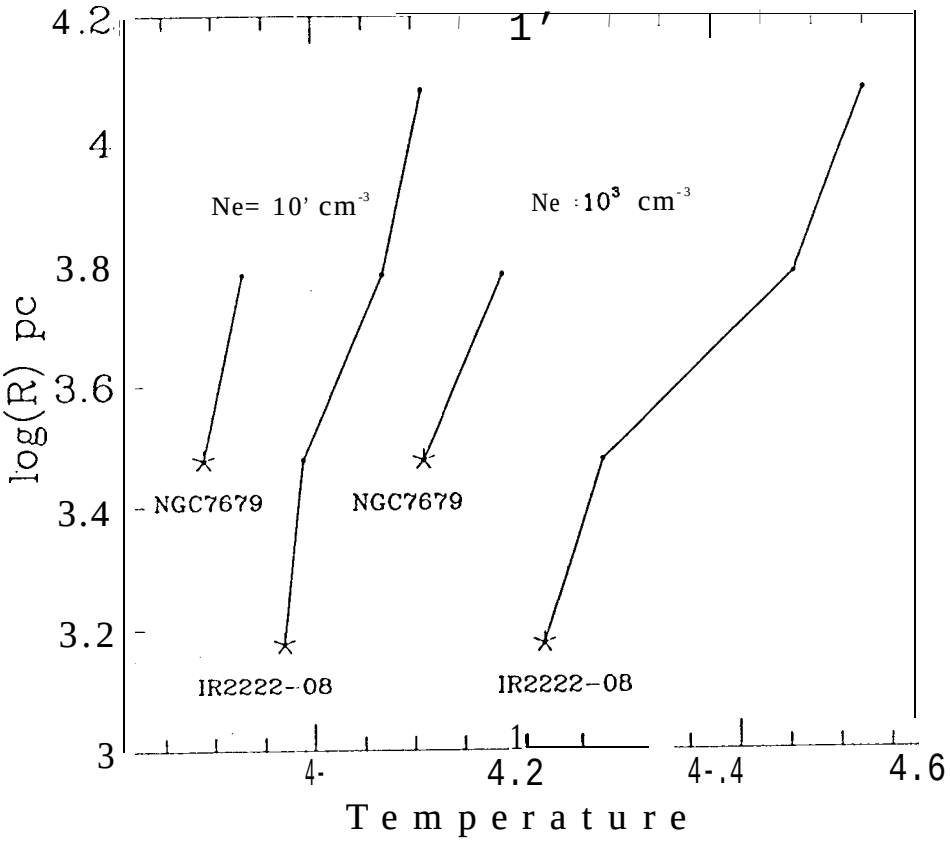
4.2
4
3.8
3.6
3.4
3.2
3
log(R) pc
Ne= 10' cm-3
Ne :10³ cm-3
NGC7679
NGC7679
IR2222-08
IR2222-08
4.2
4.6
Temperature

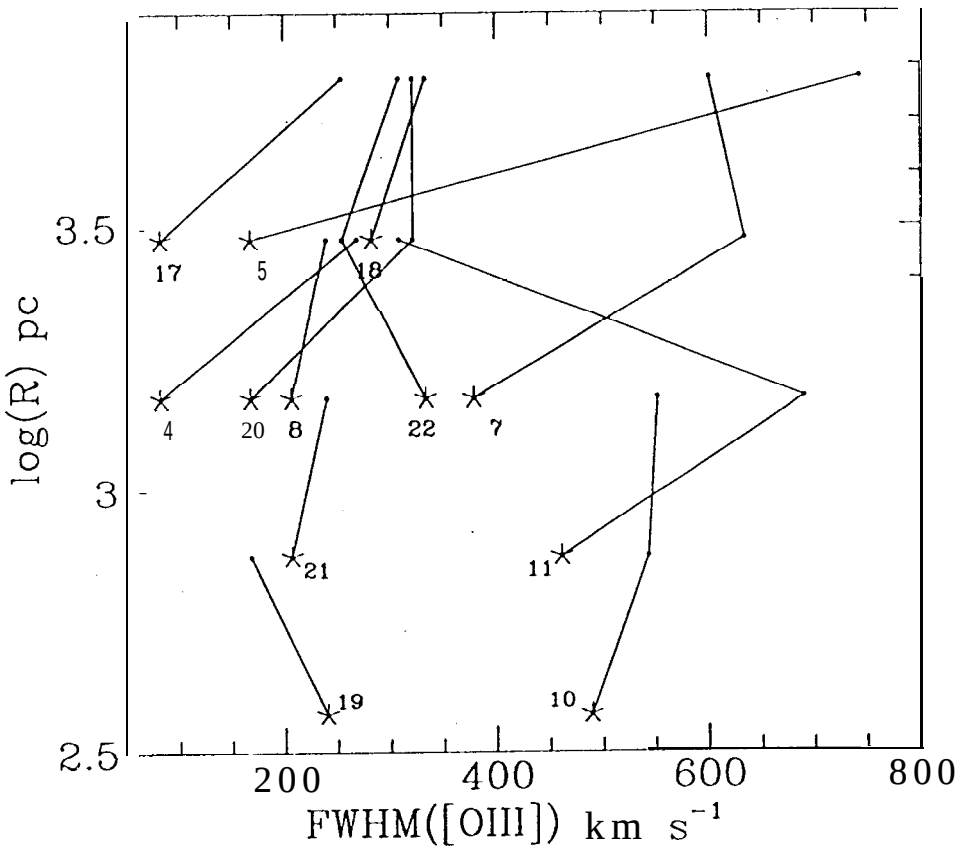
3.5
3
2.5
log(R) pc
17
5
18
4
20
8
22
7
21
11
19
10
200
400
600
800
FWHM([OIII]) km s^{-1}

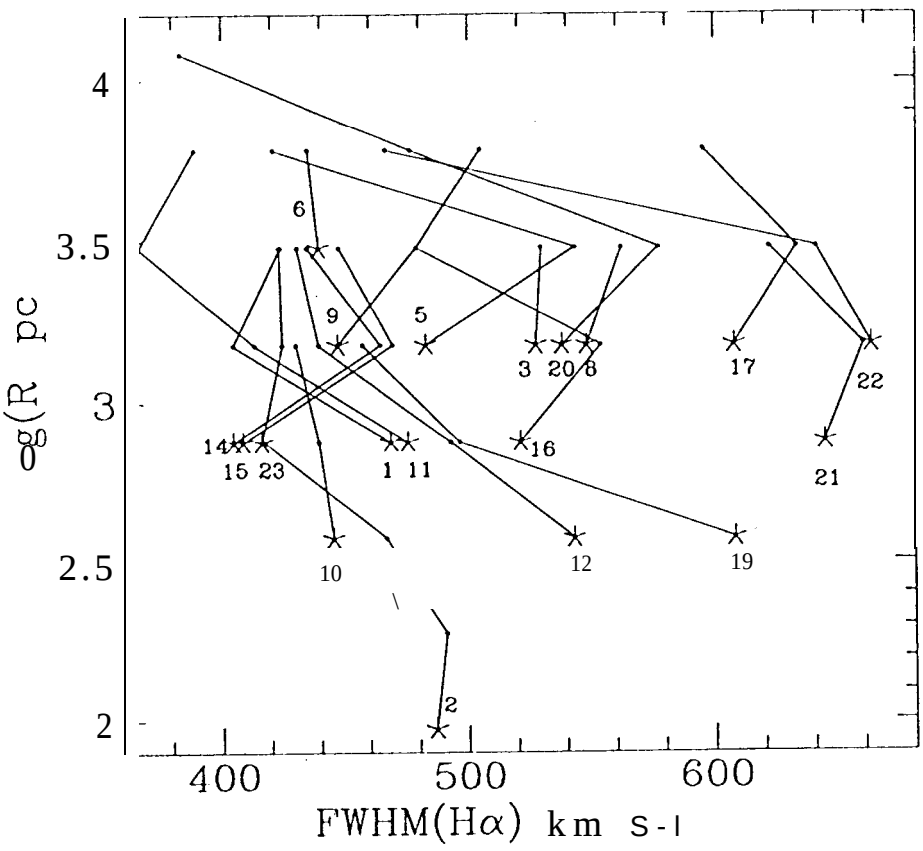
4
3.5
3
2.5
2
400
500
600
FWHM(Hα) km s-1
log(R pc
6
9
5
3 20 8
17
22
14
15 23
1 11
16
21
10
12
19
2

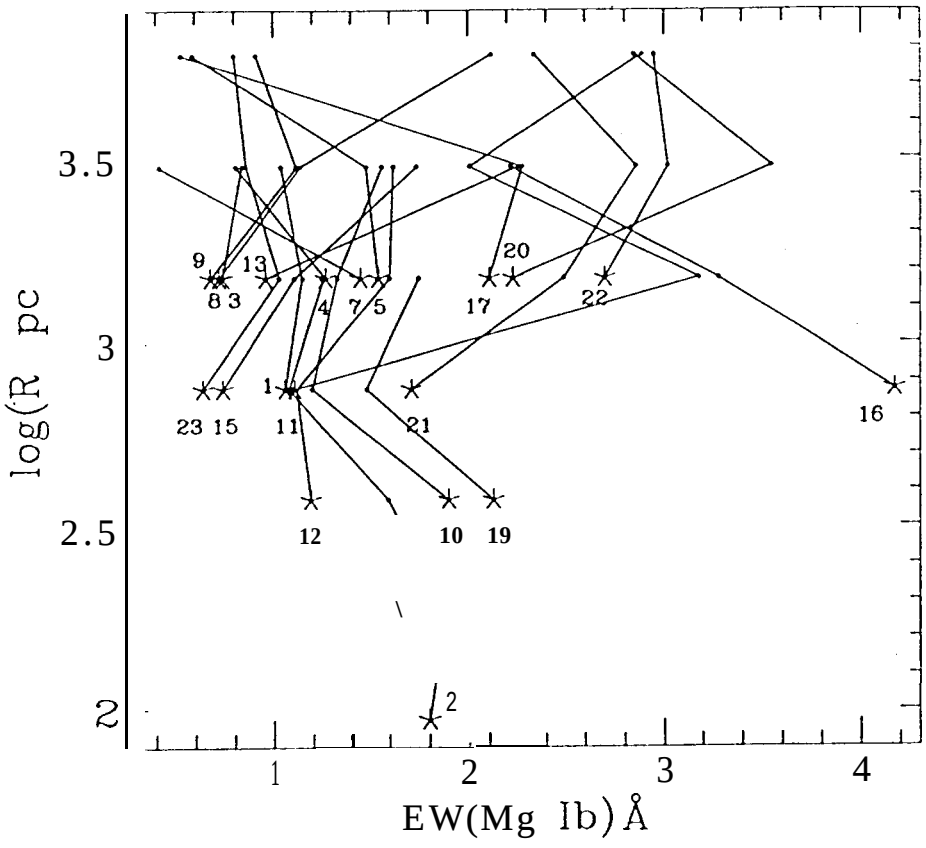
3.5
3
2.5
2
log(R pc
1
2
3
4
EW(Mg Ib) Å
9
13
8 3
4
7 5
20
17
22
23 15
1
11
21
16
12
10 19
2

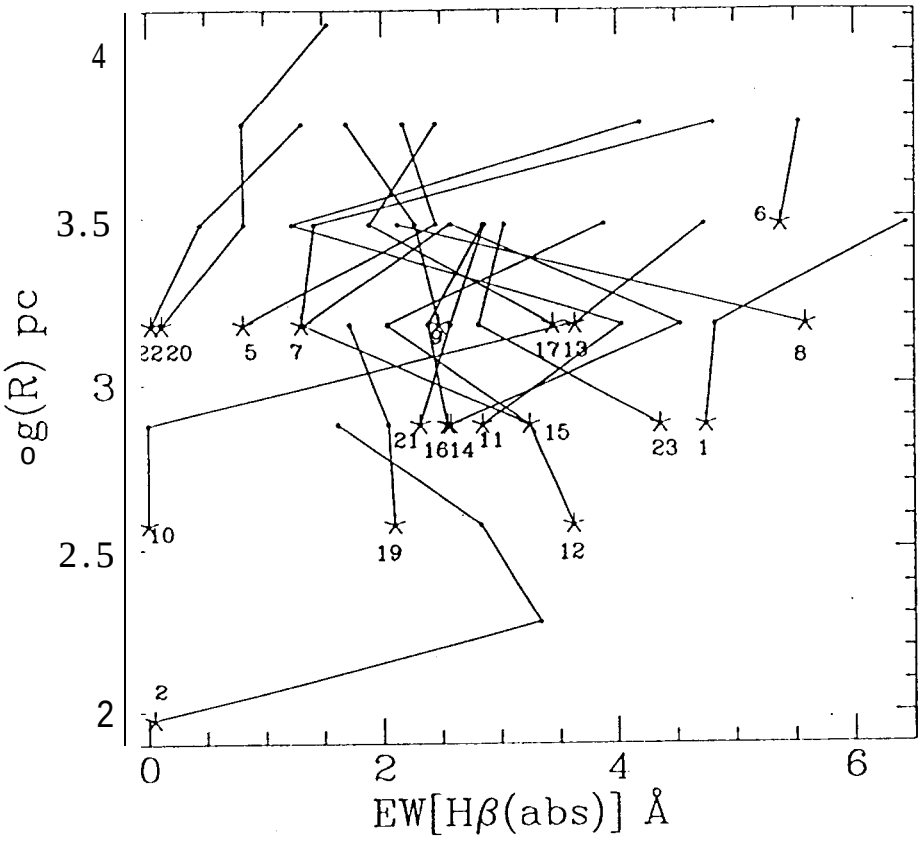
4
3.5
3
2.5
2
log(R) pc
0
2
4
6
EW[Hβ(abs)] Å
2220
5
7
1713
6
8
21
1614
11
15
23
1
10
19
12
2

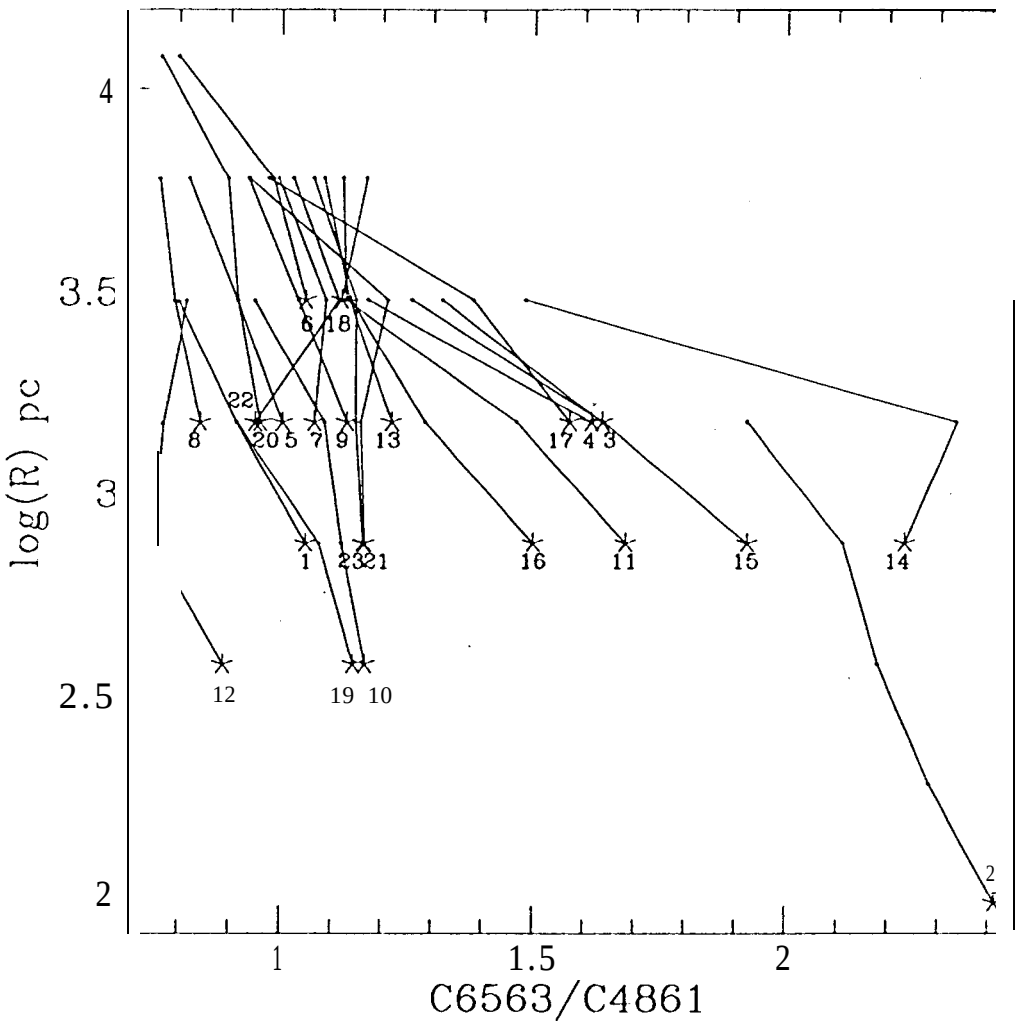
4
3.5
3
2.5
2
log(R) pc
1
1.5
2
C6563/C4861
6 18
22
8
20 5 7 9 13
17 4 3
1 23 21
16
11
15
14
12
19 10
2

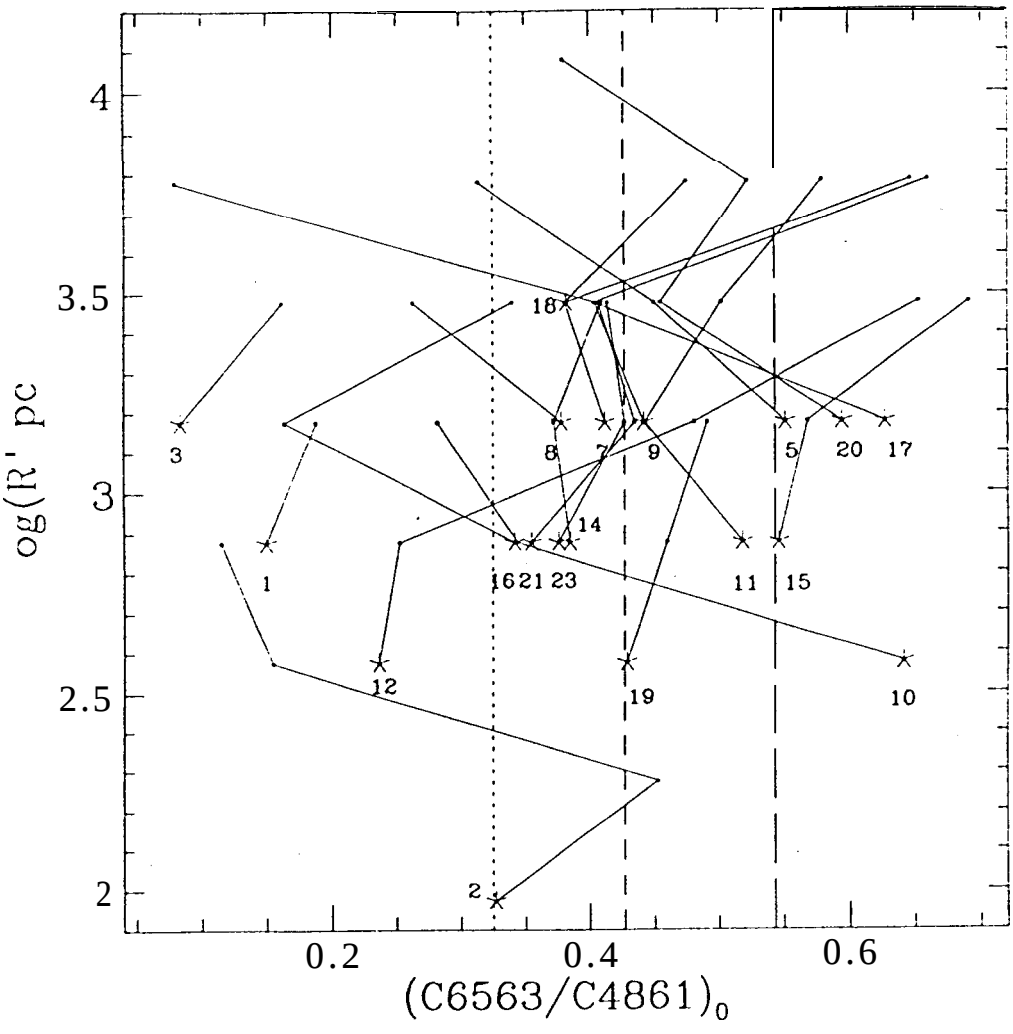
4
3.5
3
2.5
2
0.2
0.4
0.6
og(R' pc
(C6563/C4861)0
18
3
8
7
9
5
20
17
14
1
16 21 23
11
15
12
19
10
2

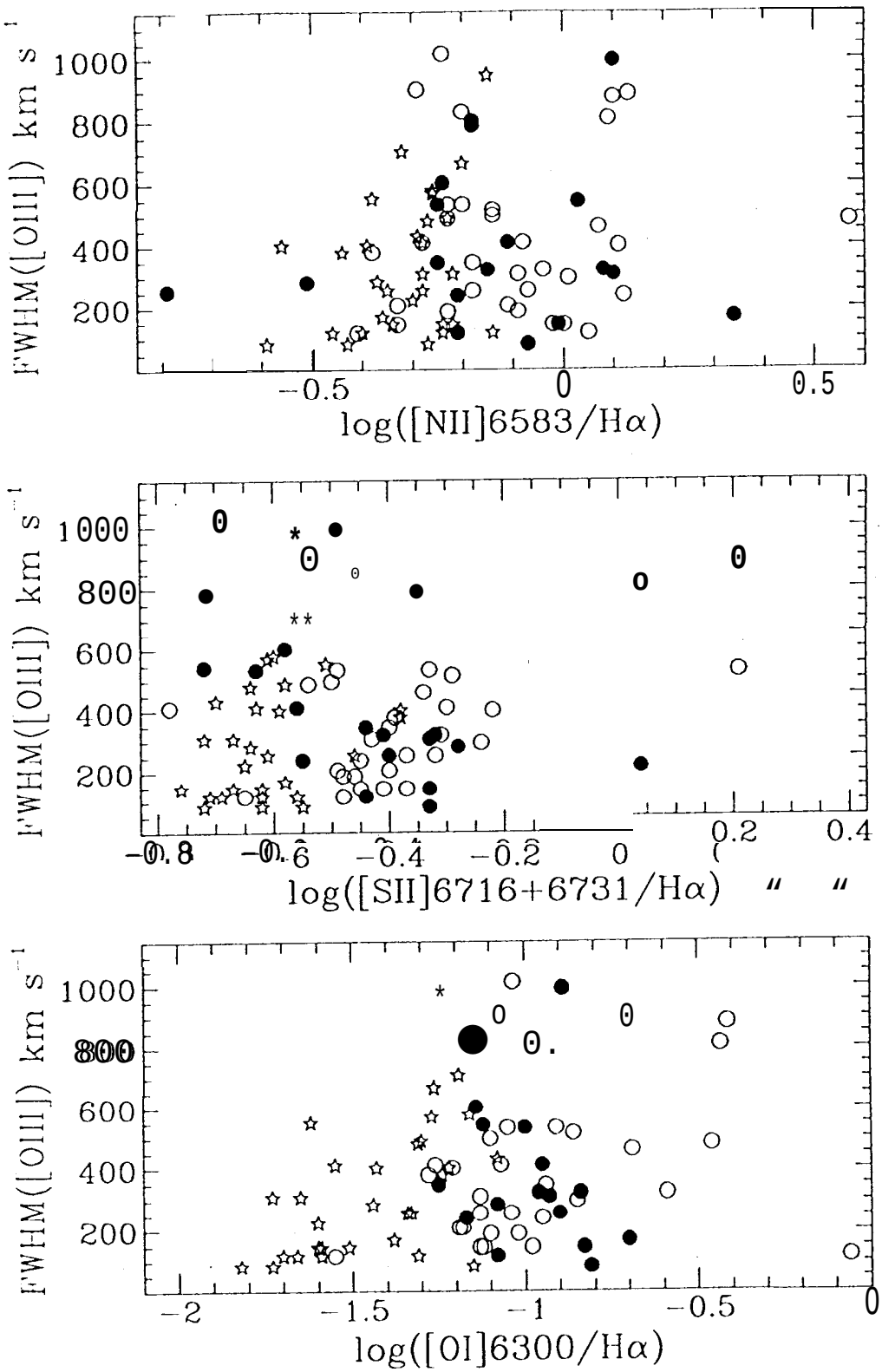
FWHM([OIII]) km s^{-1}
1000
800
600
400
200
−0.5
0
0.5
log([NII]6583/Hα)
FWHM([OIII]) km s^{-1}
1000
800
600
400
200
−0.8
−0.6
−0.4
−0.2
0
0.2
0.4
log([SII]6716+6731/Hα)
FWHM([OIII]) km s^{-1}
1000
800
600
400
200
−2
−1.5
−1
−0.5
0
log([OI]6300/Hα)